Evaluation of "Good Engineering Practice" Stack Height at the ASARCO Smelter, Hayden, Arizona -- A Physical Modeling Study

by

R.L. Petersen* and J.E. Cermak**

FLUID MECHANICS AND
WIND ENGINEERING PROGRAM

COLLEGE OF ENGINEERING

COLORADO STATE UNIVERSITY
FORT COLLINS, COLORADO

Evaluation of "Good Engineering Practice" Stack Height at the ASARCO Smelter, Hayden, Arizona -- A Physical Modeling Study

by

R.L. Petersen* and J.E. Cermak**

Prepared for

North American Weather Consultants
600 Norman Firestone Road
Goleta, California 93017

July 1979

CER79-80RLP-JEC2

*Research Assistant Professor
**Director, Fluid Dynamics and Diffusion Laboratory

ABSTRACT

North American Weather Consultants contracted with Colorado State University to conduct a fluid modeling investigation of the effects of topographic generated wakes, eddies and downwash upon the plumes emitted from stacks at the ASARCO smelter, Hayden, Arizona. The purpose of the study is to determine whether the existing 305 m (1000 ft) stack at the smelter is above or below the "good engineering practice" (GEP) stack height. The GEP height is defined in a proposed Environmental Protection Agency regulation.

The wind tunnel tests were conducted using state-of-the-art wind tunnel testing procedures. Visualization and concentration measurements of the simulated plume from stacks ranging in height from 91 to 349 m were obtained. For each stack height three wind speeds and one wind direction with and without the scale model of the upwind topography were studied. The results of the tests show that the maximum ground level SO_2 concentration exceeds the applicable National Ambient Air Quality Standard for stack heights up to and including 349 m. In addition the maximum concentration is at least 40% in excess of that without the terrain present for all stack heights studied. Hence the existing 305 m stack is below the GEP height.

LIST OF CONTENTS

Chapter		Page
	ABSTRACT	ii
	LIST OF TABLES	iv
	LIST OF FIGURES	v
	LIST OF SYMBOLS	ix
1	INTRODUCTION	1
2	SUMMARY AND CONCLUSIONS	3
3	WIND TUNNEL SIMILARITY REQUIREMENTS	5
4	EXPERIMENTAL PROGRAM	14
	4.1 Summary	14
	4.2 Scale Models and Wind Tunnel	15
	4.3 Flow Visualization	16
	4.4 Gas Tracer Technique	17
	4.5 Velocity and Temperature Measurements	22
5	VELOCITY MEASUREMENTS	28
6	PLUME TRANSPORT AND DIFFUSION RESULTS	33
	6.1 Visualization	33
	6.2 Concentration Measurements	33
	REFERENCES	40

LIST OF TABLES

Tables		Page
4.1	Model Parameters	43
4.2	Parameters for ASARCO smelter at Hayden, Arizona	44
4.3	Summary of Visualization & Concentraction Tests	45
5.1	Summary of velocity profile characteristics without the upwind terrain present	47
5.2	Summary of velocity profile characteristics with the terrain present	48
5.3	Values of the surface roughness parameter z_o . .	49
6.1	Summary of ground-level concentration measurement results for ASARCO wind tunnel modeling experiments	50

LIST OF FIGURES

Figure		Page
4.2-1	Environmental Wind Tunnel, Fluid Dynamics & Diffusion Laboratory, Colorado State University . . .	52
4.2-2	Map showing area modeled in wind tunnel	53
4.2-3	Photographs of model terrain for the 51° true azimth looking (a) upwind and (b) downwind	54
4.2-4	Photograph showing 30.5 cm spires, 3.8 cm trip and approach ramp used for developing the boundary layer of the no-upwind terrain tests	55
4.2-5	Photograph of model stacks used for GEP evaluation. .	56
4.2-6	Drawing of model stacks used for GEP evaluation . . .	57
4.4-1	Map showing tracer gas sampling locations and locations where velocity measurements were obtained	58
4.4-2	Photograph showing the sampling rake used to obtain the horizontal and vertical concentration profiles	59
4.4-3	Photographs showing (a) the tracer gas sampling system and (b) the gas chromatograph, integrator and sampling system set-up	60
4.5-1	Typical hot film calibration curve taken on June 5, 1979	61
5.1-1	Velocity profiles at the tall stack location without the upwind terrain present for the following reference velocities: ○ - 1 m/s; △ 2 m/s; □ - 3 m/s; * - 4 m/s ◇ - 5 m/s	62
5.1-2	Velocity profiles at the tall stack location with the upwind terrain present for the following reference velocities: □ 3.1 m/s; ○ - 3.4 m/s; △ - 3.9 m/s; * - 4.5 m/s.	63
5.1-3	Velocity profiles along the center of the tunnel without the upwind terrain present	64
5.1-4	Velocity profiles along the center of the tunnel with the upwind terrain present	65
5.1-5	Longitudinal turbulence intensity profiles along the center of the tunnel without the upwind terrain present	66

Figure		Page

Figure		Page
5.1-6	Longitudinal turbulence intensity profiles along the center of the tunnel with the upwind terrain present	67
5.1-7	Velocity profiles across the tunnel at the tall stack location without the upwind terrain present . .	68
5.1-8	Velocity profiles across the tunnel at the tall stack location with the upwind terrain present . . .	69
5.1-9	Longitudinal turbulence intensity profiles across the tunnel without the upwind terrain present	70
5.1-10	Longitudinal turbulence intensity profiles across the tunnel with the upwind terrain present	71
6.1-1	Photographs of plume behavior without (a) and with (b) the upwind terrain present for stack height of 91.5 m for the R&R flue and 73.2 m for the converter flue	72
6.1-2	Photographs of plume behavior without (a) and with (b) the upwind terrain present for a tall stack height of 199.7 m	73
6.1-3	Photographs of plume behavior without (a) and with (b) the upwind terrain present for a tall stack height of 249.6 m	74
6.1-4	Photographs of plume behavior without (a) and with (b) the upwind terrain present for a tall stack height of 305.3 m	75
6.1-5	Photographs of plume behavior without (a) and with (b) the upwind terrain present for a tall stack height of 349.4 m	76
6.2-1	Vertical concentration profiles for (a) 91 m stack - without terrain, (b) 200 m stack - without terrain, (c) 305 m stack - without terrain, and (d) 305 m stack with terrain	77
6.2-2	Horizontal concentration profiles for (a) 91 m stack - without terrain, (b) 200 m stack - without terrain, (c) 305 m stack - without terrain, and (d) 305 m stack - with terrain	78
6.2-3	Comparison of observed σ_y variation with that predicted for the atmosphere by Pasquill (1974, 1976)	79

Figure		Page
6.2-4	Comparison of observed σ_z variation with that predicted for the atmosphere by Pasquill (1974, 1976)	80
6.2-5	Maximum dimensionless concentration K versus dimensionless downwind distance (x/H_T) with and without the upwind terrain for a stack height of 91 m	81
6.2-6	Maximum dimensionless concentration K versus dimensionless downwind distance (x/H_T) with and without the upwind terrain for a stack height of 200 m	82
6.2-7	Maximum dimensionless concentration K versus dimensionless downwind distance (x/H_T) with and without the upwind terrain for a stack height of 250 m	83
6.2-8	Maximum dimensionless concentration K versus dimensionless downwind distance (x/H_T) with and without the upwind terrain for a stack height of 305 m	84
6.2-9	Maximum dimensionless concentration K versus dimensionless downwind distance (x/H_T) with and without the upwind terrain for a stack height of 349 m	85
6.2-10	Dimensionless concentration K versus lateral distance (y/H_T) with and without the upwind terrain at the two downwind locations of maximum concentration for a stack height of 91 m	86
6.2-11	Dimensionless concentration K versus lateral distance (y/H_T) with and without the upwind terrain at the two downwind locations of maximum concentration for a stack height of 200 m	87
6.2-12	Dimensionless concentration K versus lateral distance (y/H_T) with and without the upwind terrain at the two downwind locations of maximum concentration for a stack height of 250 m	88
6.2-13	Dimensionless concentration K versus lateral distance (y/H_T) with and without the upwind terrain at the two downwind locations of maximum concentration for a stack height of 305 m and velocity ratios of (a) 1.57, (b) 0.94, and (c) 0.66	89

Figure | Page

6.2-14 Dimensionless concentration K versus lateral distance (y/H_T) with and without the upwind terrain at the two downwind locations of maximum concentration for a stack height of 349 m and velocity ratios of (a) 1.63, (b) 0.98, and (c) 0.69 90

LIST OF SYMBOLS

Symbol	Definition	Units
A	Hot film calibration constant	(-)
B	Hot film calibration constant	(-)
C_p	Specific heat at constant pressure	($m^2s^{-2}K^{-1}$)
d	Diameter of hot film	(m)
D	Stack inside diameter	(m)
D_o	Stack outside diameter	(m)
E	Hot-film voltage	(V)
E_c	Eckert number $[u_o^2/(C_{p_o}\ \Delta T_o)]$	(-)
F_L	Lagrangian spectral function	(s)
Fr	Stack Froude number $[\frac{u_s}{\sqrt{g\gamma D}}]$	(-)
g	Acceleration due to gravity	(ms^{-2})
Gr	Grashof number $\left[\frac{gd^3(T_w-T_g}{\nu_g{}^2\ T_g}\right]$	(-)
h	Height of stack	(m)
H_b	Height of building	(m)
H_T	Height of terrain obstacle	(m)
$i_{x,y,z}$	Turbulence intensity in x, y or z direction [u'/u, v'/v, w'/u]	(1)
I	Current through wire	(a)
k	Thermal conductivity	($Wm^{-1}K^{-1}$)
K	Dimensionless concentration $(\frac{\chi}{\chi_o R})$	(-)

Symbol	Definition	Units
ℓ	Length	(m)
L	Length Scale or Monin Obukhov length scale	(m)
n	Frequency, Power Law exponent or King's Law exponent	(varies)
Nu	Nusselt number	(-)
p	Pressure	(mb)
Pr	Prandtl number $\left[\frac{\nu_o \rho_o C_{p_o}}{k_o}\right]$	(-)
Q	Emission rate	(g/s)
R	Velocity ratio (u_s/u_r)	(-)
R_c	Hot resistance at calibration conditions	(Ω)
Re	Reynolds number $(\frac{L_o u_o}{\nu_o})$	(-)
R_H	Film hot resistance	(Ω)
Ri	Richardson number $\frac{g}{T}\left[\frac{\frac{\partial\theta}{\partial z}}{\frac{\partial u^2}{\partial z}}\right]$	(-)
Ro	Rossby number $(\frac{L_o \Omega_o}{u_o})$	(-)
R_o	Film resistance at reference conditions	(-)
$R(\tau)$	Autocorrelation	(-)
t,τ,ξ	Time or time scale	(s)
T,θ	Temperature or potential temperature	(K)
t_1	Center of gravity of autocorrelation curve	(s)
t_o	Integral time scale	(s)
u	Ambient velocity	(m/s)

Symbol	Definition	Units
u_r	Ambient velocity at reference height z_h	(m/s)
u_s	Stack exit velocity	(m/s)
u_*	Friction velocity	(m/s)
V	Volume flow	$(m^3 s^{-1})$
x,y,z	Cartesian coordinates	(-)
$\bar{z}$	Center of mass	(m)
z_h	Reference height	(m)

Greek Symbols

Symbol	Definition	Units
α	Thermal coefficients of resistance	(Ω/K)
χ	Concentration	(ppm)
χ_o	Source strength	(ppm)
γ	Density Ratio $\left(\frac{\rho_a-\rho_s}{\rho_a}\right)$	(-)
Λ	Length scale	
ν	Kinematic viscosity	(m^2s^{-1})
Ω	Angular velocity	(s^{-1})
ϕ^*	Dissipation term	(-)
ρ	Density	(gm^{-3})
σ_z,σ_y	Vertical and horizontal standard deviation of concentration distribution	(m)

Subscripts

Symbol	Definition
a	Pertaining to ambient conditions
h	Pertaining to reference height z_h
i,j,k	Tensor or summation indices
m	Model
o	General reference quantity or initial condition
p	Prototype
r	Reference quantity
s	Pertaining to stack exit conditions
wo	Without terrain pressent
w	With terrain present
∞	Free stream

Superscripts

'	Root-mean-square of quantity
*	Dimensionless parameter

1 INTRODUCTION

ASARCO Incorporated operates a large smelter in Hayden, Arizona. A 305 m (1000 ft) stack was installed at the site as a means of reducing ground level concentrations. Construction of this stack began in 1973. Since the construction of the stack, a regulation was promulgated which limits credit for a stack height to be the "good engineering practice" stack height. The GEP height is defined and explained in Section 123 of the 1977 Clean Air Act Amendment for stack height (Public Law 95-95) and proposed revisions to the regulations posted in the Federal Register, Volume 44, Number 9 (Friday, January 12, 1979, pages 2608-2614). The definition is

> "the height necessary to insure that emissions from the stack do not result in excessive concentrations of any air pollutant in the immediate vicinity of the source as a result of atmospheric downwash, eddies and wakes which may be created by the source itself, nearby structures or nearby terrain obstacles and shall not exceed as appropriate: 1) 30 meters, for stacks uninfluenced by structures or terrain; 2) H_g = H + 1.5 L where H_g = good engineering practice stack height, H = height of structure or nearby structure, L = lesser dimension (height or width) of the structure or nearby structure,..., 3) such height as an owner or operator of a source demonstrates through the use of a field study or fluid model is necessary to ensure that emissions from the stack do not result in an excessive concentration of any air pollutant in the vicinity of the source."

Items 1) and 2) of the above definition do not apply since the limiting factor is a hill that is within 800 m of the stack. This hill is northeast of the smelter and at a height of 858.2 m MSL (2815 ft) - 193 m above the base of the 305 m stack. Hence a fluid modeling investigation was initiated by ASARCO to quantify the effect of the upwind topography upon plume transport and dispersion as well as define the GEP stack height.

For assessing the GEP stack height by a fluid modeling investigation the regulation defines excessive concentration as follows "a maximum concentration greater than an ambient air quality standard, due in part or whole to downwash, wakes, or eddy effects and which concentrations is at least 40 percent in excess of the maximum concentration experienced in the absence of downwash, wakes or eddy effects produced by the nearby structures or terrain."

This report presents the experimental methods and wind tunnel similarity criteria used to quantify the effect of the upwind topography and ultimately determine whether the existing 305 m stack is above or below the GEP height. The results of the study are divided into two sections: 1) velocity, and 2) plume transport and dispersion. The velocity results are presented to document the flow field within the wind tunnel and to establish that the flow field is representative of a similar full scale case. The plume transport and dispersion results include a series of photographs with and without the upwind terrain as well as maximum ground level concentrations with and without the upwind terrain. This latter information was used to assess whether the 305 m stack is above or below the GEP height.

A complete set of photographs and a motion picture supplements this report.

2 SUMMARY AND CONCLUSIONS

The effect of the topographic generated (specifically, the 193 m hill) wakes, eddies and downwash upon the plumes emitted from stacks of varying height was studied in a wind tunnel. Scale models (1 to 1920) of the stacks and terrain were constructed and positioned in the CSU Environmental Wind Tunnel. A metered quantity of gas was released from the stacks and the resulting concentration distributions were measured. One test run consisted of a fixed stack height (91, 200, 250, 305 or 349 m), a set wind speed (9.3, 15.6 or 22.1 m/s) and a terrain configuration (with or without the upwind terrain). A total of 30 full scale simulations was set in the tunnel from the above variables.

Concentration tests were used to assess whether the 305 m stack was above or below the GEP stack height as well as to establish the dispersion patterns in the wind tunnel. A complete set of photographs and motion pictures was obtained to qualitatively assess the effect of the upwind terrain upon the plume transport and dispersion. Velocity measurements were taken to document the flow field in the wind tunnel and for comparison with the profiles expected for the atmosphere.

The results of the measurement program can be summarized as follows:

- The horizontal and vertical dispersion parameters observed in the wind tunnel compared favorably with those expected for a similar stability and surface roughness in the atmosphere.
- The maximum ground level SO_2 concentrations with the terrain present were predicted to be 4.25, 1.68, 1.19, 1.01 and 0.69 ppm for respective stack heights of 91, 200, 250, 305 and 349 m.

- The percentage increase in maximum concentration with the terrain present as compared to the maximum without the terrain was observed to be greater than 40 percent for all stack heights studied.
- The velocity profiles in the wind tunnel compare favorably with those expected for the ASARCO smelter vicinity.

In conclusion the results above clearly demonstrate that the wakes, eddies and downwash generated by the upwind topography adversely affect the dispersion of the plume from the existing 305 m stack. The effect is of such a magnitude that 1) the applicable National Ambient Air Quality Standard (NAAQS) is exceeded, and 2) the percent increase in ground level concentrations due to the terrain is greater than 40 percent. Items 1 and 2 above are necessary criteria that must be met according to the stack height regulations before ASARCO can receive credit for that portion of their new stack that is "good engineering practice". The results of the study also show that the GEP stack height is above 349 m the tallest stack height studied.

3 WIND-TUNNEL SIMILARITY REQUIREMENTS

The basic equations governing atmospheric and plume motion (conservation of mass, momentum and energy) may be expressed in the following dimensionless form (Cermak, 1971; Snyder, 1972):

$$\frac{\partial \rho^*}{\partial t} + \frac{\partial(\rho^* u_i^*)}{\partial x_i^*} = 0, \qquad 3.1$$

$$\frac{\partial u_i^*}{\partial t^*} + u_j^* \frac{\partial u_i^*}{\partial x_j^*} - \left[\frac{L_o \Omega_o}{u_o}\right] 2\epsilon_{ijk}\Omega_j^* u_k^* =$$

$$- \frac{\partial p^*}{\partial x_i^*} - \left[\frac{\Delta T_o L_o g_o}{T_o u_o^2}\right] \Delta T^* g^* \delta_{i3}$$

$$+ \left[\frac{\nu_o}{u_o L_o}\right] \frac{\partial^2 u_i^*}{\partial x_k^* \partial x_k^*} + \frac{\partial}{\partial x_j^*} (-\overline{u'^*_i u'^*_j}) \qquad 3.2$$

and

$$\frac{\partial T^*}{\partial t^*} + u_i^* \frac{\partial T^*}{\partial x_i^*} = \left[\frac{k_o}{\rho_o C_{p_o} \nu_o}\right]\left[\frac{\nu_o}{L_o u_o}\right] \frac{\partial^2 T^*}{\partial x_k^* \partial x_k^*}$$

$$+ \frac{\partial}{\partial x_i^*} \overline{\theta'^* u_i'^*} + \left[\frac{\nu_o}{u_o L_o}\right]\left[\frac{u_o{}^2}{C_{p_o}(\Delta T)_o}\right] \phi^*. \qquad 3.3$$

The dependent and independent variables have been made dimensionless (indicated by an asterisk) by choosing appropriate reference values.

For exact similarity, the bracketed quantities and boundary conditions must be the same in the wind tunnel and in the plume as they are in the corresponding full-scale case. The complete set of requirements for similarity is:

1) Undistorted geometry

2) Equal Rossby number: $Ro = u_o/(L_o\Omega_o)$

3) Equal gross Richardson number: $Ri = \Delta T_o g L_o / T_o u_o^2$

4) Equal Reynolds number: $Re = u_o L_o / \nu_o$

5) Equal Prandtl number: $Pr = (\nu_o \rho_o C_{p_o})/k_o$

6) Equal Eckert number: $Ec = u_o^2/[C_{p_o} (\Delta T)_o]$

7) Similar surface-boundary conditions

8) Similar approach-flow characteristics

All of the above requirements cannot be simultaneously satisfied in the model and prototype. However, some of the quantities are not important for the simulation of many flow conditions. The parameters which can be neglected for this study and those which are important will now be discussed in detail.

- Neglected Parameters

For this study equal Reynolds number for model and prototype is not possible since the length scaling is 1:1920 and unreasonably high wind tunnel and stack exist speeds would be required. As will be discussed, this inequality is not a serious limitation.

The Reynolds number related to the stack exit is defined by

$$Re_s = \frac{u_s D}{\nu_s} .$$

Hoult and Weil (1972) reported that plumes appear to be fully turbulent for exit Reynolds numbers greater than 300. Their experimental data show that the plume trajectories are similar for Reynolds numbers above this critical value. In fact, the trajectories appear similar down to $Re_s = 28$ if only the buoyancy dominated position of the plume trajectory is considered. Hoult and Weil's study was in a laminar cross flow (water tank) with low ambient turbulence levels and hence the rise and dispersion of the plume would be predominantly dominated by the plume's own self-generated turbulence. These arguments for Reynolds number independence only apply to plumes in low ambient turbulence or to the initial stage of plume rise where the plume's self-generated turbulence dominates.

For similarity in the region dominated by ambient turbulence consider Taylor's (1921) relation for diffusion in a stationary homogeneous turbulence

$$\sigma_z^2(t) = \overline{2w'^2} \int_0^{\xi} \int_0^{t} R(\xi)d\xi dt \qquad 3.4$$

which can be simplified to (see Csanady, 1973)

$$\sigma_z^2(t) \cong \overline{w'^2t^2} \cong i_z^2x^2 \qquad 3.5$$

for short travel times; or,

$$\sigma_z^2(t) = \overline{2w'^2}t_o(t-t_1) \ ; \qquad 3.6$$

for long travel times where

$$t_o = \int_0^{\infty} R(\tau)d\tau \qquad 3.7$$

is an integral time scale and

$$t_1 = \frac{1}{t_o} \int^{\infty} \tau R(\tau)d\tau \qquad 3.8$$

is the center of gravity of the autocorrelations curve. Hence for geometric similarity at short travel times,

$$\frac{[\sigma_z^2]_m}{[\sigma_z^2]_p} = \frac{[L^2]_m}{[L^2]_p} = \frac{[i_z^2 x^2]}{[i_z^2 x^2]_p}$$

or,

$$[i_z]_m = [i_z]_p . \qquad 3.9$$

For similarity at long travel times

$$\frac{L_m^2}{L_p^2} = \frac{[\sigma_z^2]_m}{[\sigma_z^2]_p} = \frac{[\overline{w'^2 t_o}(t-t_1)]_m}{[\overline{w'^2 t_o}(t-t_1)]_p}$$

$$= \frac{[i_z^2]_m}{[i_z^2]_p} \frac{[t_o(t-t_1)/u^2]_m}{[t_o(t-t_1)/u^2]_p} = \frac{[Li_z^2\ \Lambda]_m}{[Li_z^2\ \Lambda]_p}$$

if it is assumed $t_1 << t$, $t_o/u = \Lambda$ and $t/u = L$. Thus the turbulence length scales must scale as the ratio of the model to prototype length scaling if $(i_z)_m = (i_z)_p$ or,

$$\frac{L_m}{L_p} = \frac{\Lambda_m}{\Lambda_p} . \qquad 3.10$$

An alternate way of evaluating the similarity requirement is by putting 3.4 in spectral form or (Snyder, 1972),

$$\sigma_z^2 = \overline{w'^2} t^2 \int_0^\infty F_L(n) \left[\frac{\sin \pi nt}{\pi nt}\right]^2 dn = \overline{w'^2} t^2 I \qquad 3.11$$

where

$$I = \int_0^\infty F_L(n) \left[\frac{\sin \pi nt}{\pi nt}\right]^2 dn$$

F_L = Lagrangian spectral function

The quantity in brackets is a filter function the form of which can be seen in Pasquill (1974). In brief for $n > \frac{1}{t}$ the filter function is very small and for $n < \frac{1}{10t}$ virtually unity.

For geometric similarity of the plume the following must be true:

$$\frac{L_m^2}{L_p^2} = \frac{[\sigma_z^2]_m}{[\sigma_z^2]_p} = \frac{[\overline{w'^2}t^2 I]_m}{[\overline{w'^2}t^2 I]_p} = \frac{[L^2 i_z^2]_m}{[L^2 i_z^2]_p}$$

or

$$\frac{[i_z^2 I]_m}{[i_z^2 I]_p} = 1 \qquad 3.12$$

If $[i_z]_m = [i_z]_p$ the requirement is $I_m = I_p$. For short travel times the filter function is essentially equal to one; hence, $I_m = I_p = 1$ and the same similarity requirement as previously deduced for short travel times is obtained (equation 3.9).

For long travel times the larger scales (smaller frequencies) of turbulence progressively dominate the dispersion process. If the spectra in the model and prototype are of a similar shape then similarity would be achieved. However for a given turbulent flow a decrease in the ambient Reynolds number (hence wind velocity) decreases the range (or energy) of the high frequency end of the spectrum. Fortunately, due to the nature of the filter function, the high frequency (small wavelength) components do not contribute significantly to the dispersion. There would be, however, some critical Reynolds number below which too much of the high frequency turbulence is lost. If a study is run with a Reynolds number in this range similarity may be impaired.

To evaluate whether geometric similarity of the plumes was achieved for this study the σ_y and σ_z values obtained in the wind tunnel were compared with those quoted as being representative of atmospheric dispersion rates (Pasquill, 1976). If the model σ_y and σ_z values compare well for the corresponding atmospheric flow the inference is that Reynolds number independence was achieved.

The ambient flow field affects the plume trajectories and consequently similarity of this field between model and prototype is required. The mean flow field will become independent of Reynolds number if the flow is fully turbulent. The critical Reynolds number for this criteria to be met is based on the work of Nikuradse as summarized by Schlichting (1968) and Sutton (1953) and is given by

$$(Re)_{k_s} = \frac{k_s u^*}{\nu} > 75.$$

or assuming $k_s = 30\ z_o$

$$Re_{z_o} = \frac{z_o u^*}{\nu} > 2.5.$$

In this relation k_s is a uniform sand grain height and z_o is the surface roughness factor. Re_{z_o} values were computed and will be discussed in Section 6.

The <u>Rossby number</u> Ro is a quantity which indicates the effect of the earth's rotation on the flow field. In the wind tunnel equal Rossby numbers between model and prototype cannot be achieved. The effect of the earth's rotation becomes significant if the distance scale is large. Snyder (1972) puts a conservative cutoff point at 5 km for diffusion studies. He states that for length scales above this value the Rossby number should be considered. For this particular study, the maximum range over which the plume is transported is 13 km in the horizontal and approximately 1 km in the vertical. Hence, the earth's rotation may affect plume transport for similar full scale conditions but was neglected for this study.

When equal Richardson numbers are achieved, equality of the Eckert number between model and prototype cannot be attained. This is not a serious compromise since the Eckert number is equivalent to a Mach number squared. Consequently, the Eckert number is small compared to unity for laboratory and atmospheric flows.

- Relevant Parameters

Since air is the transport medium in the wind tunnel and the atmosphere, near equality of the Prandtl number is assured.

Equality of plume transport will be assured if the following conditions are met (Snyder, 1979):

1) Fix effluent Reynolds number as large as possible - preferably above 300.
2) Match the following parameters in model and prototype

$$R = \frac{u_s}{u_r}$$

$$Fr = \frac{u_s}{\sqrt{g\gamma D}}$$

$$\gamma = \frac{\rho_a - \rho_s}{\rho_a}$$

$$\lambda = D/h$$

Implementing the above scaling criteria would give the following relation between model and prototype velocities:

$$(u_r)_m = (u_r)_p \left(\frac{D_m}{D_p}\right)^{1/2}$$

and for $D_m/D_p = 1:1920$

$$(u_r)_m = 0.0228\ (u_r)_p.$$

The range of ambient free-stream velocities to be simulated range from 9 to 24 m/s* or 0.21 to 0.57 m/s in the wind tunnel. Since the tunnel is hard to control at these low speeds and Reynolds number effects may become important, a distorted scaling technique was employed. The technique involved neglecting the plume buoyancy thus requiring equality of only the velocity ratio (R). An alternate technique of relaxing the density ratio (γ) equality was also considered but the wind tunnel speeds were still found to be less than 1 m/s.

The justification for neglecting plume buoyancy ($Fr = \infty$) is:

1) the wind tunnel speeds can be set at any reasonable value - maintained at approximately 3 m/s for all tests,
2) the stack Reynolds numbers can be maintained at values exceeding 300 for the majority of the tests,
3) atmospheric turbulence will quickly dominate the rise of the plume since the velocity ratios are all below 2 and the ambient turbulence intensity levels are high (> 10%),
4) the assumption is conservative in that the plume rise without the upwind terrain will be less resulting in higher ground level concentrations,
5) Huber (1978) recommended this procedure.

*See Taylor (1979) for discussion and justification of test wind speeds.

In summary the following scaling criteria were applied for this study

1) $R_m = R_p$; $R = u_s/u_r$.

2) $Re_s > 300$; $Re_s = \dfrac{u_s D}{\nu_s}$

3) $Re_{z_o} > 2.5$; $Re_{z_o} = \dfrac{u^* z_o}{\nu_a}$

4) Similar geometric dimensions.

5) Equality of dimensionless boundary conditions.

4 EXPERIMENTAL PROGRAM

4.1 Summary

The objective of this study is to evaluate the adverse aerodynamic effect of the nearby terrain obstacles upon the transport and diffusion of the plume emitted from the ASARCO stacks. To meet this objective a 1:1920 scale model of ASARCO stacks and topography was constructed and placed in the CSU Environmental Wind Tunnel. A neutral boundary layer was developed naturally over the topographic surface and tracer gas releases were made through the model stacks simulating wind speeds of approximately 9, 15 and 22 m/s.

The model operating conditions are given in Table 4.1 and for reference the full-scale plant conditions are enumerated in Table 4.2. A total of 33 tests conditions was simulated in the wind tunnel. The run number, terrain configuration, stack height, velocity ratio and wind speed for each test are given in table 4.3.

All tests were conducted in a similar manner. A neutral boundary layer characteristic of the smelter vicinity was established and measurements of velocity were made at 13 locations with and 13 without the upwind terrain present. The profiles were analyzed to 1) assess the effect of the terrain upon the flow field, 2) to verify that the boundary layer was representative of the site, and 3) document the wind tunnel flow characteristics.

After completing the velocity measurements a metered quantity of buoyant gas was allowed to flow from the model stacks and the wind tunnel was adjusted to simulate the desired ambient wind speed. Aerial distributions of the resulting plume were made at four locations for select cases with and without the terrain to document the dispersion patterns in the wind tunnel. For all tests at least 48 ground-level samples were obtained to establish the maximum ground level concentration.

To qualitatively document the flow pattern the plumes were made visible by passing the gas mixture through titanium tetrachloride prior to emission from the stacks. Stills (color and black and white) and motion pictures of the tests in Table 4.3 were obtained.

A more detailed description of every facet of the study will now be given.

4.2 Scale Models and Wind Tunnel

A topographic model with equal vertical and horizontal scales of 1:1920 was designed and constructed for study in the CSU Environmental Wind Tunnel (EWT) shown in Figure 4.2-1. The model was constructed by cutting styrofoam sheets of 0.64 cm thickness to match contour lines on a topographic map enlarged to the 1:1920 scale. The wind direction modeled in the tunnel was approximately 51^{o} true azimuth--the direction of the 858.2 m (2815 ft, MSL) hill directly upwind of ASARCO's tall stack. A map of the modeled terrain is shown in Figure 4.2-2 and represents a 7.0 by 25.8 km area (3.66 by 13.44 m in the tunnel). The ASARCO stack was positioned 6.3 m (12 km in prototype) from the beginning of the terrain model. A picture of the complete terrain model looking up- and downwind is shown in Figure 4.2-3.

Two terrain configurations were employed: the first with the upwind terrain present (Figure 4.2-3) and the second without the terrain upwind of the stack. A 1.22 m ramp was used as a transition from the tunnel to the model for both cases. For the flat upwind terrain case the ramp rose 11.4 cm and for the terrain case the ramp rose 15.2 cm. A 3.8 cm trip and twenty evenly spaced 30.5 cm high epliptic spires were used to stimulate the boundary layer for the no-upwind terrain case. The spire-trip arrangement is shown in Figure 4.2-4.

The 1:1920 scale was chosen so that sufficient topography upwind and downwind of the smelter could be included. The approach terrain was modeled beyond Lee Mountain to a location where a low point in the undulating terrain was found. The required downwind fetch was chosen to be approximately 12 km since the maximum concentration for a 305 m stack could occur at that distance.

A scale model of the stacks for the R&R flue and converter flue as well as for tall stacks of 200, 250, 305 and 349 m prototype height were constructed of Plexiglas. A diagram for each stack is shown in Figure 4.2-5 and a photo of the model stacks is shown in Figure 4.2-6. A sharp edged orifice was used in all stacks (as indicated in Figure 4.2-5) to insure that the flow upon exit was fully turbulent.

4.3 Flow Visualization

The purpose of this phase of the study is to visually assess the transport of the plumes released from the ASARCO stacks. The data collected consist of a series of photographs of the smoke emitted from the stacks for the different tests enumerated in Table 4.3.

The smoke was produced by passing compressed air through a container of titanium tetrachloride located outside the wind tunnel and transported through the tunnel wall by means of a tygon tube terminating at the stack inlets. The plume was illuminated with high intensity lamps and a visible record was obtained by means of black and white photographs taken with a supergraphic camera (lens focal length 127 mm) and color slides taken with a Canon F1 camera (focal length 28 mm). The shutter speed for the black and white photographs was 1/25 of a second and for the color slides 1/30 of a second. The black and white photographs are actually a composite of five superimposed pictures taken consecutively. This procedure was performed to obtain an average plume trajectory and not lose the detail of the turbulent motion as happens at longer shutter speeds. The black and white and color photographs were taken at an angle perpendicular to the tunnel such that the field of view extended from the stack to approximately 9 km (4.9 m in the model) downwind.

A series of 16 mm motion pictures was taken of all tests. A Bolex movie camera was used with a speed of 24 frames per second. The movies consisted of taking an initial close-up of the smoke release after which the camera was panned from the model stack(s) to approximately 9 km downwind in the prototype.

4.4 Gas Tracer Technique

The purpose of this phase of the experimental study is to provide quantitative information on the transport and dispersion of the plume emitted from the ASARCO stacks with and without the upwind terrain present. Specifically this phase must demonstrate the magnitude of the SO_2 concentration produced with the terrain present and also the ratio of maximum concentration with and without the terrain. To meet this goal a comprehensive set of concentration measurements was taken. The data obtained included ground level samples, a horizontal array of samples elevated above the ground and an array of samples along the center of the tunnel in the vertical direction.

An array of 69 sampling tubes was run into the tunnel under the model terrain and fastened to brass tubes having outlets at the model surface. The location of these points is shown in Figure 4.4-1. To sample all 69 points it was necessary to take two independent runs using the same tunnel and stack settings, since the sampling device had only 50 sample retention chambers. A sampling rake shown in Figure 4.4-2 with 50 tubes in the vertical and 50 in a vertically traversing horizontal array was also used for the four runs indicated in Table 4.3. A vertical distribution of the plume was obtained using 15 of the sampling tubes at four downwind locations. Thereafter a horizontal distribution was obtained at the height of maximum concentration using 15 of the sampling tubes. The coordinates of the horizontal and vertical samples for each run are given on the graphs which will be discussed in Section 6.2.

The test procedure consisted of: 1) setting the proper tunnel wind speed, 2) releasing a metered mixture of source gas (ethane-nitrogen-helium and methane-nitrogen-carbondioxide*) of the required density (that of air) from the release stacks, 3) withdraw samples of air from the tunnel at the locations designated, and 4) analyze the samples with a flame ionization gas chromatograph (FIGC). Photographs of the sampling system and gas chromatograph are shown in Figure 4.4-3. The samples were drawn into each syringe over a 45s (approximate) time and consecutively injected into the FIGC.

The procedure for analyzing air samples from the tunnel was as follows: 1) a 2 cc sample volume drawn from the wind tunnel is introduced into the flame ionization detector (FID), 2) the output from the electrometer (in microvolts) is sent to the Hewlett Packard 3380 Integrator, 3) a digital record is integrated and an ethane concentration determined by multiplying the integrated signal (μvs) times a calibration factor (ppm/μvs), and 4) a summary of the integrator

*Methane mixture was used only for the converter stack. Data from these tests were not analyzed or reported herein since they were not essential for determining GEP stack height.

analysis (ethane concentration, peak height, integrated voltage, etc.) is printed out on the integrator at the wind tunnel. Prior to any data collection a known concentration of propane is introduced into the FID to determine the calibration factor.

The FID operates on the principle that the electrical conductivity of a gas is directly proportional to the concentration of charged particles within the gas. The ions in this case are formed by the effluent gas being mixed in the FID with hydrogen and then burned in air. The ions and electrons formed enter an electrode gap and decrease the gap resistance. The resulting voltage drop is amplified by an electrometer and fed to the HP3380A integrator. When no effluent gas is flowing, a carrier gas (nitrogen) flows through the FID. Due to certain impurities in the carrier some ions and electrons are formed creating a background voltage or zero shift. When the effluent gas enters the FID the voltage increases above this zero shift in proportion to the degree of ionization or correspondingly the amount of tracer gas present. Since the chromatograph[2] used in this study features a temperature control on the flame and electrometer, there is very low zero drift. In case of any zero drift the HP3380A which integrates the effluent peak also subtracts out the zero drift.

The lower limit of measurement (approximately 0.5 ppm or an equivalent SO_2 concentration of approximately 0.04 ppm) is imposed by the instrument sensitivity and the background concentration of ethane within the air in the wind tunnel. Background concentrations were measured and subtracted from all data quoted herein.

The wind-tunnel concentration data for all tests in this report are presented in the following dimensionless form

---

[2]A Hewlett-Packard 5700 gas chromotograph was used in this study.

$$K = \frac{\chi}{\chi_o R}$$

where χ is the observed concentration, χ_o is the source strength of the tracer gas and $R = u_s/u_r$. The tracer gas source strength was measured during the period of measurement and the appropriate observed value was used in tabulating the data.

To determine a corresponding full-scale concentration from the model K values the K-model (K_m) is set equal to K-prototype (K_p). Equality of these two parameters can be verified by considering the equation for conservation of mass, or,

$$\left[\int_{-\infty}^{\infty}\int \frac{\chi u}{Q}\, dydz\right]_m = \left[\int_{-\infty}^{\infty}\int \frac{\chi u}{Q}\, dydz\right]_p = 1.$$

Since $(dy)_m = \frac{(H_b)_m}{(H_b)_p}(dy)_p$ and $(dz)_m = \frac{(H_b)_m}{(H_b)_p}(dz)_p$, the equation can be rearranged to give

$$\int_{-\infty}^{\infty}\int \left[\left(\frac{\chi u}{Q}\right)_p - \left(\frac{\chi u}{Q}\right)_m \frac{(H_b^2)_m}{(H_b^2)_p}\right] (dydz)_p = 1$$

For this equality to be true requires

$$\left(\frac{\chi u}{Q}\right)_p = \left(\frac{\chi u}{Q}\right)_m \frac{(H_b^2)_m}{(H_b)_p}$$

or

$$\left(\frac{\chi u}{Q}\ H_b^2\right)_m = \left(\frac{\chi u H_b^2}{Q}\right)_p$$

Solving for χ_p and letting $u = u_r$, $Q = \chi_o \frac{\pi D^2}{4} u_s$, and recognizing that $\left(\frac{H_b}{D}\right)_m = \left(\frac{H_b}{D}\right)_p$ yields the following equation which is used in this report to calculate prototype concentrations

$$\chi_p = K_m (\chi_o)_p \qquad 4.2$$

The concentration data were computer processed to obtain the center of mass $(\bar{z})$ and the standard deviation (σ_z or σ_y). The parameters were determined by numerically integrating the following equations over the height (and width, where appropriate) of the concentration profiles:

$$Q' = \int_0^\infty K dz \qquad 4.3$$

$$\bar{z} = (1/Q') \int_0^\infty zK dz \qquad 4.4$$

$$\sigma_z^2 = (1/Q') \int_0^\infty (z-\bar{z})^2 \, K dz \qquad 4.5$$

The numerical integration was obtained using the trapezoidal rule.

To determine the averaging time for the predicted concentrations from wind-tunnel experiments the dispersion parameters--σ_y and σ_z--for the undisturbed flow in the wind tunnel were compared to those used for numerical modeling studies in the atmosphere. The dispersion rates used in the atmosphere are referred to as the Pasquill-Gifford curves and are given in Turner (1969) and modified values are given in Pasquill (1974, 1976). The results of this comparison as discussed in Section 6 showed that the σ_y and σ_z values in the wind tunnel compare (when multiplied by the length scaling factor 1920) with those expected for the atmosphere. Hence the method used for converting numerical model predictions to different averaging times should also be used for converting the wind-tunnel tests. The EPA guideline series for evaluating new stationary sources (Budney, 1977) conservatively assumes that the Pasquill-Gifford σ_y and σ_z values represent 1-hour average values. To convert to a 3-hour concentration the document recommends multiplying the 1-hour value by 0.9 ± 0.1 and if aerodynamic disturbances are a problem the factor should be as high as 1. Huber (1979) recommended using the wind-tunnel predictions of SO_2 concentration as a 3-hour value. To be consistent with EPA recommendations the results presented herein will be assumed to represent 3-hour average SO_2 concentrations.

4.5 Velocity and Temperature Measurements

Mean and turbulent velocity measurements were performed to 1) monitor and set flow conditions, and 2) document the flow conditions in the wind tunnel. Instrumentation used for this study included 1) one Thermo-Systems, Inc. (TSI) 1050 series anemometer, 2) a TSI Model 1210 hot-film sensor, 3) a type 120 Equibar pressure meter and pitot tube, and 4) TSI model 1125 calibrator for velocity calibration. Since all tests were conducted under neutral stratification no detailed temperature measurements were required. The techniques used to obtain the velocity data with this assortment of equipment and the data processing techniques will now be discussed in more detail.

- Hot-Film Anemometry--Principle of Operation and Calibration Technique

The transducer used for measuring velocities for this study was a Model 1210 hot-film sensor. The sensor consists of a platinum film on a single quartz fiber. The diameter of the sensor is 0.0025 cm. The sensor has the capability of resolving one component of velocity in turbulent flow fields.

The basic theory of operation is based on the physical principle that the heat transfer from the wire equals the heat supplied to the wire by the anemometer or in equation form (see Hinze, 1975),

$$I^2 R_H = \pi \ell k_g (T_w - T_g)\ \mathrm{Nu} \qquad 4.6$$

where

I = current through wire

k_g = heat conductivity of gas

ℓ = length of wire

T_w = temperature of wire

T_g = temperature of gas

Nu = Nusselt number

$= F\left(\mathrm{Re}, \mathrm{Pr}, \mathrm{Gr}, \frac{T_w - T_g}{T_g}, \frac{\ell}{d}\right)$

$\mathrm{Re} = \frac{ud}{\nu_g}$

$\mathrm{Pr} = \frac{C_p \mu_g}{k_g}$

$\mathrm{Gr} = \frac{g d^3 (T_w - T_g)}{\nu_g^{\ 2}\ T_g}$

d = diameter of wire

R_H = operating resistance of wire

For most wind-tunnel applications an empirical equation evolved by Kramers as reported in Hinze (1975) is adequate for representing Nu for a Reynolds number range $0.01 < \mathrm{Re} < 1000$, or

$$\mathrm{Nu} = 0.42\ \mathrm{Pr}^{0.2} + 0.56\ \mathrm{Pr}^{0.33}\ \mathrm{Re}^{0.5}.$$

Free convection from the wire can be neglected for $\mathrm{Re} > 0.5$ when

$$GrPr < 10^{-4}.$$

Alternately buoyancy may be neglected when

$$Gr < Re^3 .$$

The temperature dependence of the resistance of the wire is assumed to follow the ensuing relation

$$R_H = R_o[1 + b_1(T_w - T_o) + b_2(T_w - T_o)^2 + \ldots]$$

where b_i are temperature coefficients. Normally the higher order terms are neglected and

$$R_w = R_o[1 + b_1(T_w - T_o)].$$

Substituting the appropriate relations yields the following equation

$$\frac{I^2 R_w}{R_w - R_c} = A + B(\rho_c u)^n \qquad 4.7$$

where

R_c = resistance of wire at calibration temperature

ρ_c = density of air at calibration temperature

$$A = \frac{\pi \ell k_f}{b_1 R_o} 0.42(Pr)^{0.2}$$

$$B = \frac{\pi \ell k_f}{b_1 R_o} 0.57(Pr)^{0.33}(\frac{d}{\mu})$$

For this study A, B and u were obtained by calibrating the wire over a range of known velocities and determining A, B and n by a least-squares analysis. Since the calibration temperature of the wire is nearly equal to the temperature in the wind tunnel no corrections for temperature were applied and the following equation was used to calculate the instantaneous velocity:

$$u = \left[\frac{\frac{I^2 R_w}{R_w - R_c} - A}{B} \right]^{1/n}$$

Calibration of the hot film was performed with the model 1125 TSI calibrator and a type 120 Equibar pressure meter where the following relation applies:

$$u = \sqrt{\frac{2 \Delta p R T_a}{p_a}}$$

which gives the following error equation

$$\frac{W_u}{u} = \left[\left(\frac{1}{2} \frac{W_{\Delta p}}{\Delta p} \right)^2 + \left(\frac{1}{2} \frac{W_{p_a}}{p_a} \right)^2 + \left(\frac{1}{2} \frac{W_{T_a}}{T_a} \right)^2 \right]^{1/2}$$

where W_i are associated errors for each component (T_a, Δp, ect.). The predominant factor for this case is the differential pressure measurement. Instrument specifications on the type 120 Equibar pressure meter are an accuracy of 3% of full scale readings which gives the following

Full Scale Reading	$W_{\Delta p}$ (mm Hg)	W_{T_a} (C)	W_{p_a} (mm Hg)
.01	± 0.0003	1	.1
.1	± 0.003	1	.1

The lowest calibration point was $\Delta p = 0.001$ mm Hg. The error at the low velocity is

$$\frac{W_u}{u} = 0.15 \quad \text{for} \quad u = 0.525 \text{ m/s.}$$

The highest calibration point was $\Delta p = .07$ mm Hg. The error at the high velocity is

$$\frac{W_u}{u} = 0.02 \quad \text{for} \quad u = 4.38 \text{ m/s}$$

A typical calibration curve is shown in Figure 4.5-1. A calibration was performed at the beginning of each day's measurement.

After the wire was calibrated, the desired flow condition was set in the wind tunnel. The free-stream velocity was monitored with the type 120 Equibar pressure meter and pitot tube. Once the desired condition at the reference height was obtained the pressure meter setting was recorded and used to set and monitor the tunnel conditions for all remaining tests. During all subsequent velocity measurements, care was taken to ensure that the pressure meter reading remained constant.

- Data Collection

Velocity profiles were measured at 13 locations. The profiles were taken at locations shown in Figure 4.4-1.

The manner of collecting the data was as follows:

1) the hot-film probe was attached to a carriage,
2) the bottom height of the profile was set to 0.0127 meters,
3) a vertical distribution of velocity was obtained using a vertically traversing mechanism which gave a voltage output corresponding to the height of the wire above the ground,
4) the signals from the anemometer and potentiometer device indicating height were fed directly to a Hewlett-Packard Series 1000 Real Time Executive Data Acquisition System,
5) samples were stored digitally in the computer at a rate of 208.3 samples per second, and
6) the computer program converted each voltage into a

velocity (m/s) using the equation

$$u = \left[\frac{\dfrac{E^2}{R_H(R_H - R_c)} - A}{B} \right]^{1/n}$$

At this point the program computes several useful quantities using the following equations:

$$\bar{u} = \frac{1}{N} \sum_{i=1}^{N} u_i$$

$$\overline{u'} = \frac{1}{N-1} \sum_{i=1}^{N} (u_i - \bar{u})^2$$

where N is the number of velocities considered (a 30 second average was taken, hence 6016 samples were obtained). The mean velocity and turbulence intensity at each measurement height were stored on a file in addition to being returned to the operator at the wind tunnel on a remote terminal.

5 VELOCITY MEASUREMENTS

Velocity measurements were obtained to: 1) establish the correct operating speeds in the tunnel, 2) assess the representativeness of the wind tunnel velocity profile in comparison to those observed in the atmosphere, and 3) document the flow conditions in the wind tunnel. To meet this objective a total of 34 vertical profiles of horizontal wind speed and turbulence intensity was obtained. Nine profiles were taken at the location of the tall stack. Four free-stream velocities were set for the profiles taken with the upwind terrain present and five were set without the upwind terrain. This series of profiles was used to check the variation of the velocity and turbulence field with free-stream velocity. Figure 5.1-1 shows the profiles without the terrain present and Figure 5.1-2 the profiles with the upwind terrain present. As is evident, the profiles remain nearly constant down to a free-stream velocity as low as 1 m/s. Since all tests were conducted at free-stream velocities greater than 3 m/s, Reynolds number independence of the flow field is inferred by these results. The remaining 24 profiles consisted of 12 profiles taken at similar locations with and without the terrain present. The locations are shown in Figure 4.4-1. For each terrain configuration six profiles were taken down the center of the tunnel test section and six lateral to the test section.

To assess the flow characteristics in the wind tunnel and to aid in comparing to atmospheric flows the velocity profiles with a reference velocity approximately equal to 3 m/s were analyzed to obtain the surface roughness factor (z_o), the displacement height (d), the friction velocity (u_*), the turbulent Reynolds number (Re_{z_o}), and the power law exponent (n). The estimated values for each profile with and without the terrain are given in Table 5.1 and 5.2 respectively. The values of z_o and u_* were determined by finding the z_o and u_* which gave the best fit (by least squares) to the following equation which is characteristic of atmospheric (Businger, 1972) and wind tunnel flows (Cermak, 1971):

$$\frac{u}{u_*} = \frac{1}{k} \ln \frac{z-d}{z_o} .$$

The expected value for z_o in the vicinity of the ASARCO smelter can be estimated by referring to Table 5.3 from Engineering Science Data Unit, 1972. The site can be characterized somewhere between "desert" and "very hilly or mountainous areas" depending upon location which gives an expected z_o range of 0.04 to 200 cm. For wind tunnel similarity the model z_o should equal the atmospheric value divided by the scale factor of 1920. This results in desired values for a model z_o from 0.0002 to 0.52 mm. As can be seen from Tables 5.1 and 5.2, the range of values for the wind-tunnel profiles was from 0.00 to 7.44 mm without the upwind terrain present and from 0.00 to 29.60 with the upwind terrain present. In general the results cover the range expected and show wide variation depending upon terrain complexity upwind.

The power law exponent was computed by fitting the data by least squares to the following equation:

$$\frac{u}{u_r} = \left(\frac{z}{z_r}\right)^n$$

Counihan (1975) presents the following equation for estimating n as a function of z_o

$$n = 0.096 \log_{10} z_o + 0.016(\log_{10} z_o)^2 + 0.24.$$

where z_o is in meters. Using the expected z_o range of 0.0004 to

2.0 meters for the site gives an expected n range of 0.10 to 0.27. The exponent for the velocity profiles in the tunnel ranged from 0.09 to 0.42 without the upwind terrain present and from 0.07 to 0.60 with the terrain. In general the exponent was greatest when high topographic features were directly upwind and lowest for profiles taken on a hill or rise. Overall the values observed in the tunnel for n and z_o are reasonable for similar atmospheric flows.

The turbulent Reynolds numbers in Tables 5.1 and 5.2 range from 0.00 to 131.9 without the terrain present and from 0.00 to 5013 with the terrain present. The majority of the estimates of Re_{z_o} exceed the critical value of 2.5 as discussed in Section 3 and implies Reynolds number independence was achieved. Reynolds number independence is also inferred due to the close agreement between the atmospheric and laboratory dispersion rates as discussed in Section 6.2.

A representative boundary layer thickness was estimated from the velocity profile taken 0.91 meters upwind of the tall stack location (designated by $x = -0.91$, $y = 0$) when the upwind terrain was removed. The boundary layer thickness is assumed to be the height where the free-stream value is reduced by 10 percent. Assuming a power law wind profile:

$$\frac{u(\delta)}{u_\infty} = 0.9 = \left(\frac{\delta}{z_\infty}\right)^n .$$

Rearranging δ can be calculated as follows:

$$\delta = z_\infty (0.9)^{1/n}$$

where $z_\infty = 0.61$ and $n = 0.14$. The δ-value computed for this profile is 0.29 m in the model or 552 m in the full scale. The atmospheric boundary layer for neutral stratification and flat topography is typically taken to be 600 m (Counihan, 1975). The boundary layer thickness is generally greater than the 600 m over rough topography as is the case for the wind tunnel which can be inferred by referring to profiles that will be discussed below.

Figures 5.1-3 and 5.1-4 show the respective velocity profiles without and with the upwind terrain taken down the center of the tunnel ($y = 0$). The profiles were taken at $x = -0.91$, 0.91, 1.83, 2.74, 3.66 and 4.57 m with $x = 0.0$ being the tall stack location. The profiles at the tall stack location are plotted in Figures 5.1-1 and 5.1-2 and were briefly discussed above. In general the shape of the velocity profiles for x greater than 0.91 m are similar with and without the terrain as is reflected by the near equality of the power law exponents for corresponding profiles in Tables 5.1 and 5.2. At $x = -0.91$ m the profile with the terrain present is flatter than that without the terrain since the former was taken on a hill. At the tall stack location ($x = 0$, $y = 0$) the velocity with the terrain (Figure 5.1-2) is reduced below 16 cm compared to that without the upwind terrain (Figure 5.1-1). The reduction is due to the close proximity of the upwind terrain obstacle.

The respective turbulence intensity profiles taken along the center of the tunnel without and with the upwind terrain are shown in Figures 5.1-5 and 5.1-6. The profiles show a general increase in turbulence intensity when the upwind terrain is present. This increase is most pronounced for those profiles taken at the plant site ($x = 0$, $y = 0$) as shown in Figures 5.1-1 and 5.1-2. Below 16 cm the turbulence intensity is two to three times greater when the upwind terrain is present.

Velocity profiles were taken across the tunnel at the location of the plant site (x = 0) for y = -1.68, -1.22, -0.61, 0.61, 1.22 and 1.68 m. The respective profiles without and with the upwind terrain are shown in Figure 5.1-7 and 5.1-8. The profiles at y = -1.68, -1.22 and -0.61 show the greater decrease in velocity with the upwind terrain present. This is due to the higher terrain feature upwind of these measurement sites as is evident by referring to Figure 4.2-3 (top picture left side). The profiles without the upwind terrain (Figure 5.1-7) show the uniformity of the tunnel flow between -1.22 and 1.22 m.

The corresponding longitudinal turbulence intensity profiles taken without and with the upwind terrain are shown in Figures 5.1-9 and 5.1-10. The extreme increase in turbulence with the upwind terrain is noticible for those profiles taken at -1.68, -1.22 and -0.61 m - - the locations directly downwind of the highest terrain features. There is a slight increase in turbulence for those profiles on the other side of the tunnel (y = 0.61, 1.22 and 1.68 m) but the increase is much less since no significant terrain features were directly upwind.

In summary the velocity profiles show that the boundary layer in the wind tunnel is well established and is characteristic of a full scale rough terrain site. The profiles also show the expected trend of decreased velocity and increased turbulence in the wake of a terrain obstacle.

6 PLUME TRANSPORT AND DIFFUSION RESULTS

6.1 Visualization

The visualization of plume dispersion from the model stacks was performed to qualitatively assess the downwash effects of the upwind terrain. Figures 6.1-1 through 6.1-5 show the visualization with and without the upwind terrain for the high velocity ratio tests associated with each stack configuration. In all cases there is a dramatic difference between the photo with and without the upwind terrain. The terrain acts to mix the effluent quickly to the ground and spread it more in the vertical. This increased vertical spread when the terrain is present is evident in the photographs.

In summary the photographic results demonstrate qualitatively that the terrain has an adverse effect on plume dispersion for a stack as high as 349.4 m. The effect on ground level concentrations will be discussed in the following section.

6.2 Concentration Measurements

The purpose of this phase of the study is to quantify the magnitude of the SO_2 concentrations downwind of the smelter stacks. This was done by releasing a metered quantity of tracer gas (ethane) from a scale model of the stacks in the environmental wind tunnel. The resulting concentrations were measured with and without the upwind terrain present to comply with the EPA Stack Height Credit Regulation requirement (Huber, 1979). Normally for an existing source to be able to raise their stack heights to a GEP stack height, the owner or operator (ASARCO) must first demonstrate that air quality standards or PSP limits are exceeded and second that the maximum concentration with the upwind terrain is at least 40 percent in excess of that without the upwind terrain.

Hence this section of the report will discuss 1) the wind tunnel dispersion characteristics, 2) ground level concentrations, and 3) implication of results on GEP stack height.

- Dispersion Characteristics

To determine whether the wind tunnel dispersion parameters (σ_y and σ_z) agree with those for the atmosphere, the vertical and horizontal concentration profiles were analyzed to determine σ_y, σ_z and $\bar{z}$ as discussed in Section 4.4. The model values were then scaled to prototype values by multiplying by the length scaling factor (1920). The results for each vertical and horizontal profile are tabulated on the profile plots which are given in Figures 6.2-1 and 6.2-2.

The atmospheric values for σ_y and σ_z are often assumed to follow the Pasquill-Gifford curves as given in Turner (1969). However, Pasquill (1976) has recommended a different method for computing these parameters. For σ_y Pasquill recommends the following formula for sampling times up to one hour

$$\sigma_y = i_y \, x \, f(x)$$

where $f(x)$ is defined as follows

x(km)	0.1	0.2	0.4	1.0	2.0	4.0
f(x)	0.8	0.7	0.65	0.6	0.5	0.4

For this study only the intensity of turbulence in the longitudinal direction i_x was measured; i_y was not. It will be assumed here that $i_y \cong i_x$. For σ_z Pasquill (1976) recommends using the Turner Workbook curves when the surface roughness is 3 cm. For other roughness he recommends using nomograms or equations in Pasquill (1974). The equations used here for σ_z are

$$\sigma_z = 0.038\ x^{0.76} \qquad z_o = 10\ \text{cm}$$
$$\sigma_z = 0.050\ x^{0.68} \qquad z_o = 100\ \text{cm}$$

where x is in kilometers and the constants were derived from Pasquill (1974) for the indicated surface roughness values.

Figure 6.2-3 shows the expected σ_y dispersion rates for the atmosphere with $i_y = 0.1$ and 0.2 in comparison to that observed in the wind tunnel. Consider first the no-upwind terrain cases. At 0.5 km the σ_y values show a variation with stack height. The highest σ_y corresponds with the lowest stack height. This is expected since σ_y is proportional to turbulence intensity and the turbulence intensity decreases with height. At 2, 5 and 9 km the σ_y values for each stack height agree with one another and indicate a lateral turbulence intensity of 10% or less. This suggests that the turbulence field effecting the lateral dispersion is nearly constant with height over the depth of the plumes studied. At 9 km the σ_y values are less than those at 5 km. This may possibly be explained by the terrain configuration at this location. The plume is traveling up a converging drainage basin (Smith Wash) which is probably inducing a convergence in the stream lines and hence a narrowing of the plume. The case with the terrain present shows a greater σ_y at all downwind locations beyond 0.5 km. This result reflects the increased turbulence in the wake of the upwind terrain. Overall these results suggest that the variation of σ_y with downwind distance is representative of similar atmospheric dispersion rates.

Figure 6.2-4 shows the expected variation of σ_z for the atmosphere using $z_o = 10$ cm and 100 cm in comparison with that observed in the wind tunnel. The wind tunnel σ_z values compare closely with those expected for a 1 m surface roughness. The σ_z values for each stack height without the upwind terrain agree closely except at 0.5 km. The tallest stack shows the highest σ_z, a result that is anticipated by Pasquill (1976). Since the upwind terrain acts to increase the surface roughness, the σ_z values for this case are higher than those without the upwind terrain.

The vertical concentration profiles in Figure 6.2-1 show the nature of the plume spread as a function of downwind distance, stack height and with and without the upwind terrain. Figures 6.2-1c and 6.2-1d show the respective vertical concentration profiles without and with the upwind terrain for a stack height of 305 m. The greater vertical extent of the plume and rapid mixing toward the ground when the terrain is present is evident in Figure 6.2-1d. The horizontal concentration profiles taken at the height where the maximum concentration in the vertical was observed are shown in Figure 6.2-2. Several features are observed: 1) the general increase in spread with downwind distance, 2) a slight decrease in plume spread with stack height, and 3) an increase in plume spread when the upwind terrain is present (Figure 6.2-2d).

- Ground-level Concentrations

The ground level concentration measurements are summarized in two forms as outlined by Huber (1979). The maximum measured concentration at each horizontal array location was identified for each run and a plot of the maximum ground-level concentration versus downwind distance (nondimensionalized with a hill height equal to 193 m) was made. Figures 6.2-5 through 6.2-9 show the plots of dimensionless concentrations $K(= \frac{\chi}{\chi_o R})$ versus x/H_T. Each figure has the corresponding results (fixed stack height) for the cases run with and without the upwind terrain. A second series of graphs was also prepared. Huber (1979) requires that "two to four lateral ground-level profiles including one at the position of maximum ground-level concentration" be prepared. Correspondingly two lateral profiles for each run indicated in Table 4.3 were prepared and are presented in Figures 6.2-10 through 6.2-14. The implications of these figures will now be discussed.

Figure 6.2-5 show a plot of K versus x/H_T for the 91.4 m stack with and without the upwind terrain present. The dimensionless maximum concentration without the terrain is 65.6×10^{-5} and occurred at $x/H_T = 14.3$. It is evident from the figure that the maximum concentration with the upwind terrain was not observed and occurred closer to the plant than measured in the sampling network. A conservative estimate of the maximum concentration is 95.4×10^{-5} based on some results by Huber (1976) for diffusion in the wake of a building. Huber found that for $h/H_b = 1.2$, and $R = 0.7$ the maximum dimensionless concentration was $K = 95.4 \times 10^{-5}$ and occurred at $x/H_b = 3$.

The longitudinal ground level profiles with and without the upwind terrain for a stack height of 199.7 m are shown in Figure 6.2-6. The maximum concentration of $K = 15.2 \times 10^{-5}$ occurred at 19.4 with the upwind terrain present and a maximum of 8.5×10^{-5} was observed at $x/H_T = 36.4$ without the upwind terrain present. These results clearly demonstrate the effect of the upwind terrain; namely to increase the maximum concentration and cause it to occur closer to the plant site.

Figure 6.2-7 shows maximum longitudinal ground level concentrations with and without the upwind terrain for a stack height of 249.6 m. The maximum dimensionless concentration with the terrain present was observed at $x/H_T = 19.4$ to be $K = 8.2 \times 10^{-5}$. The maximum value without the terrain is $K = 4.1 \times 10^{-5}$ at $x/H_T = 36.4$.

The longitudinal profiles with and without the upwind terrain for a 305.3 m stack and 3 velocity ratios for each terrain configuration are shown in Figure 6.2-8. The maximum dimensionless concentration increases as velocity ratio decreases from 1.6 to 1.0. This is due to the associated decrease in plume rise with decreasing velocity ratio and corresponding increase in concentration. When the velocity ratio changes from 1.0 to 0.7 the concentration decreases indicating the decreasing plume rise effect is not as significant as the dilution due to increased wind speed. For $R = 1.57$ with the terrain present the maximum K value is 7.4×10^{-5} at $x/H_T = 14.7$ without the terrain and $R = 1.63$ the maximum K is 4.9×10^{-5} at $x/H_T = 62.14$. Similar results are evident for the other velocity ratios.

Figure 6.2-9 shows the maximum longitudinal concentration profiles with and without the terrain for a 349.4 m stack and three velocity ratios for each terrain configuration. For this stack height the maximum K values show a consistent increase with decreasing velocity ratio. Again the maximum concentration with the upwind terrain is considerably higher than that without the upwind terrain and for a comparable velocity ratio. Also the maximum occurs closer to the plant when the terrain is present.

The two horizontal ground level profiles at the downwind location of the two highest concentrations are plotted in Figures 6.2-10 through 6.2-14. These results are presented to document the horizontal distribution of the plume and to show that the maximum concentration was indeed measured. These figures in general show that a representative maximum concentration was obtained for each run. In some cases the distribution was irregular and can be explained by the irregularity of the terrain.

- Implication of Results on GEP Stack Height

For ASARCO to receive credit for the 305 m stack two criteria must be met according to the EPA Stack Height Credit Regulation. They are 1) for a nonattainment area (as is the smelter vicinity) the source must demonstrate that NAAQS limits are exceeded, and 2) the maximum concentration with the terrain must be at least 40 percent in excess of that without the upwind terrain. These criteria must be met for the old plant configuration (R&R and converter flue stacks) as well as the present configuration (305 m stack). Table 6.1 presents the necessary information from the wind tunnel evaluation to assess whether these criteria are met.

For the old plant configuration with the 91 m stack the maximum SO_2 concentration is 4.25 ppm with the terrain and 3.03 ppm without the terrain giving a ratio of χ_w/χ_{wo} = 1.40 or a 40% increase due to the presence of the terrain. The measured concentration with the upwind terrain is also in excess of the 3-hour NAAQS limit of 0.50 ppm (1300 $\mu g/m^3$). Thus for the old plant configuration criteria 1 and 2 above are met. It is apparent that the existing 305 m stack also meets both criteria. The maximum concentration with the terrain is 1.01 ppm which exceeds the NAAQS and the ratio of maximum concentration with and without the upwind terrain ranges from 1.35 to 1.68 depending upon ambient wind speed.

In summary the results of the wind tunnel test show that the existing 305 m stack conforms with the requirements of the stack height regulation in that the stack is not above GEP. In fact the results in Table 6.1 show that the GEP height is at least 349 m - the tallest height investigated.

REFERENCES

Budney, L.J., "Procedures for Evaluating Air quality Impact of New Stationary Sources." Guidelines for Air Quality Maintenance Planning and Analysis, Volume 10 (QAQPS No. 1.2-029R) Environmental Protection Agency, Research Triangle Park, North Carolina, 27711, July, 1977.

Businger, J.A., "The Atmospheric Boundary Layer," Chapter 6 in Remote Sensing of the Troposphere, edited by V.E. Derr, U.S. Department of Commerce, National Oceanic and Atmospheric Administration, 1972.

Cermak, J.E., "Laboratory Simulation of the Atmospheric Boundary Layer," AIAA Journal, Volume 9, No. 9, 1971.

Counihan, J., "Adiabatic Atmospheric Boundary Layers: A Review and Analysis of Data from the period 1880-1972, "Atmospheric Environment, Vol. 9, pp. 871-905, 1975.

Engineering Science Data Unit Item Number 72026, "Characteristic of Wind Speed in the Lower Layers of the Atmosphere near the Ground: Strong Winds (Neutral Atmosphere)," November, 1972.

Hinze, O.J., Turbulence, 2nd Edition, McGraw-Hill, Inc., 1975.

Hoult, D.P. and Weil, J., "Turbulent Plume in a Laminar Cross Flow," Atmospheric Environment, 6:513-531, 1972.

Huber, A.H. and Snyder, W.H., "Building Wake Effects on Short Stack Effluents," Third Symposium on Atmospheric Turbulence Diffusion and Air Quality, Raleigh, NC, p. 235-241, October 19-22, 1976.

Huber, A.H., personal communication, April, 1979.

Huber, A.H., memorandum to Joseph A. Tikvart, Chief Source Receptor Analysis Brach, subject: Evaluation of the Proposed Kemmer Wind Tunnel Study, May, 1978.

Huber, A.H., "Guideline for Use of Fluid Modeling to Determine Good Engineering Practice Stack Height," USEPA Office of Air, Noise, and Radiation, Research Triangle Park, North Carolina 27711, Draft for Public Comment EPA-450/4-79-015, June, 1979.

Pasquill, F., Atmospheric Diffusion, 2nd Edition, John Wiley and Sons, New York, 1974.

Pasquill, F., "Atmospheric Dispersion Parameters in Gaussian Plume Modeling, Part II," EPA Report No. EPA-600/4/-76-0360, 1976.

Schlichting, H., Boundary Layer Theory, McGraw-Hill, Inc., New York, 1968.

Snyder, W.H., "Similarity Criteria for the Application of Fluid Models to the Study of Air Pollution Meteorology," Boundary Layer Meteorology, Vol. 3, pp. 113-134, 1972.

Snyder, W.H., "Guideline for Fluid Modeling of Atmosphere Diffusion" USEPA Office of Air, Noise, and Radiation, Research Triangel Park, North Carolina 27711, Draft for Public Comment EPA-450/4-79-016, June, 1979.

Sutton, O.G., Micrometeorology, McGraw-Hill, Inc., New York, 1953.

Taylor, G.H., "A Wind Tunnel Investigation of Good Engineering Practice (GEP) Stack Height at the ASARCO SMELTER, HAYDEN, ARIZONA," North American Weather Consultants, Goleta, California, Report # SBAQ-79-10, July, 1979.

Taylor, G.I., "Diffusion by Continuous Movements," Proceedings, London Meteorological Society, Vol. 20, pp. 196-211, 1921.

Turner, P.B., Workbook of Atmospheric Dispersion Estimates, U.S. Department of Health, Education and Welfare, Public Health Service Publ. No. 999, Cincinnati, Ohio, AP-26, 88 p., 1969.

TABLES

Table 4.1. Model Parameters

	Parameter	R&R Flue	Con-verter Flue	Tall Stack 1	Tall Stack 2	Tall Stack 3	Tall Stack 4
1)	Stack height h(cm)	4.76	3.97	10.4	13.0	15.9	18.2
2)	Stack Inside Diameter - D(cm)	0.406	0.254	0.310	0.267	0.272	0.267
3)	Exit Velocity - u_s (cm/s)	149	137	376	507	489	507
		90	91	225	304	293	304
		59	68	159	214	207	214
4)	Stack Reynolds number - Re_s	403	232	777	902	887	902
		244	154	465	541	531	541
		160	115	329	381	375	381
5)	Volume Flow - $V(cm^3/s)$	19.32	6.92	28.41			
		11.67	4.61	17.00			
		7.67	3.46	12.00			
6)	Exit Temperature - T_s(K)	293	293	293			
7)	Molecular weight of - m_s(g) Stack gas	28.9	28.9	28.9			
8)	Molecular weight of - m_a(g) Air	28.9	28.9	28.9			
9)	Source Strength χ_o(%)						
	(a) Methane	-	15.0	-			
	(b) Ethane	10.2	-	10.2			
10)	Reference height z_h (cm)	30.5					
11)	Friction velocity u_* (m/s)	0.15					
12)	Surface roughness z_o (mm)	0.17					

Table 4.2. Parameters for ASARCO smelter at Hayden, Arizona

	Parameter	R&R Flue	Converter Flue	Tall Stack
1)	Stack Height - h(m)	91.46	76.22	304.9
2)	Stack Inside Diameter - D(cm)	7.62	4.88	5.18
3)	Stack Outside Diameter - D_o(m)	9.15	5.79	9.76
4)	Stack Base (ft, MSL)	2224	2123	2182
5)	Exit Velocity - u_s(m/s)	5.15	4.54	15.18
6)	Volume Flow - V (m^3/s)	234.9	85.0	319.9
7)	Exit temperature - T_s(K)	394.1	344.1	380.7
8)	SO_2 Emission Rate - Q_s(g/s)	5669	1680	7348
9)	SO_2 Source Strength* - χ_o(ppm)	9282	7602	8834
10)	Ambient temperature - T_a(K)	300	300	300

*For ambient temperature and standard pressure

Table 4.3. Summary of Visualization & Concentration Tests[1)]

Run	Upwind Terrain	Stack Height h(m)		Velocity Ratio R		Ambient Velocity (m/s) at 585 m, AGL (1213 m, MSL)	
1[2)]	Out	91.5	(76.22)	0.50	(0.46)	9.89	(9.99)
2				0.30	(0.30)	16.37	(15.00)
3				0.20	(0.23)	24.91	(19.98)
4[2)]		199.7		1.25		9.16	
5				0.75		15.31	
6				0.53		21.68	
7		249.6		1.69		9.16	
8				1.01		15.31	
9				0.71		21.68	
10[2)]		305.3		1.63		9.16	
11				0.98		15.31	
12				0.69		21.68	
13		349.4		1.69		9.16	
14				1.01		15.31	
15				0.71		21.68	
16**	In	91.5	(76.22)	0.32	(0.30)	14.83	(14.99)
17**				0.20	(0.18)	24.56	(24.93)
18**				0.13	(0.15)	37.37	(29.97)
19**		199.7		0.97		11.85	
20**				0.58		19.80	
21**				0.41		28.04	
22**		249.6		1.48		10.47	
23**				0.89		17.50	
24**				0.62		24.79	
25[2)]		305.3		1.57		9.49	
26				0.94		15.87	
27				0.66		22.48	
28		349.4		1.63		9.49	
29				0.98		15.87	

30	349.4		0.69	22.48	
31*	91.4	(73.2)	0.48 (0.44)	10.25	(10.36)
32*	199.7		1.21[3)]	9.49[3)]	
33*	249.6		1.63	9.50	

*No pictures were taken for these cases.
**Concentration data for these tests were not analyzed since the ambient conditions were not comparable to the no terrain cases.

1)The numbers in parenthesis are the converter flue parameters.
2)Runs for which horizontal and vertical distribution of plume were obtained at four downwind locations.

Table 5.1. Summary of velocity profile characteristics without the upwind terrain present

x (m)	y (m)	z_o (mm)	u* (m/s)	d (cm)	$Re_{z_o}^*$	n	e_{z_o} 1)	e_n 2)
0.00	-1.68	0.000	0.060	1.23	0.00	0.11	0.178	0.228
0.00	-1.22	0.000	0.095	1.09	0.00	0.13	0.100	0.176
0.00	-0.61	0.169	0.161	0.76	1.81	0.22	0.059	0.167
0.00	0.00	0.069	0.142	-0.21	0.65	0.14	0.020	0.028
0.00	0.61	1.390	0.206	0.67	19.09	0.35	0.153	0.350
0.00	1.22	0.122	0.154	1.05	1.25	0.27	0.137	0.348
0.00	1.68	0.000	0.041	1.26	0.00	0.09	0.169	0.230
-0.91	0.00	0.168	0.148	-0.87	1.66	0.14	0.041	0.041
0.91	0.00	1.890	0.205	-0.71	25.83	0.23	0.045	0.075
1.88	0.00	7.440	0.266	-4.59	131.94	0.21	0.028	0.049
2.74	0.00	1.940	0.205	-2.06	26.51	0.19	0.017	0.024
3.66	0.00	0.072	0.131	-1.16	0.63	0.12	0.025	0.020
4.57	0.00	3.580	0.216	0.34	51.55	0.42	0.018	0.262

$*\nu = 0.15\ cm^2/s$

1) the root-mean-square error (m/s) between log-law and observation

2) the root-mean-square error (m/s) between power-law and observation

Table 5.2. Summary of velocity profile characteristics with the terrain present

x (m)	y (m)	z_o (mm)	u* (m/s)	d (cm)	Re_{z_o} *	n	e_{z_o} 1)	e_n 2)
0.00	-1.68	20.40	0.294	-3.59	399.84	0.36	0.052	0.078
0.00	-1.22	100.00	0.752	-10.40	5013.33	0.60	0.215	0.263
0.00	-0.61	43.50	0.558	-4.59	1618.20	0.52	0.205	0.284
0.00	0.00	11.20	0.345	-2.31	257.60	0.318	0.131	0.165
0.00	0.61	29.60	0.382	-8.25	753.81	0.27	0.037	0.065
0.00	1.22	0.14	0.228	1.09	2.13	0.29	0.137	0.393
0.00	1.68	0.00	0.084	1.12	0.00	0.12	0.200	0.218
-0.91	0.00	0.00	0.102	-1.75	0.00	0.07	0.062	0.064
0.91	0.00	4.05	0.256	-3.41	69.12	0.20	0.058	0.074
1.88	0.00	5.00	0.260	-5.41	86.67	0.18	0.027	0.056
2.74	0.00	1.23	0.208	-2.09	17.06	0.17	0.033	0.032
3.66	0.00	0.00	0.105	0.53	0.00	0.109	0.053	0.062
4.57	0.00	1.18	0.208	0.71	16.36	0.34	0.027	0.205

*ν = 0.15 cm^2/s

1) the root-mean-square error (m/s) between log-law and obervation

2) the root-mean-square error (m/s) between power-law and observation

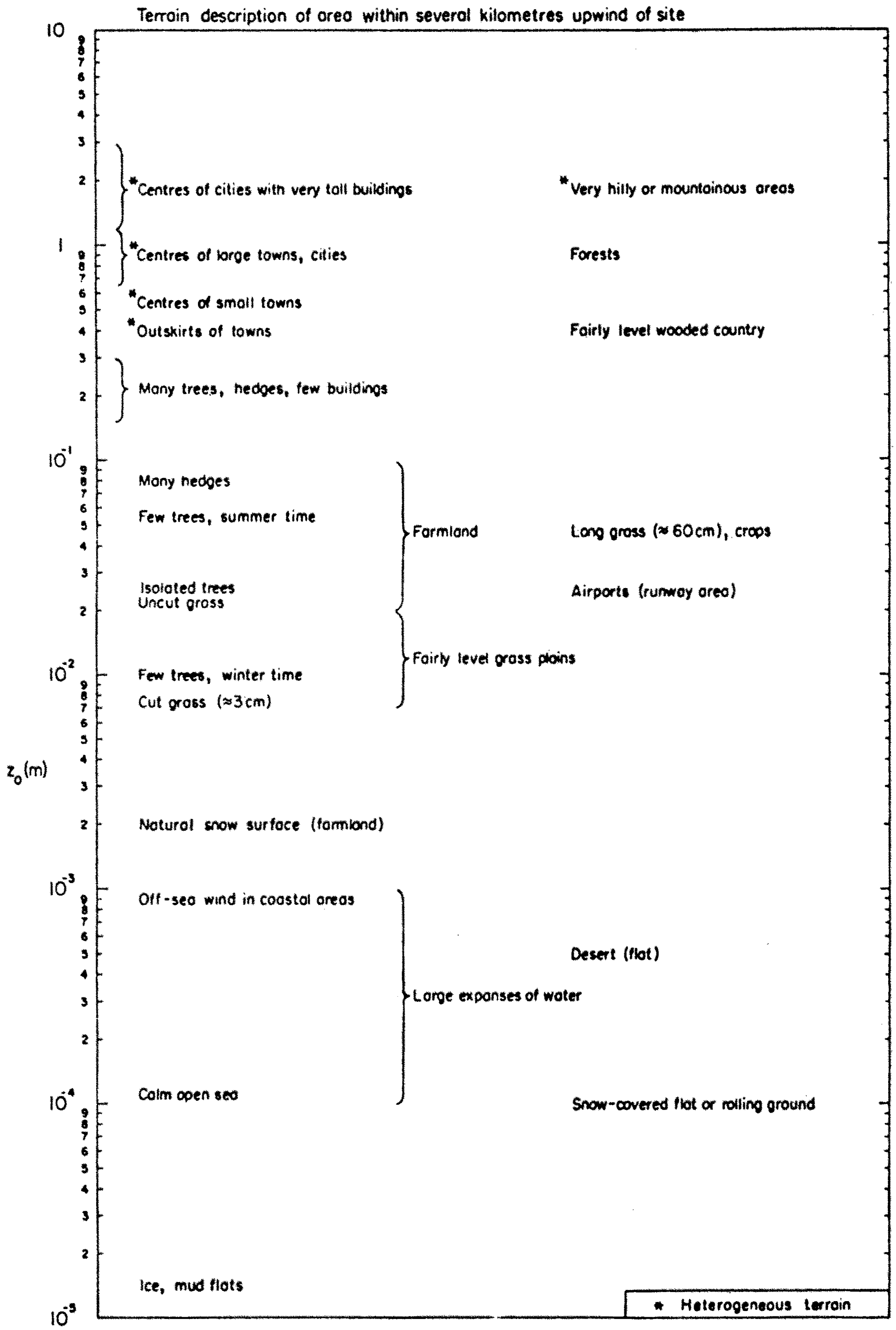

Table 5.3. Values of the surface roughness parameter z_o (ESDU, 1972)

Table 6.1. Summary of ground-level concentration measurement results for ASARCO wind tunnel modeling experiments

Stack Height (m)	Wind Speed (m/s)*	Maximum Observed Equivalent SO_2 Concentration (ppm)**		
		With Terrain (a)	No Terrain (b)	Ratio (a)/(b)
91	10.1	4.25***	3.03	1.40**
200	9.3	1.68	0.95	1.72
250	9.3	1.19	0.61	1.94
305	9.3	1.01	0.60	1.68
	15.6	0.57	0.42	1.35
	22.1	0.51	0.33	1.52
349	9.3	0.69	0.27	2.52
	15.6	0.51	0.25	2.08
	22.1	0.62	0.26	2.41

*Approximate free-stream velocity at 585 m above the stack base.

**Equivalent SO_2 emissions -- 91 m stack: R&R flue 5669 g/s (9282 ppm)

200 - 349 m stacks: 7348 g/s (8834 ppm)

***The maximum concentrations for 91 m stack with terrain occurred too near the stack to be detected in receptor grid and is conservatively estimated to be this value based on Huber (1976).

FIGURES

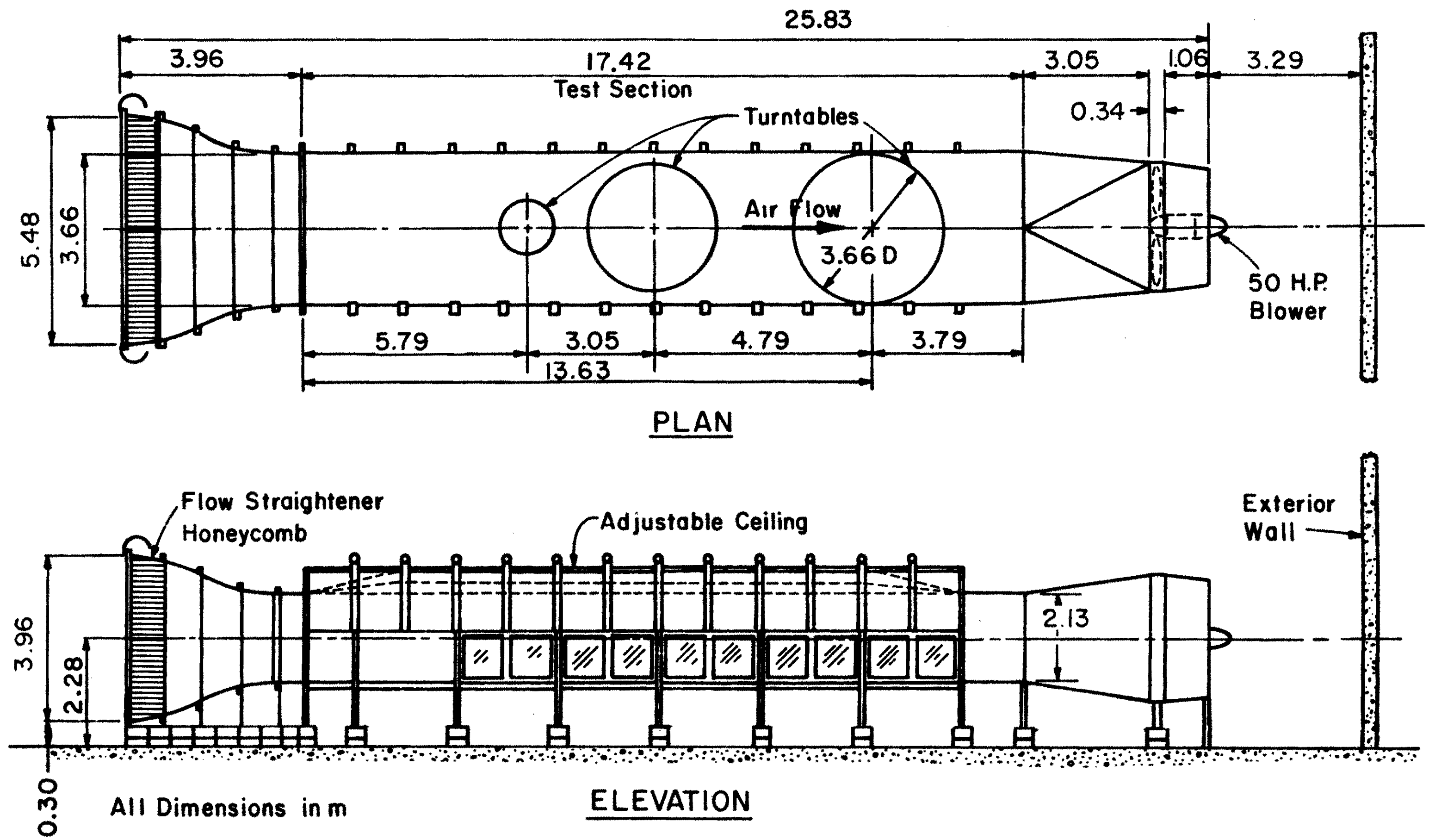

Figure 4.2-1. Environmental Wind Tunnel, Fluid Dynamics & Diffusion Laboratory, Colorado State University.

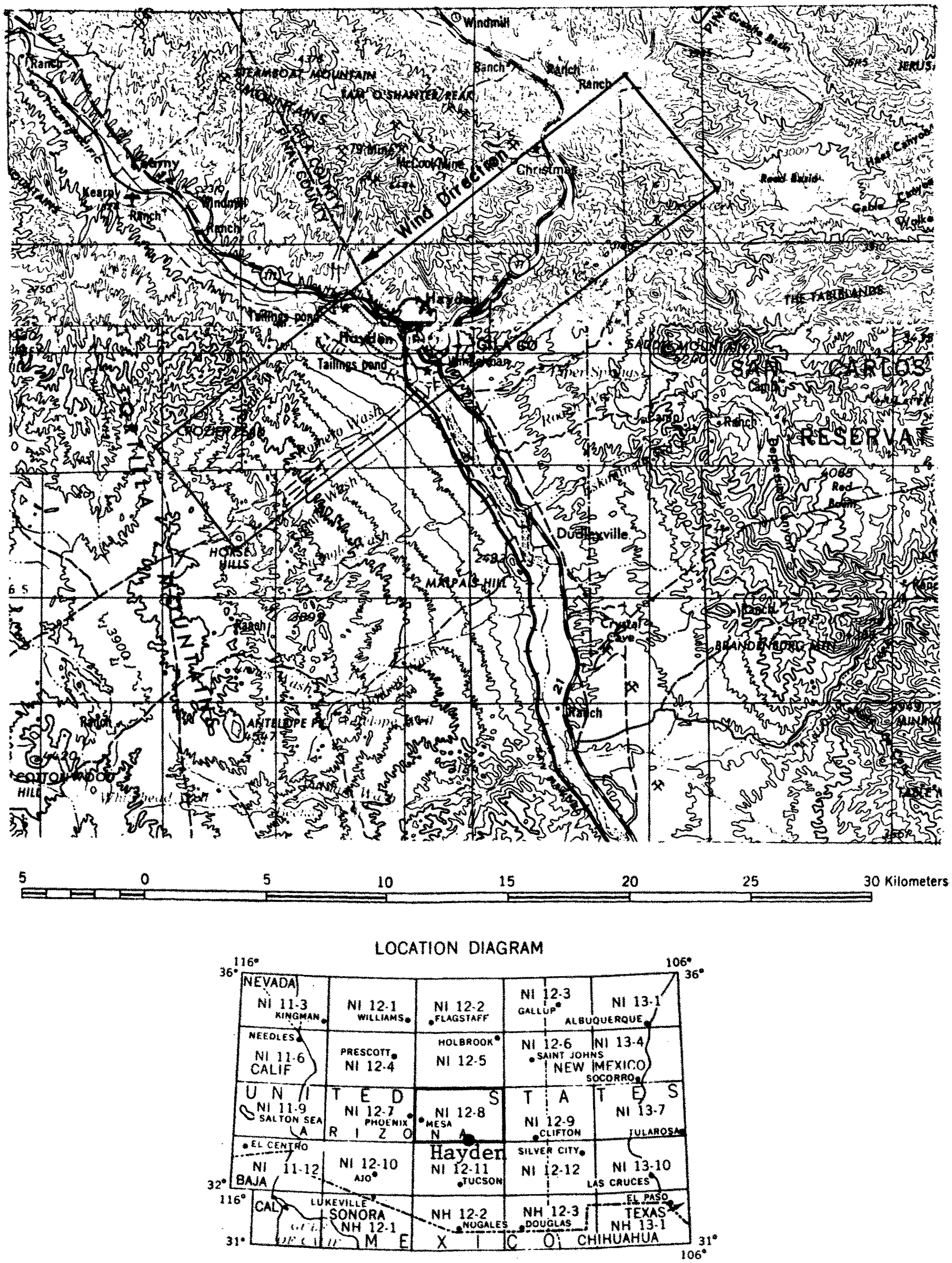

Figure 4.2-2. Map showing area modeled in wind tunnel.

a

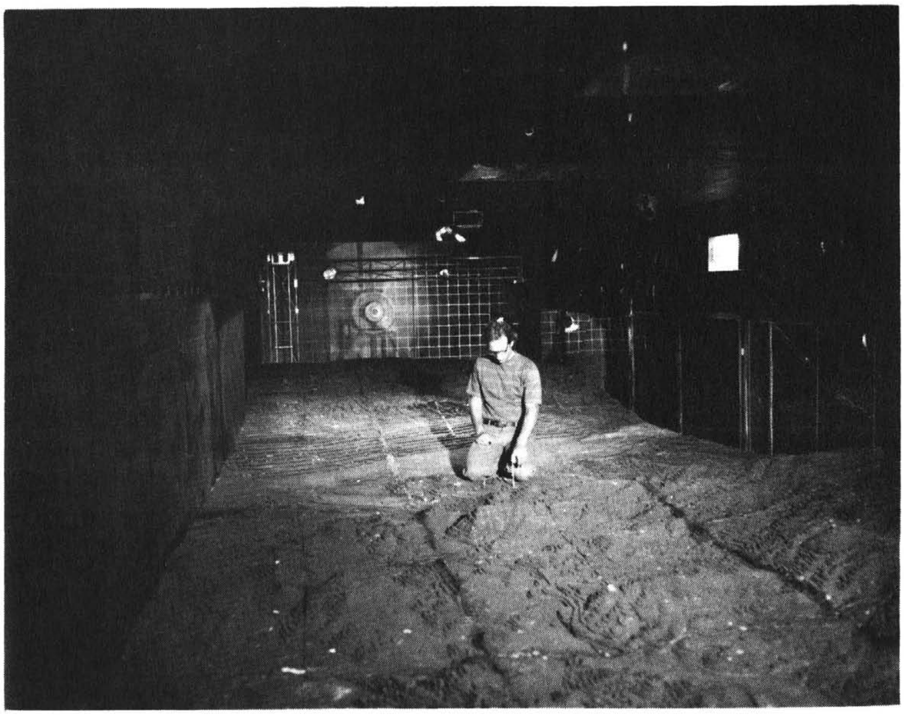

b

Figure 4.2-3. Photographs of model terrain for the 51^{o} true azimuth looking (a) upwind and (b) downwind

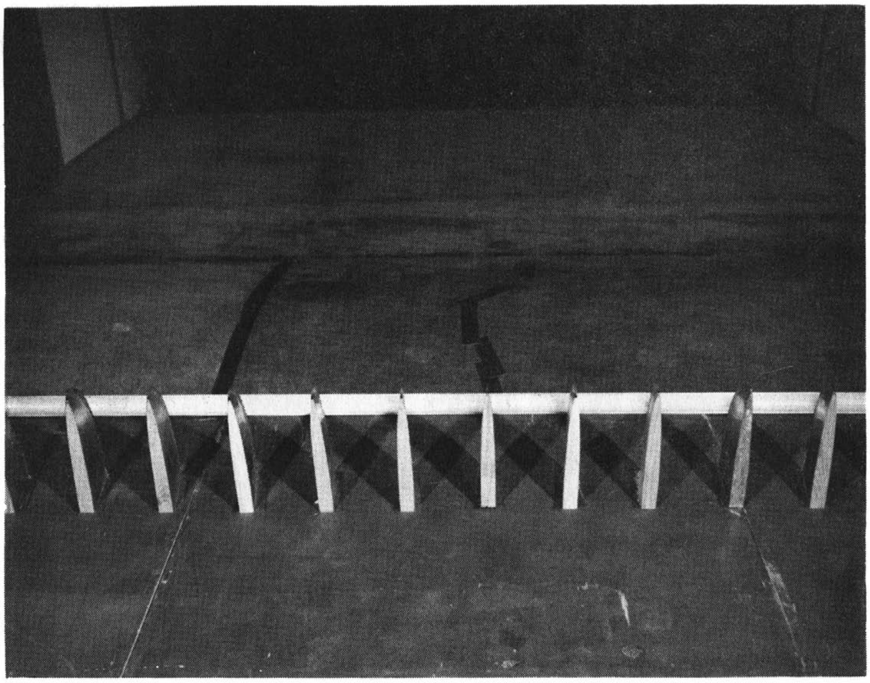

Figure 4.2-4. Photograph showing 30.5 cm spires, 3.8 cm trip and approach ramp used for developing the boundary layer of the no-upwind terrain tests.

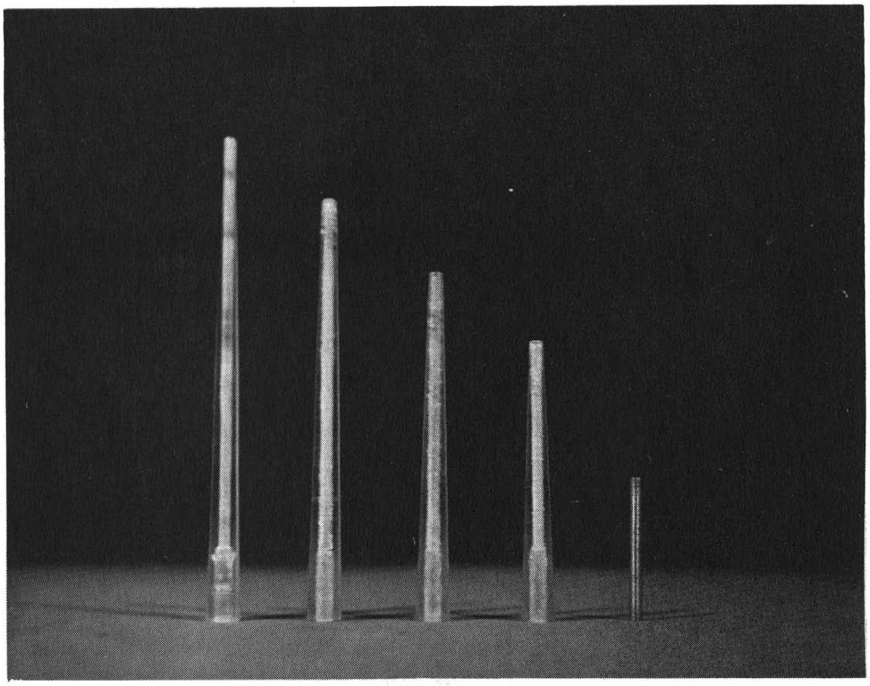

Figure 4.2-5. Photograph of model stacks used for GEP evaluation.

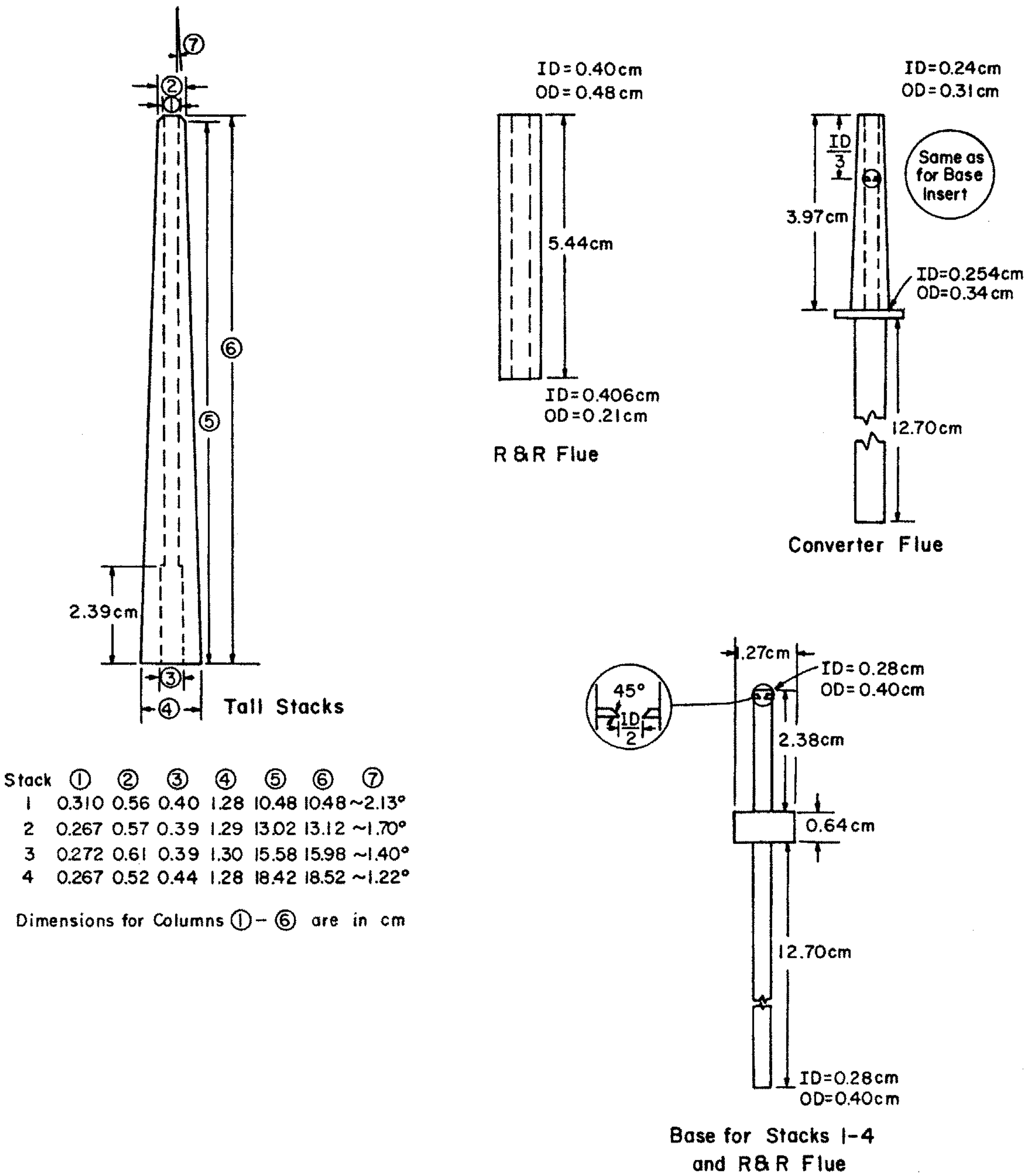

Stack	①	②	③	④	⑤	⑥	⑦
1	0.310	0.56	0.40	1.28	10.48	10.48	~2.13°
2	0.267	0.57	0.39	1.29	13.02	13.12	~1.70°
3	0.272	0.61	0.39	1.30	15.58	15.98	~1.40°
4	0.267	0.52	0.44	1.28	18.42	18.52	~1.22°

Dimensions for Columns ①– ⑥ are in cm

Figure 4.2-6. Drawing of model stacks used for GEP evaluation.

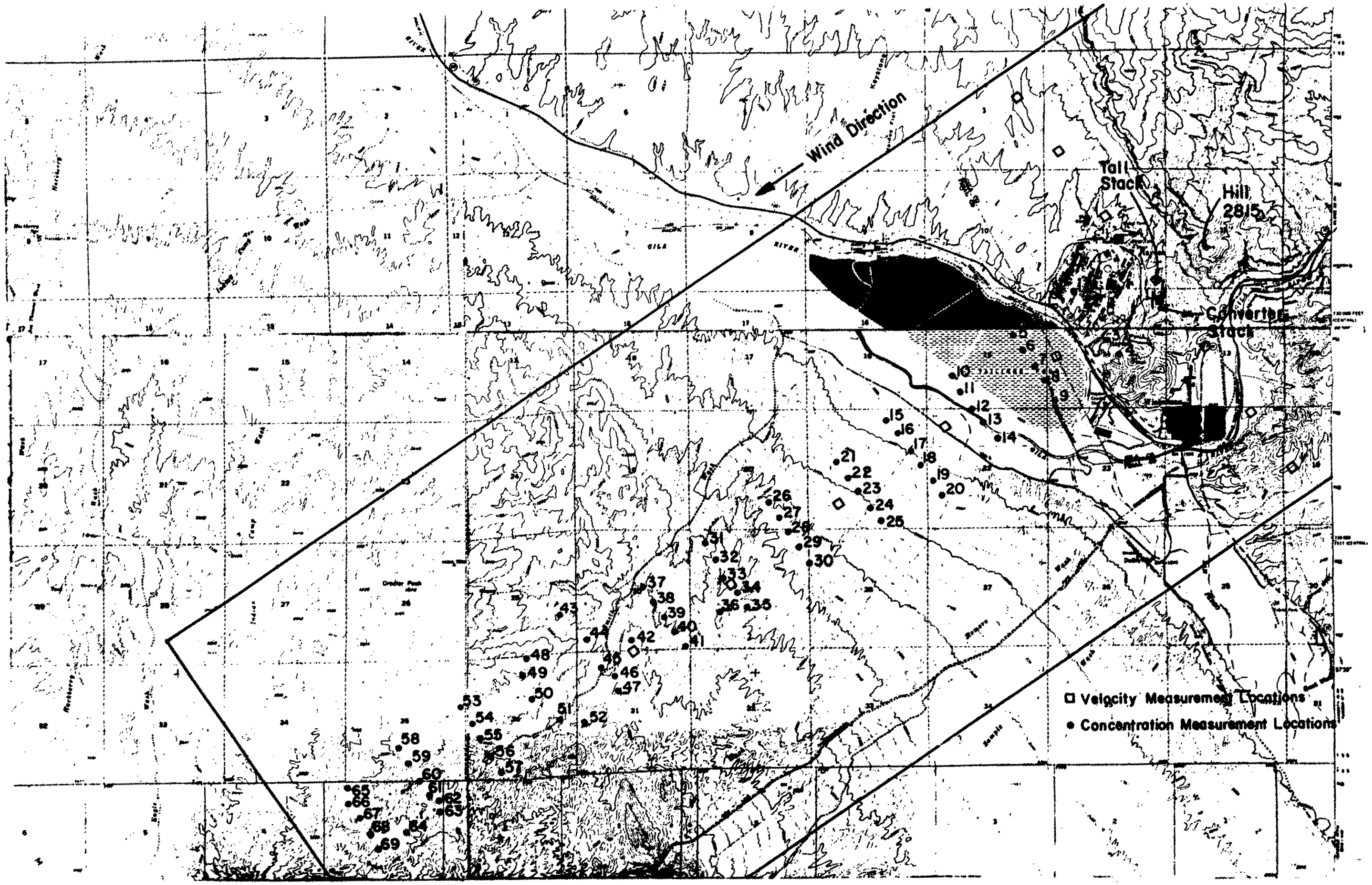

Figure 4.4-1. Map showing tracer gas sampling locations and locations where velocity measurements were obtained.

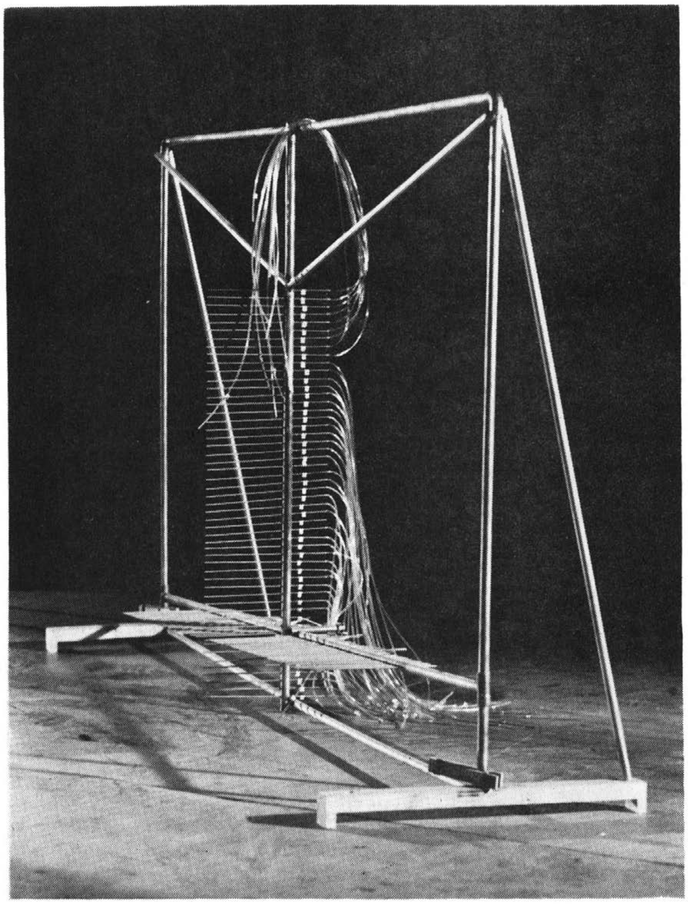

Figure 4.4-2. Photograph showing the sampling rake used to obtain the horizontal and vertical concentration profiles.

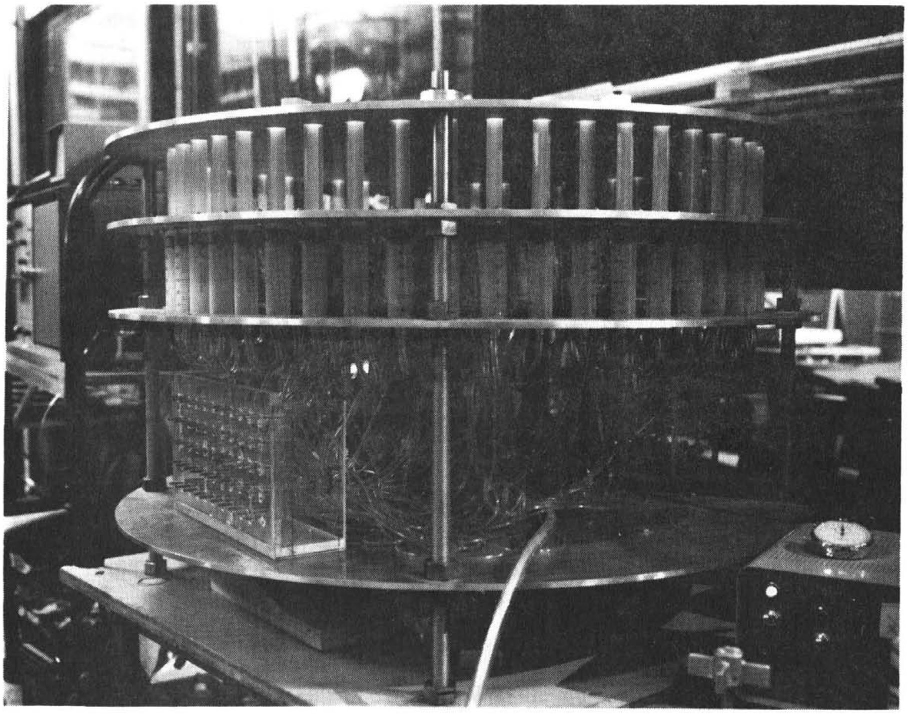

a

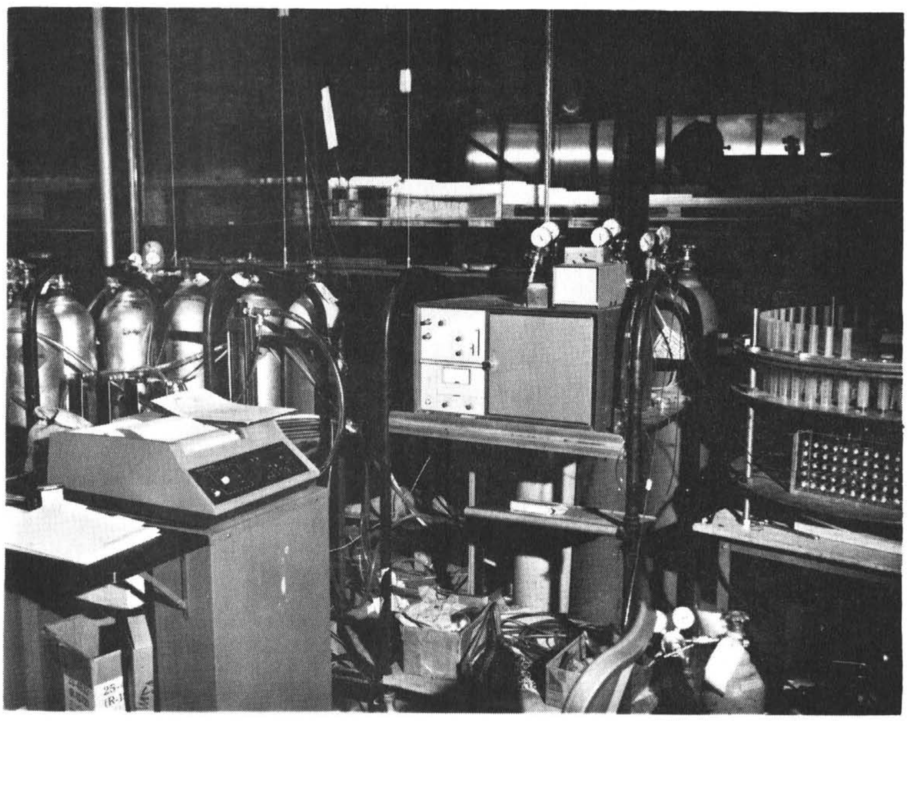

b

Figure 4.4-3. Photographs showing (a) the tracer gas sampling system and (b) the gas chromatograph, integrator and sampling system set-up.

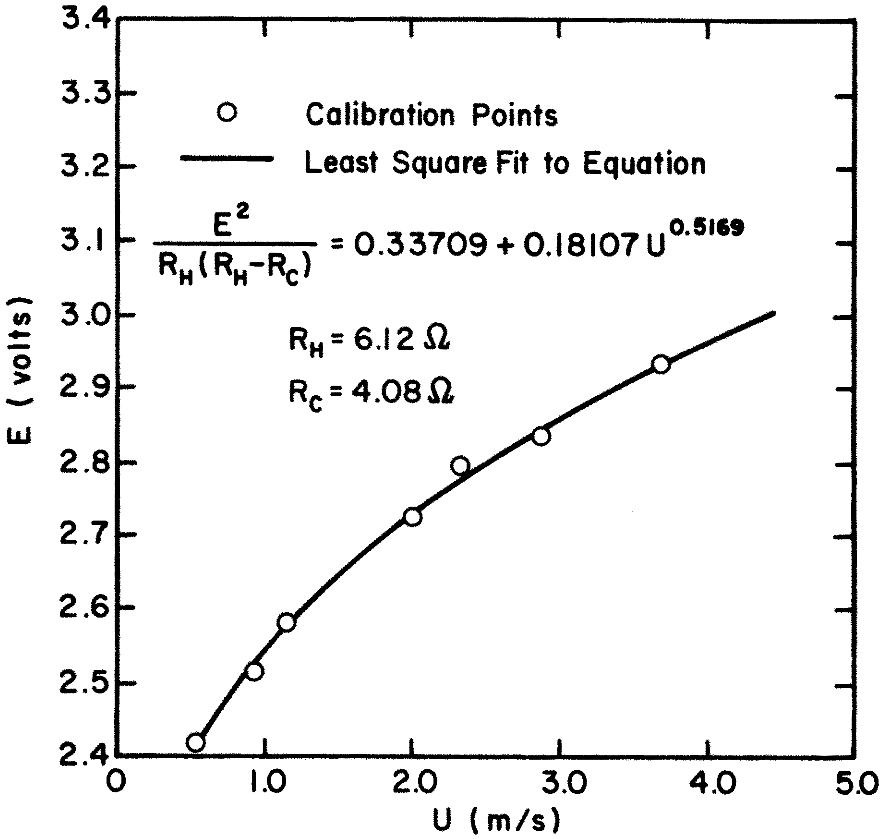

Figure 4.5-1. Typical hot film calibration curve taken on June 5, 1979.

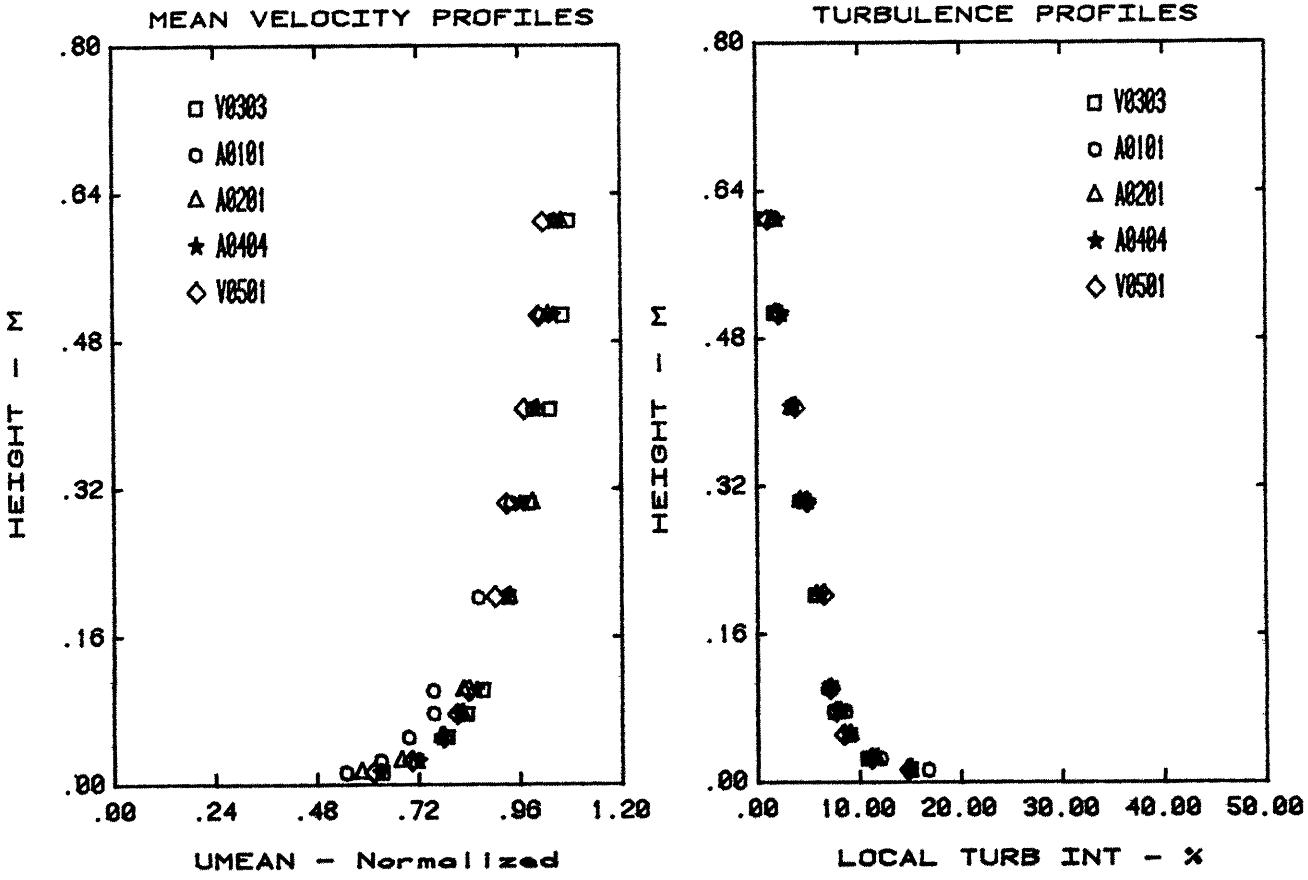

Figure 5.1-1. Velocity profiles at the tall stack location without the upwind terrain present for the following reference velocities: ○ - 1 m/s; Δ - 2 m/s; □ - 3 m/s; * - 4 m/s; ◇ - 5 m/s.

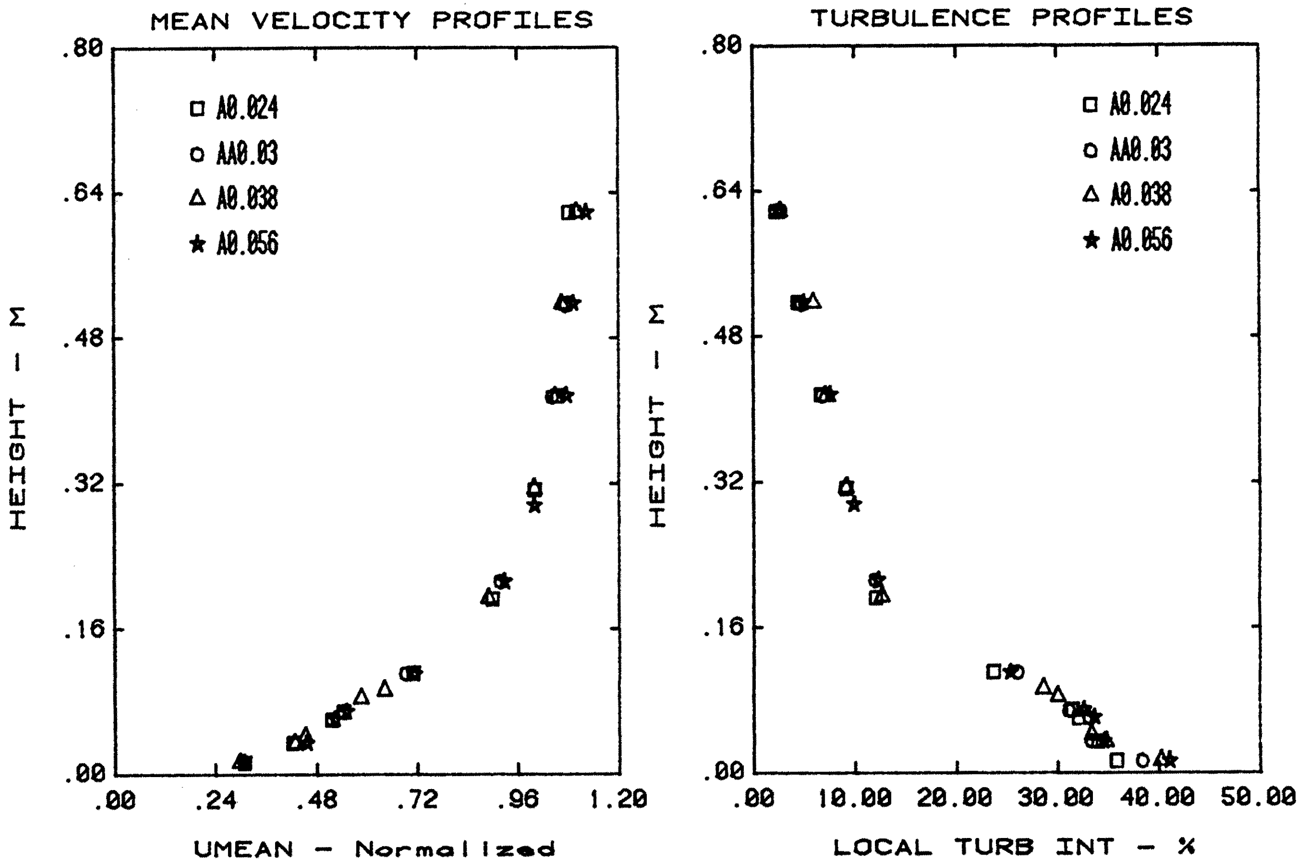

Figure 5.1-2. Velocity profiles at the tall stack location with the upwind terrain present for the following reference velocities: ◘ - 3.1 m/s; ○ - 3.4 m/s; Δ - 3.9 m/s; * - 4.5 m/s.

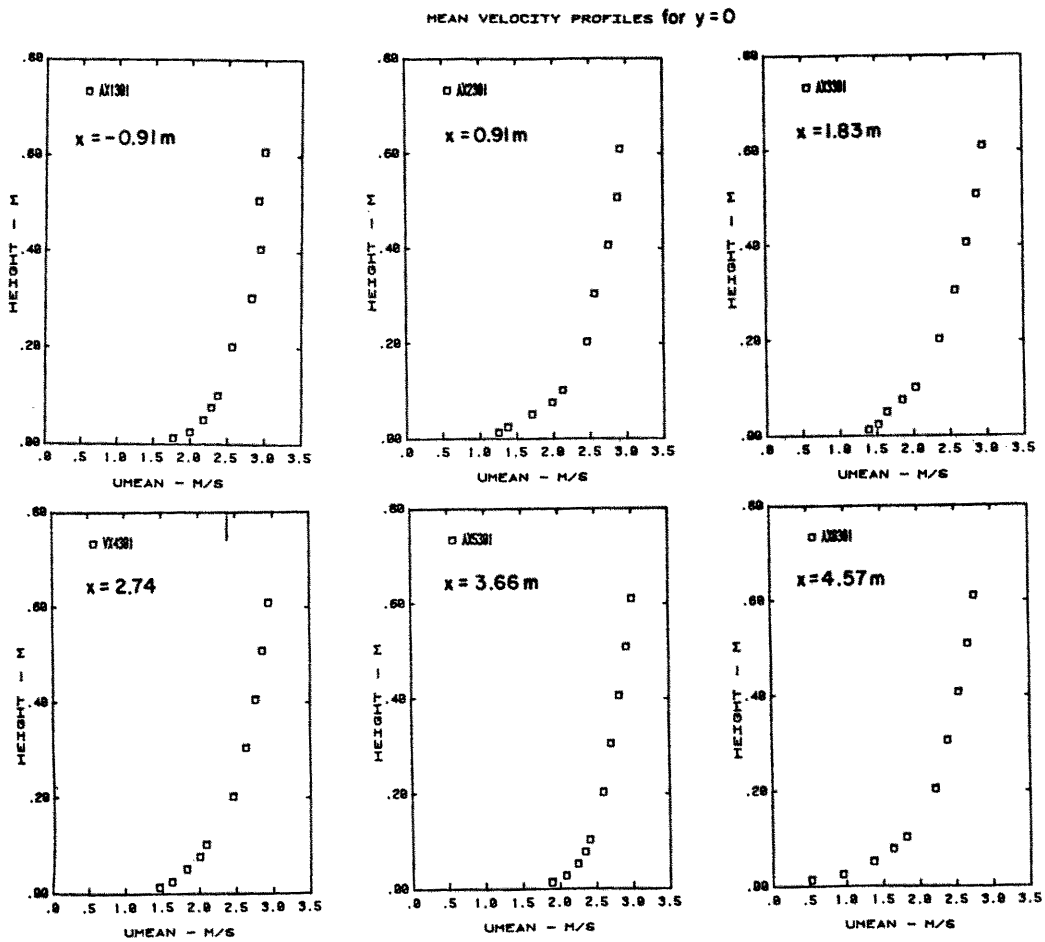

Figure 5.1-3. Velocity profiles along the center of the tunnel without the upwind terrain present.

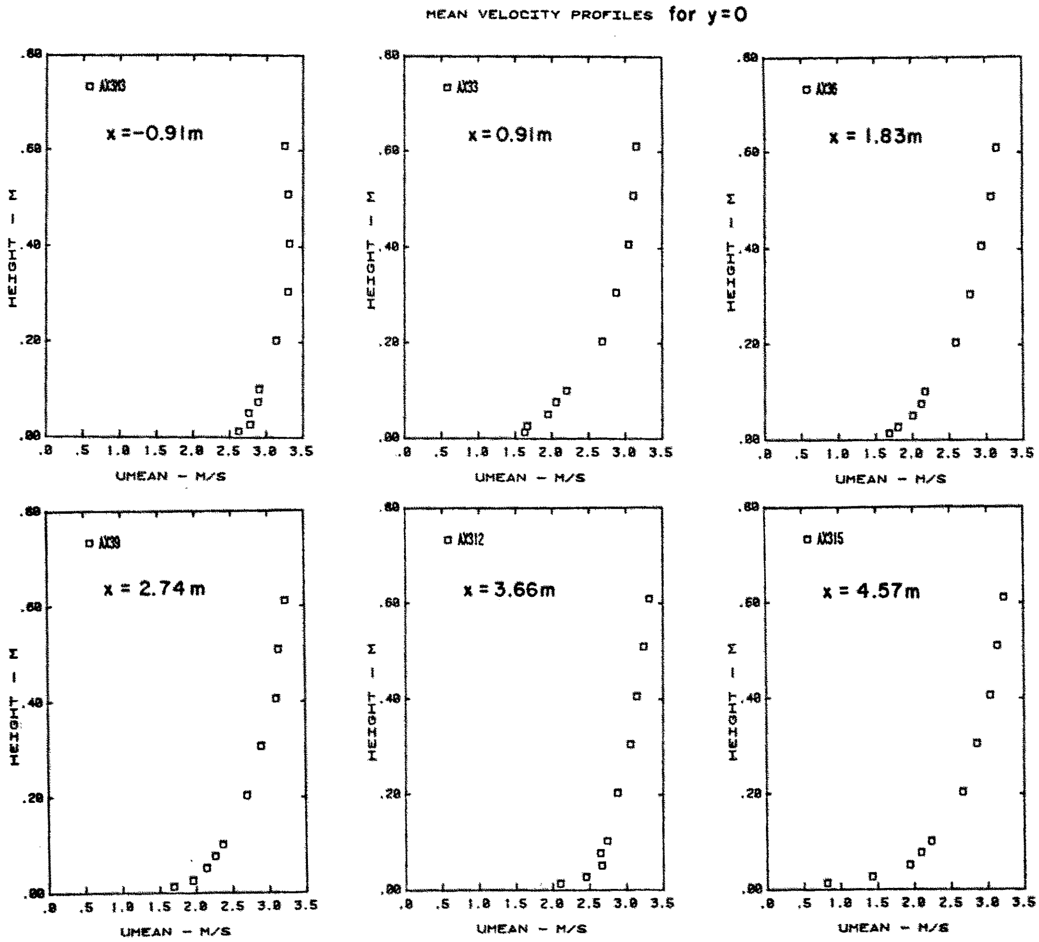

Figure 5.1-4. Velocity profiles along the center of the tunnel with the upwind terrain present.

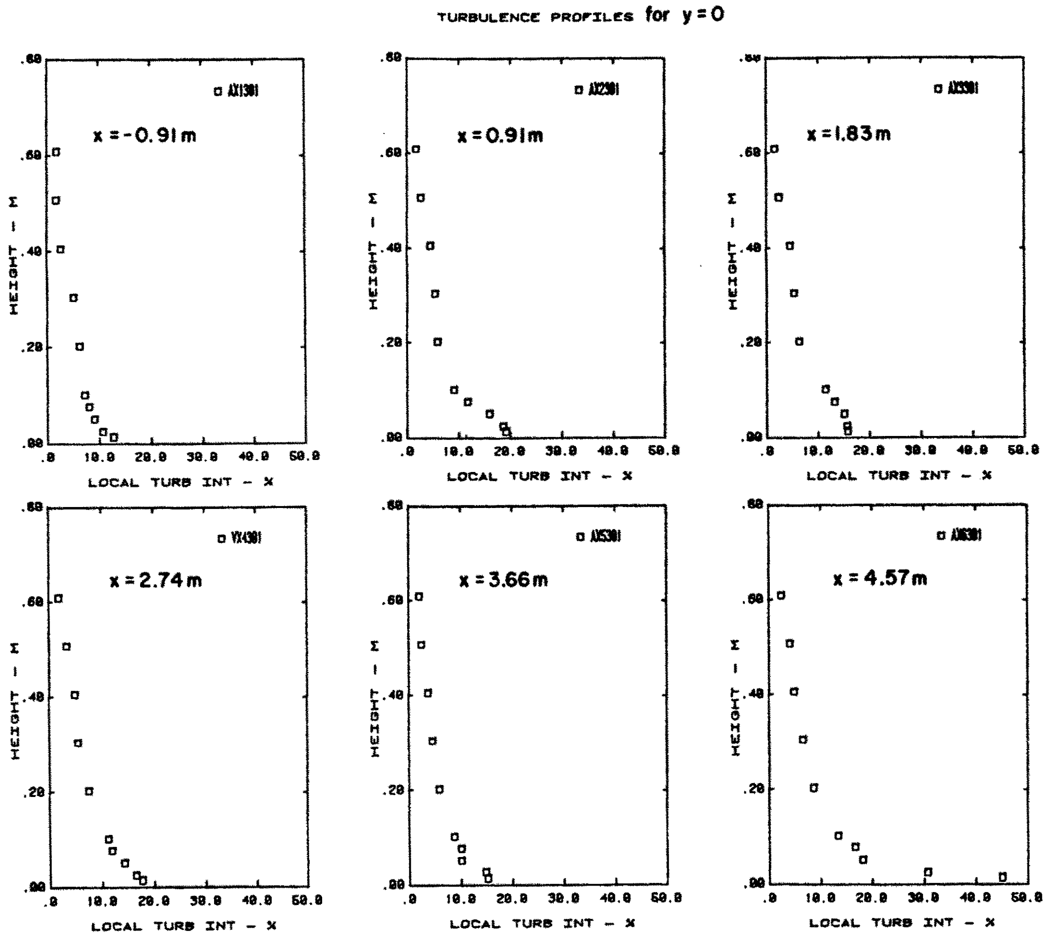

Figure 5.1-5. Longitudinal turbulence intensity profiles along the center of the tunnel without the upwind terrain present.

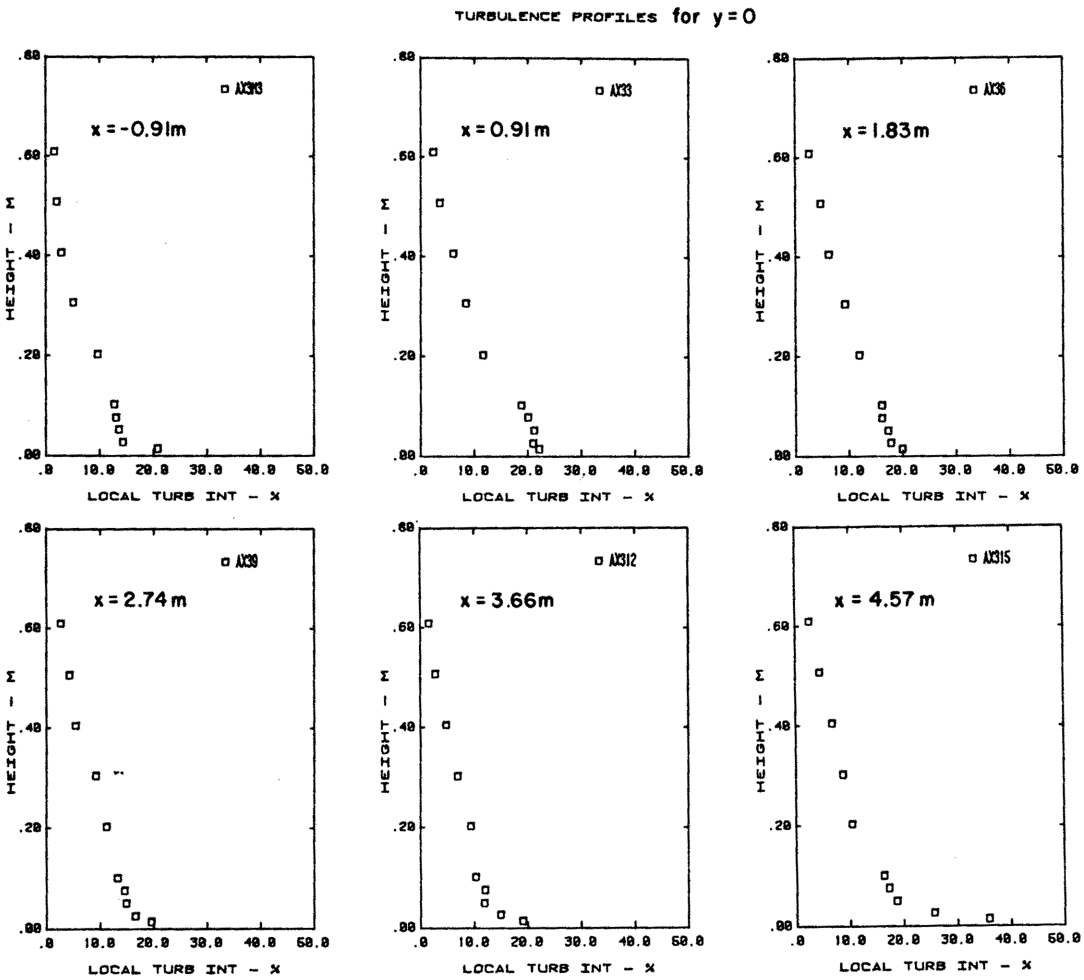

Figure 5.1-6. Longitudinal turbulence intensity profiles along the center of the tunnel with the upwind terrain present.

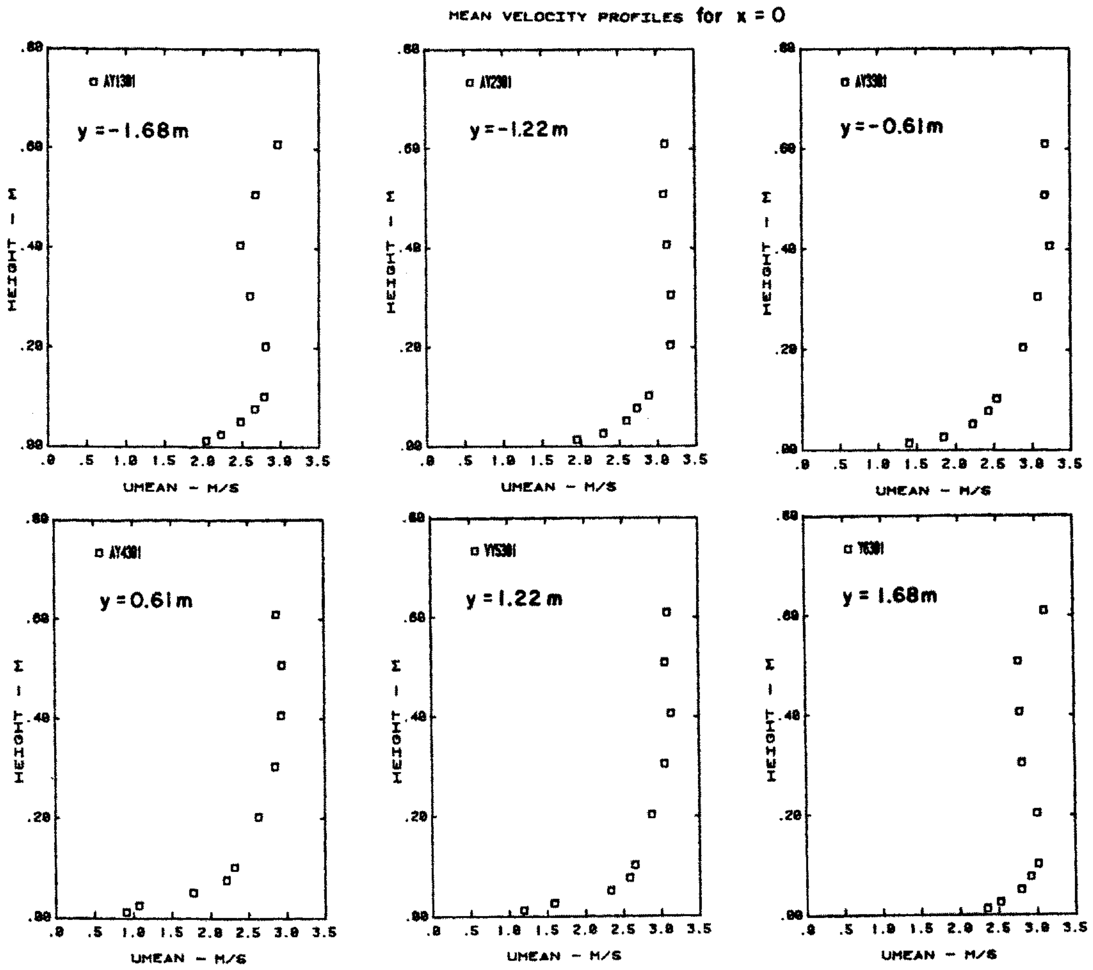

Figure 5.1-7. Velocity profiles across the tunnel at the tall stack location without the upwind terrain present.

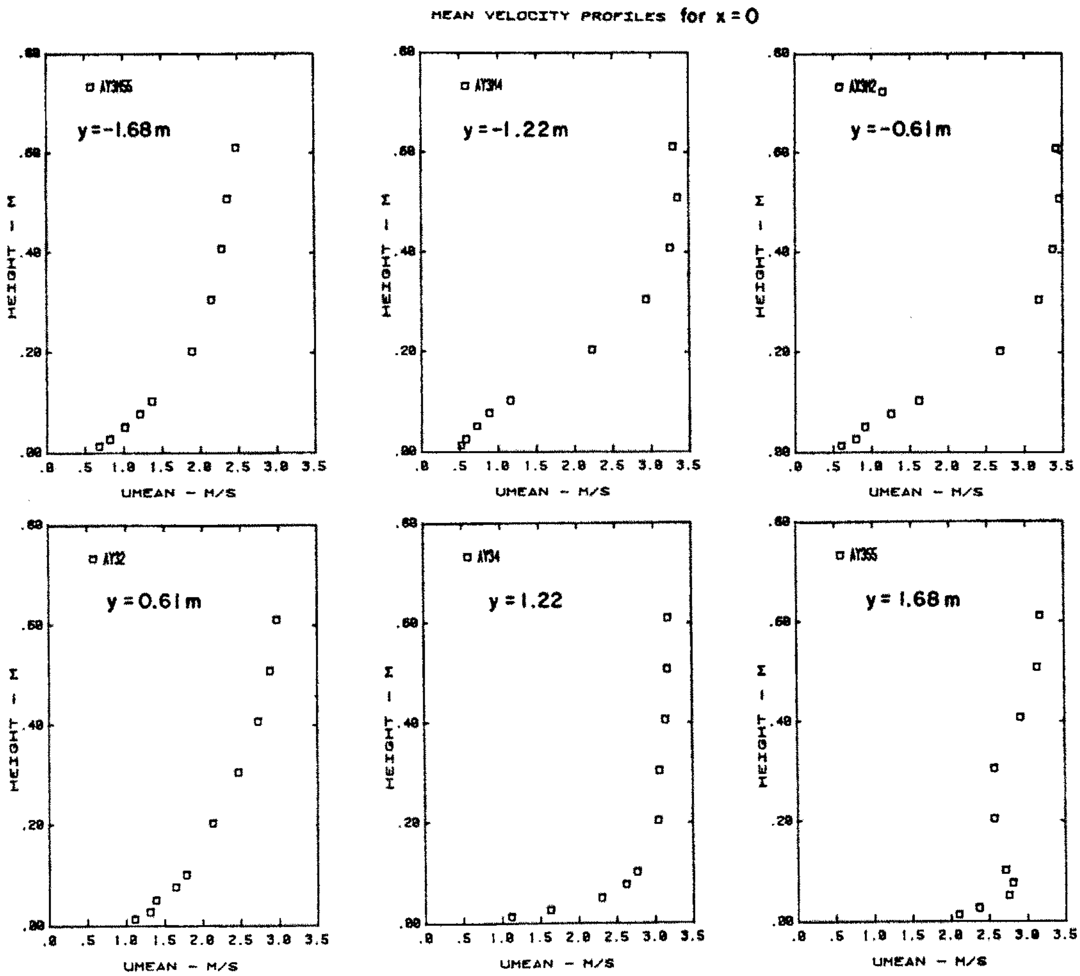

Figure 5.1-8. Velocity profiles across the tunnel at the tall stack location with the upwind terrain present.

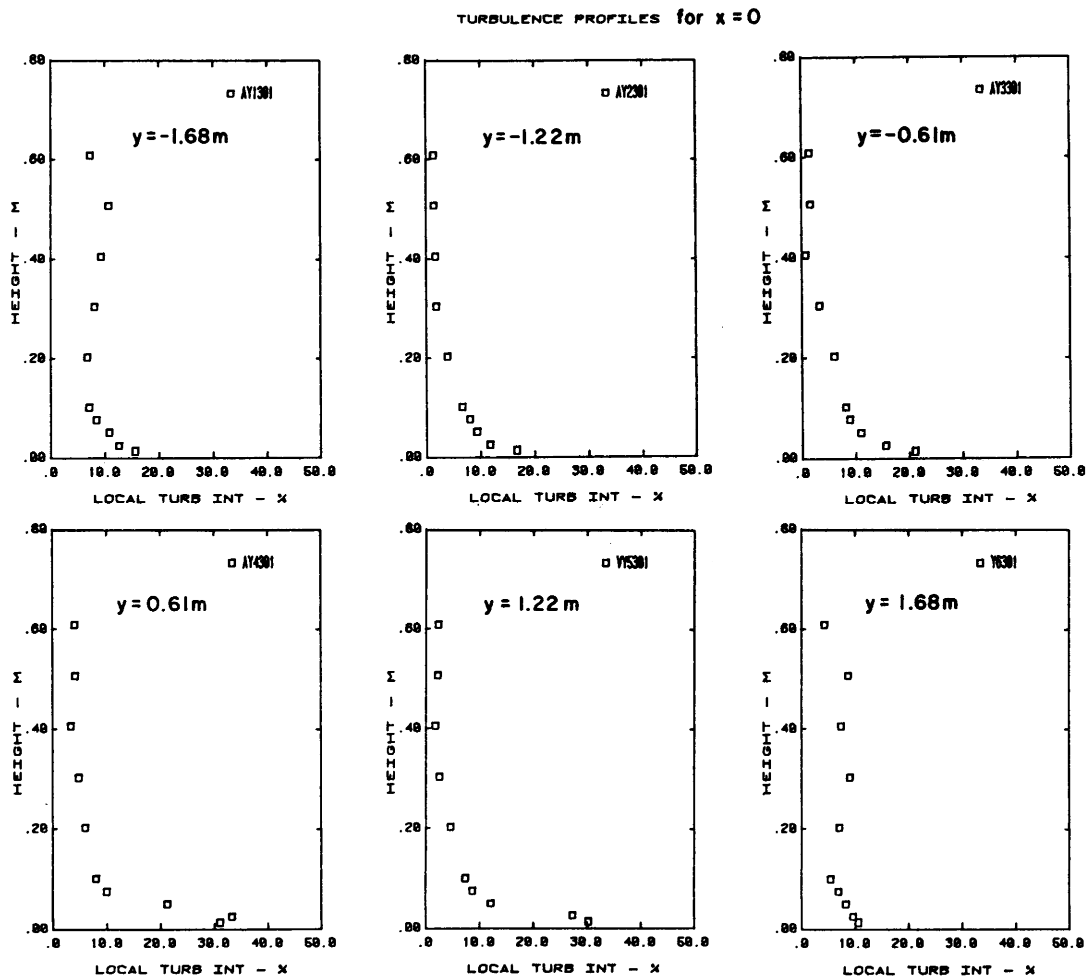

Figure 5.1-9. Longitudinal turbulence intensity profiles across the tunnel without the upwind terrain present.

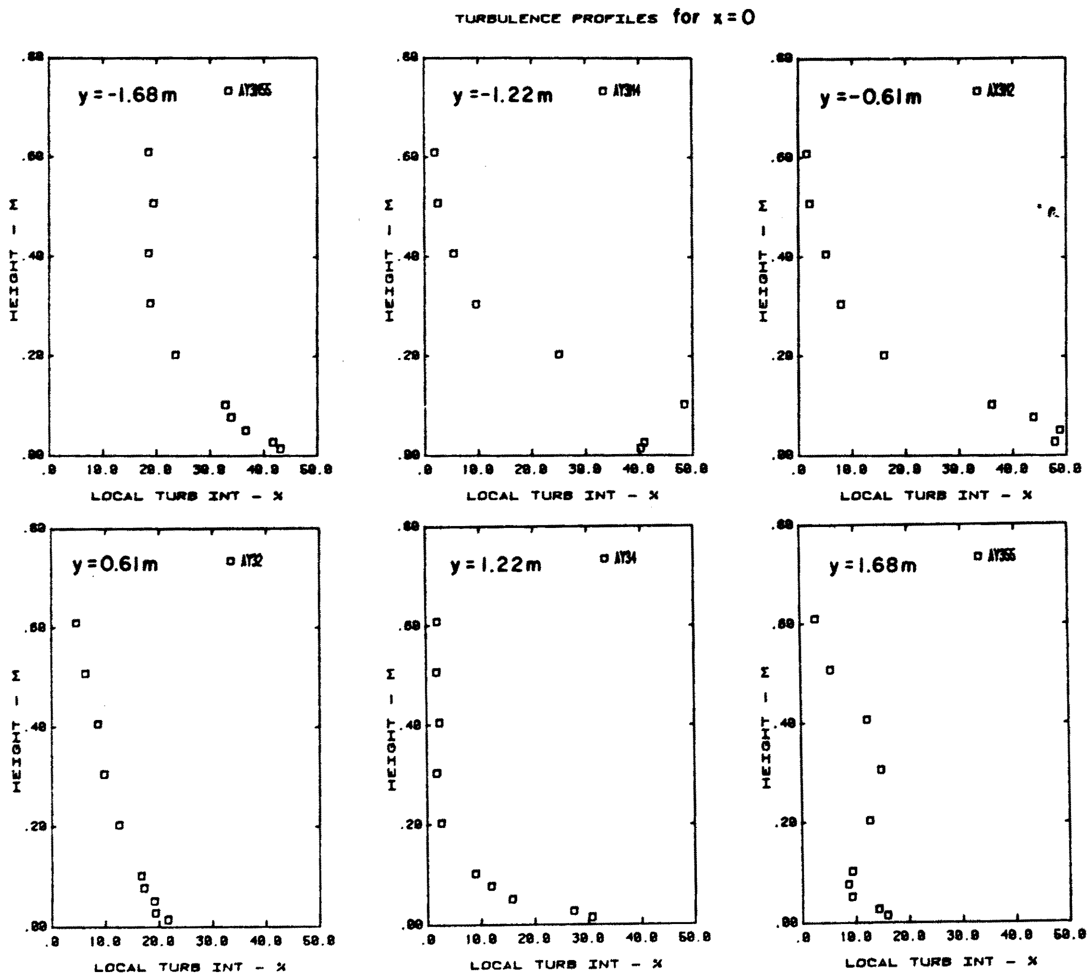

Figure 5.1-10. Longitudinal turbulence intensity profiles across the tunnel with the upwind terrain present.

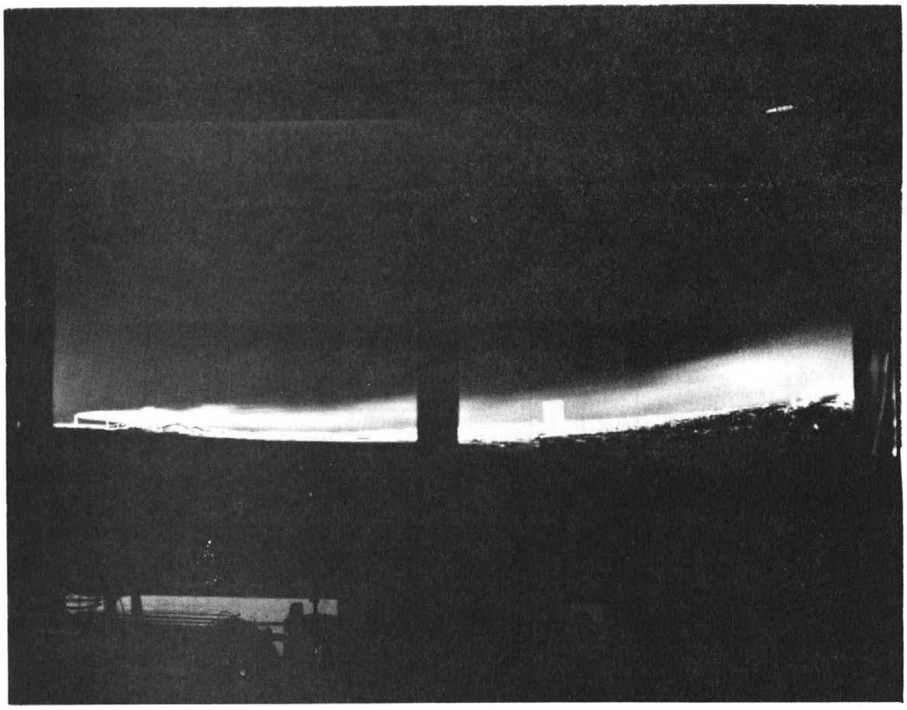

a

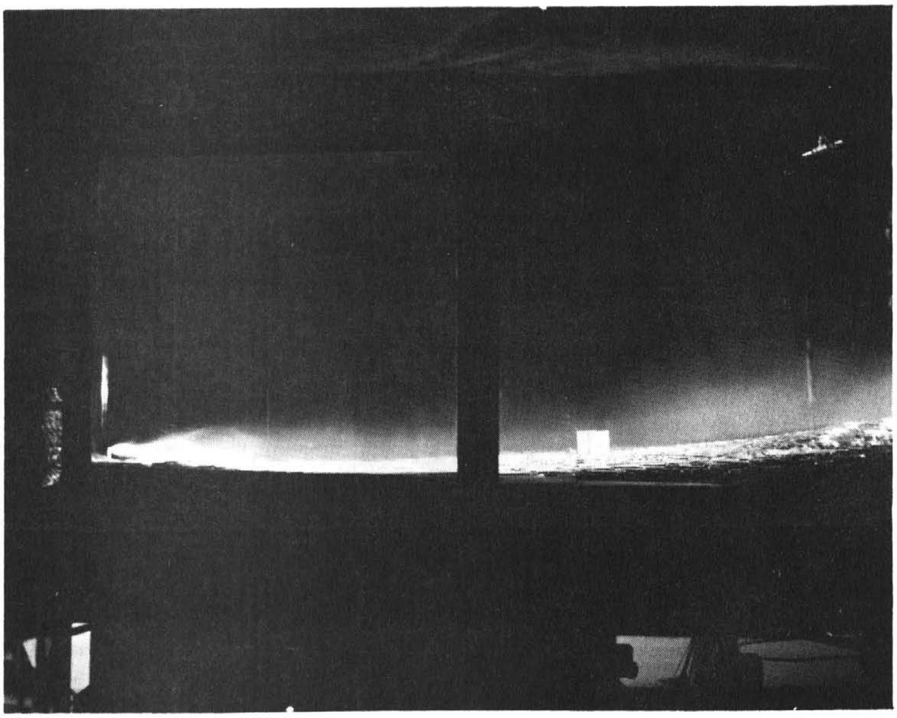

b

Figure 6.1-1. Photographs of plume behavior without (a) and with (b) the upwind terrain present for stack height of 91.5 m for the R&R flue and 73.2 m for the converter flue.

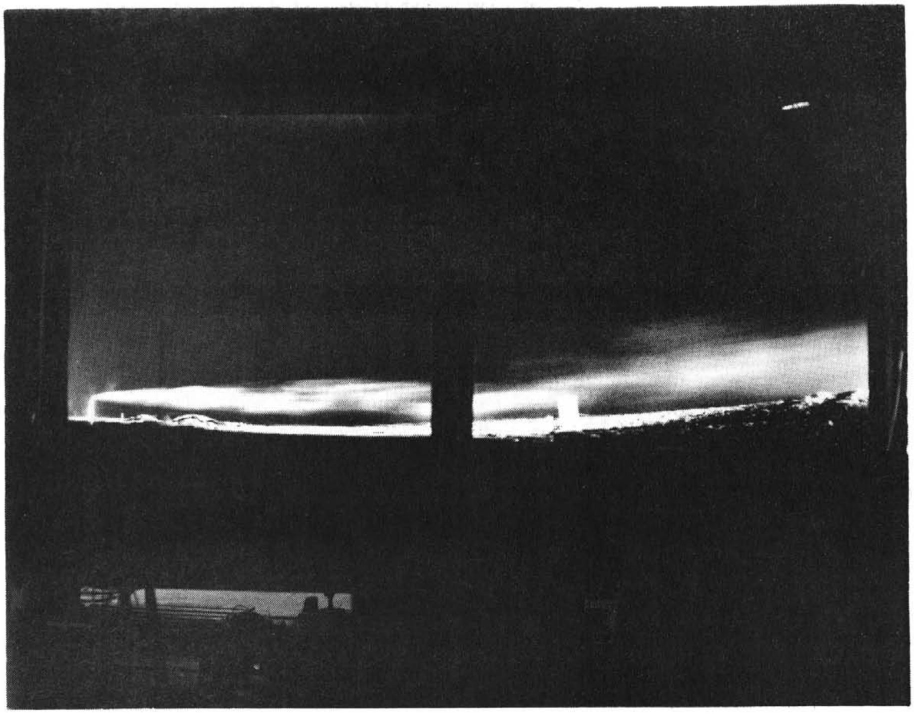

a

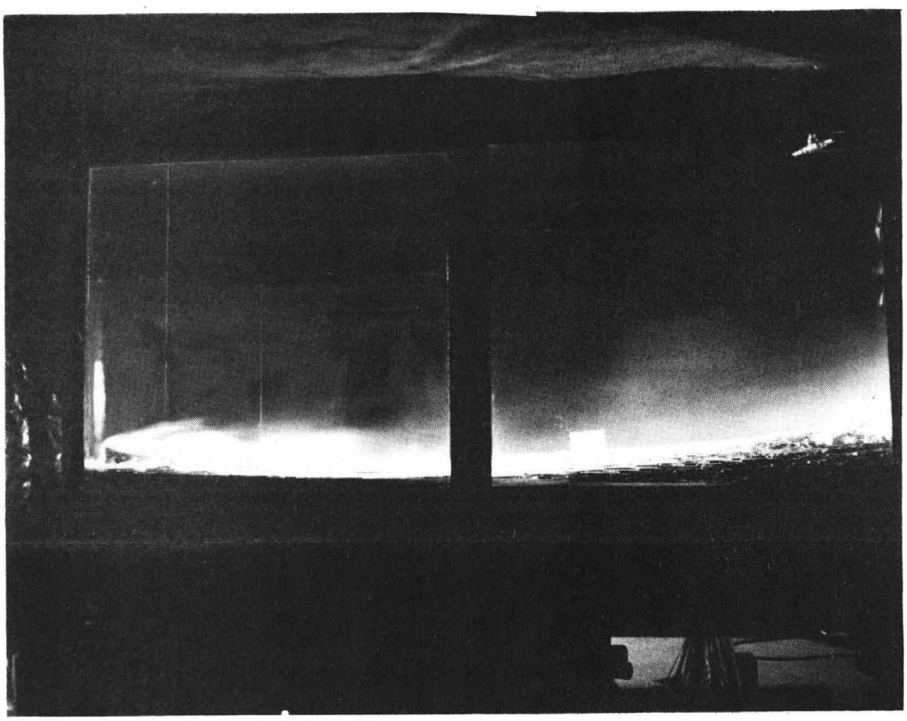

b

Figure 6.1-2. Photographs of plume behavior without (a) and with (b) the upwind terrain present for tall stack height of 199.7 m.

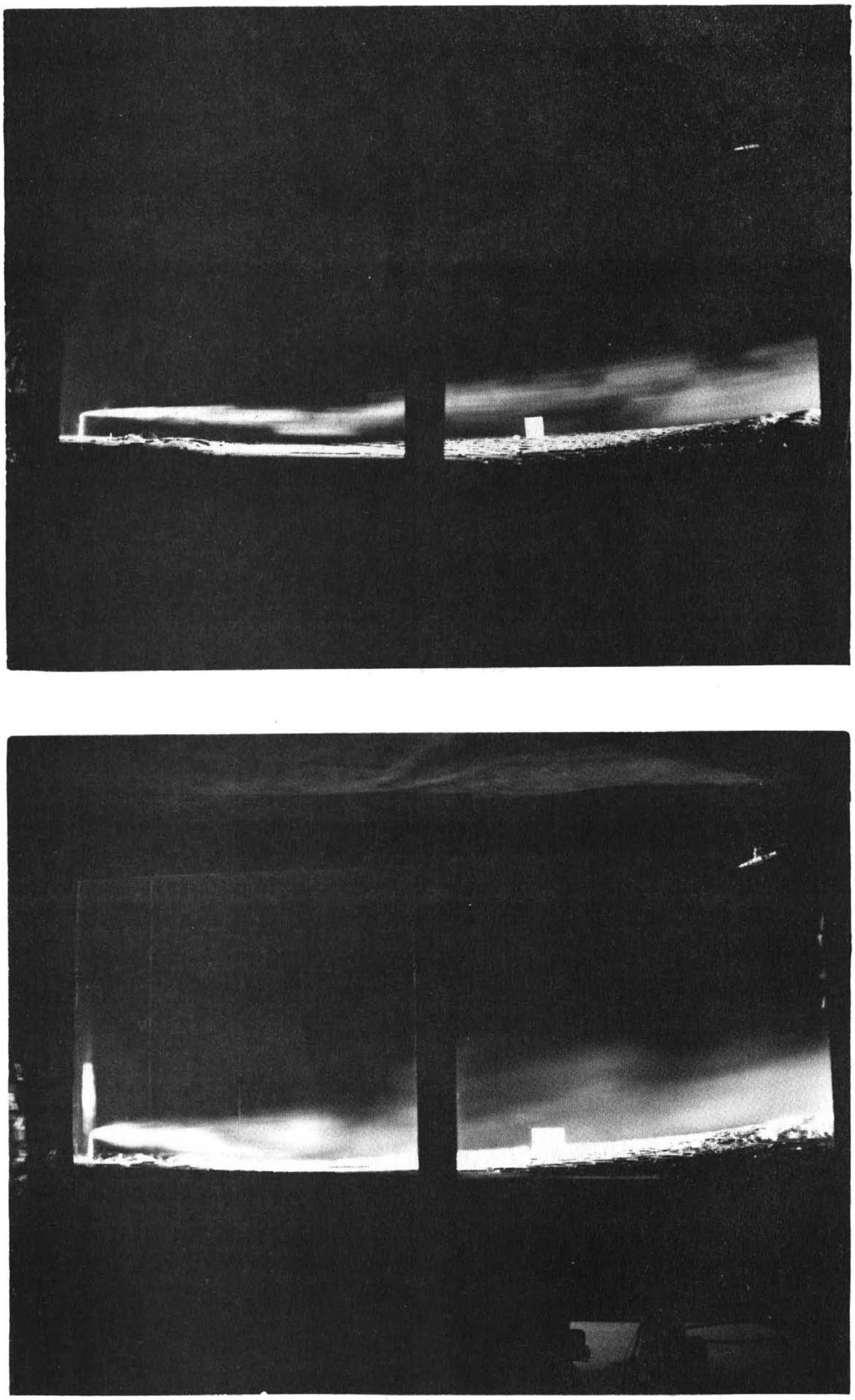

a

b

Figure 6.1-3. Photographs of plume behavior without (a) and with (b) the upwind terrain present for a tall stack height of 249.6 m.

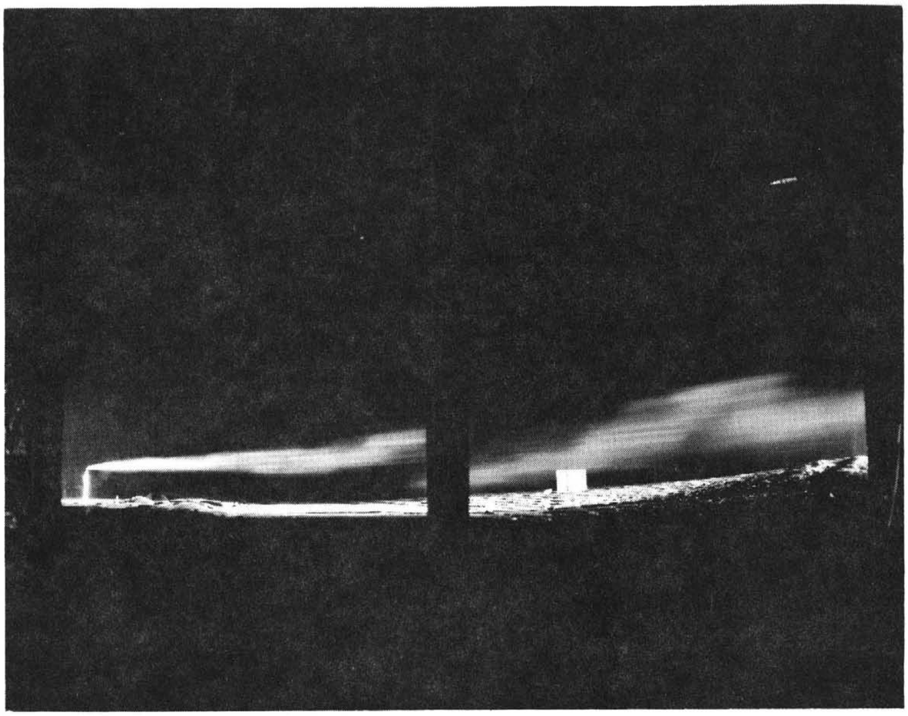

a

b

Figure 6.1-4. Photographs of plume behavior without (a) and with (b) the upwind terrain present for a tall stack height of 305.3 m.

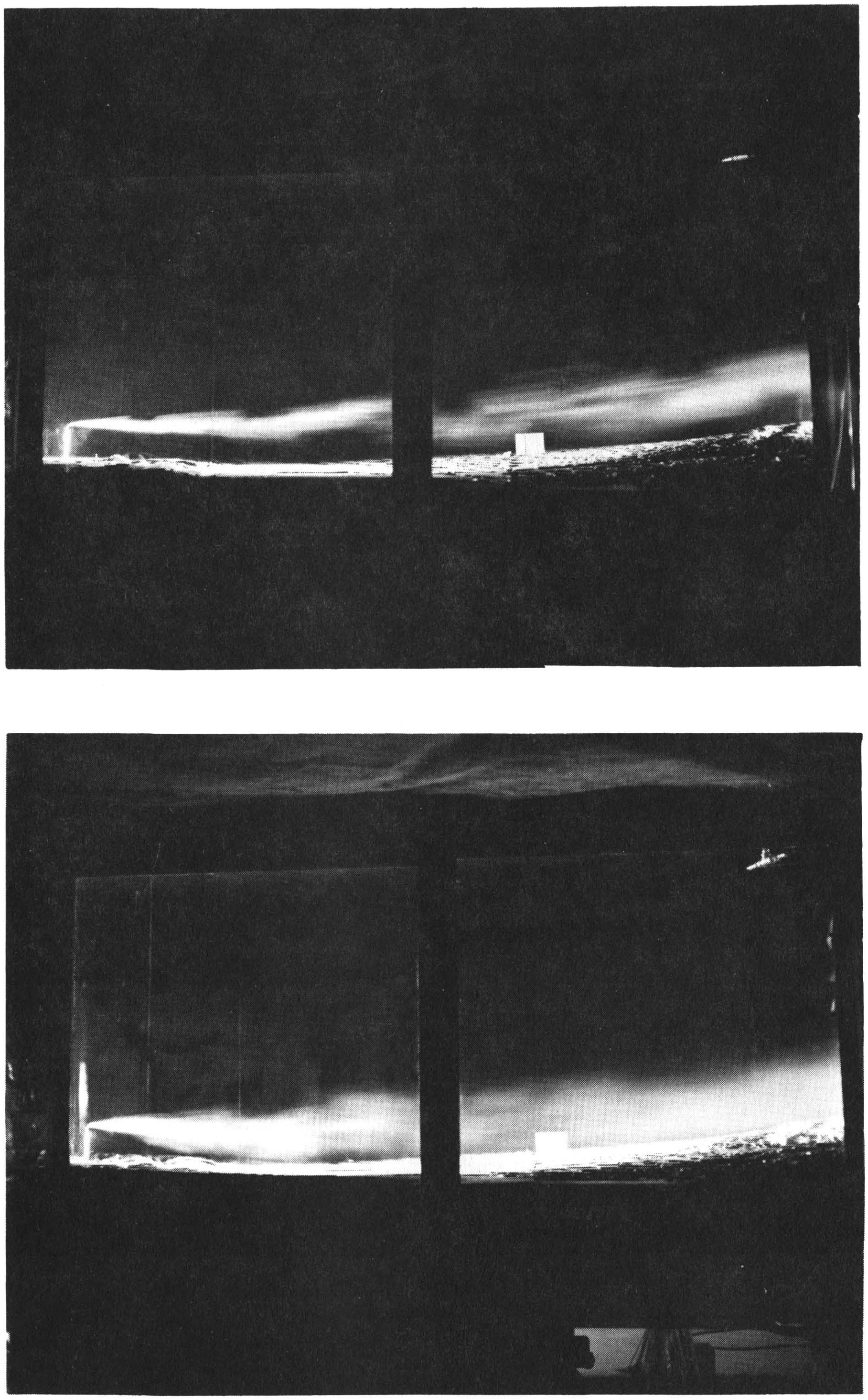

a

b

Figure 6.1-5. Photographs of plume behavior without (a) and with (b) the upwind terrain present for a tall stack height of 349.4 m.

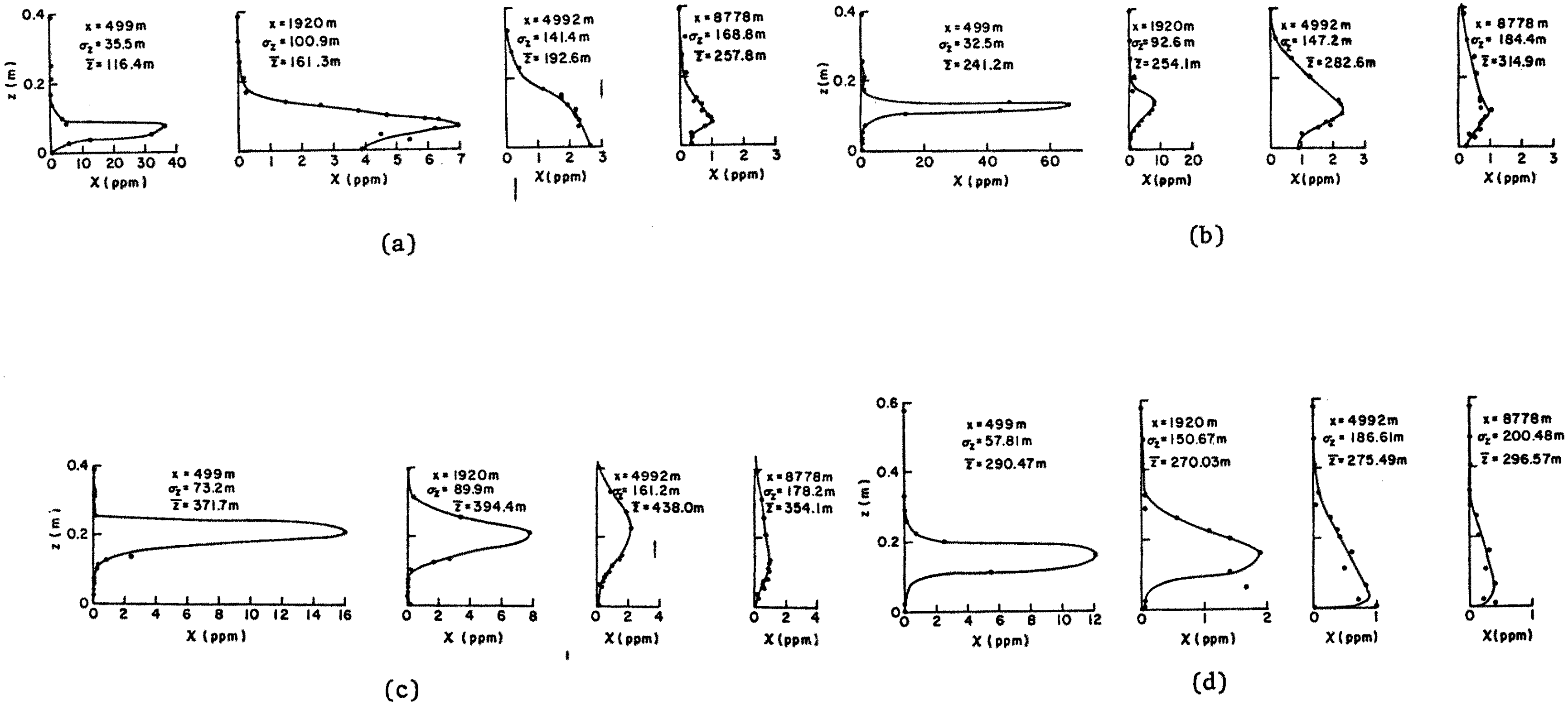

Figure 6.2-1. Vertical concentration profiles for (a) 91 m stack - without terrain, (b) 200 m stack - without terrain, (c) 305 m stack - without terrain, and (d) 305 m stack with terrain.

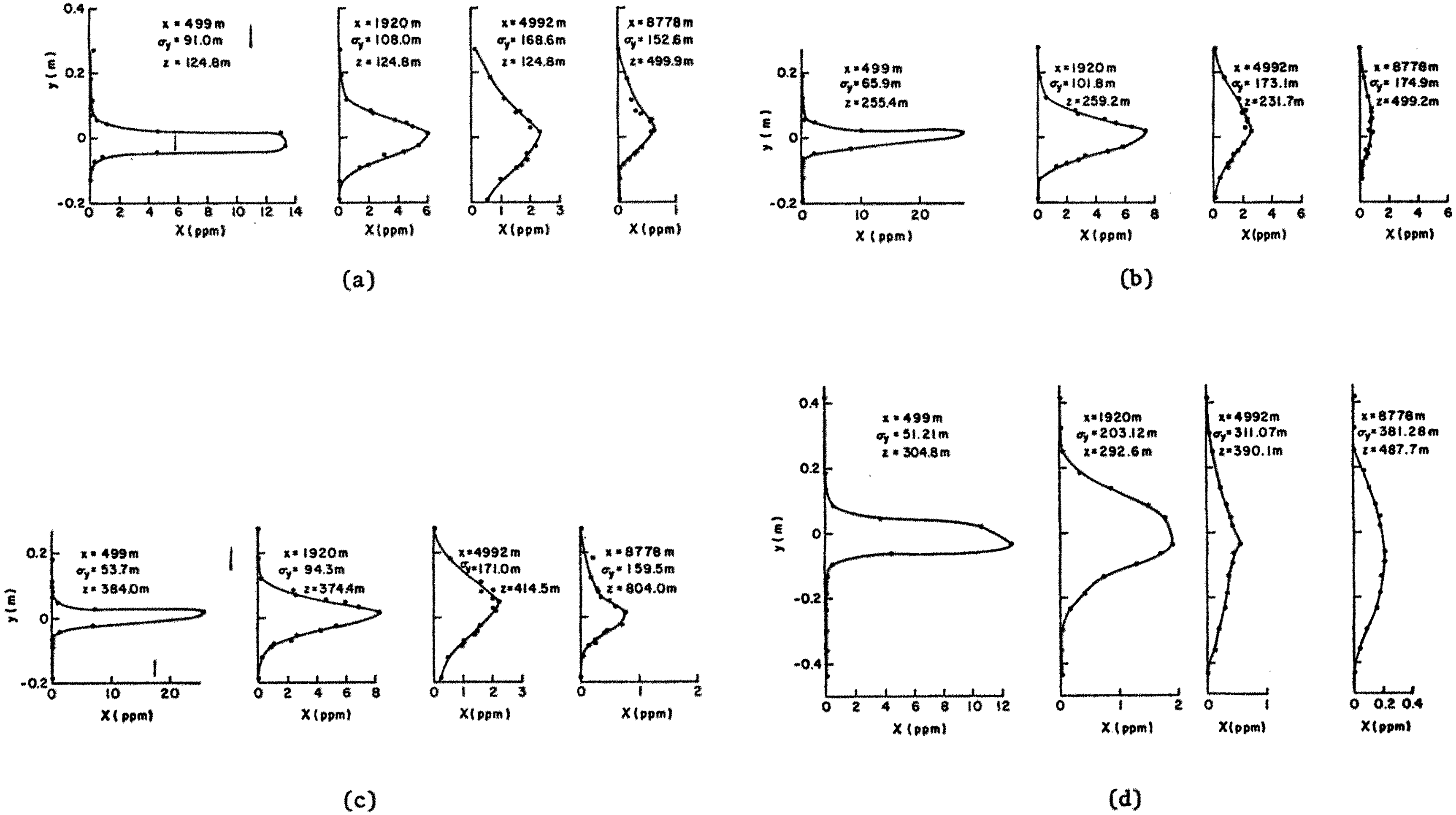

Figure 6.2-2. Horizontal concentration profiles for (a) 91 m stack - without terrain, (b) 200 m stack - without terrain, (c) 305 m stack - without terrain, and (d) 305 m stack - with terrain.

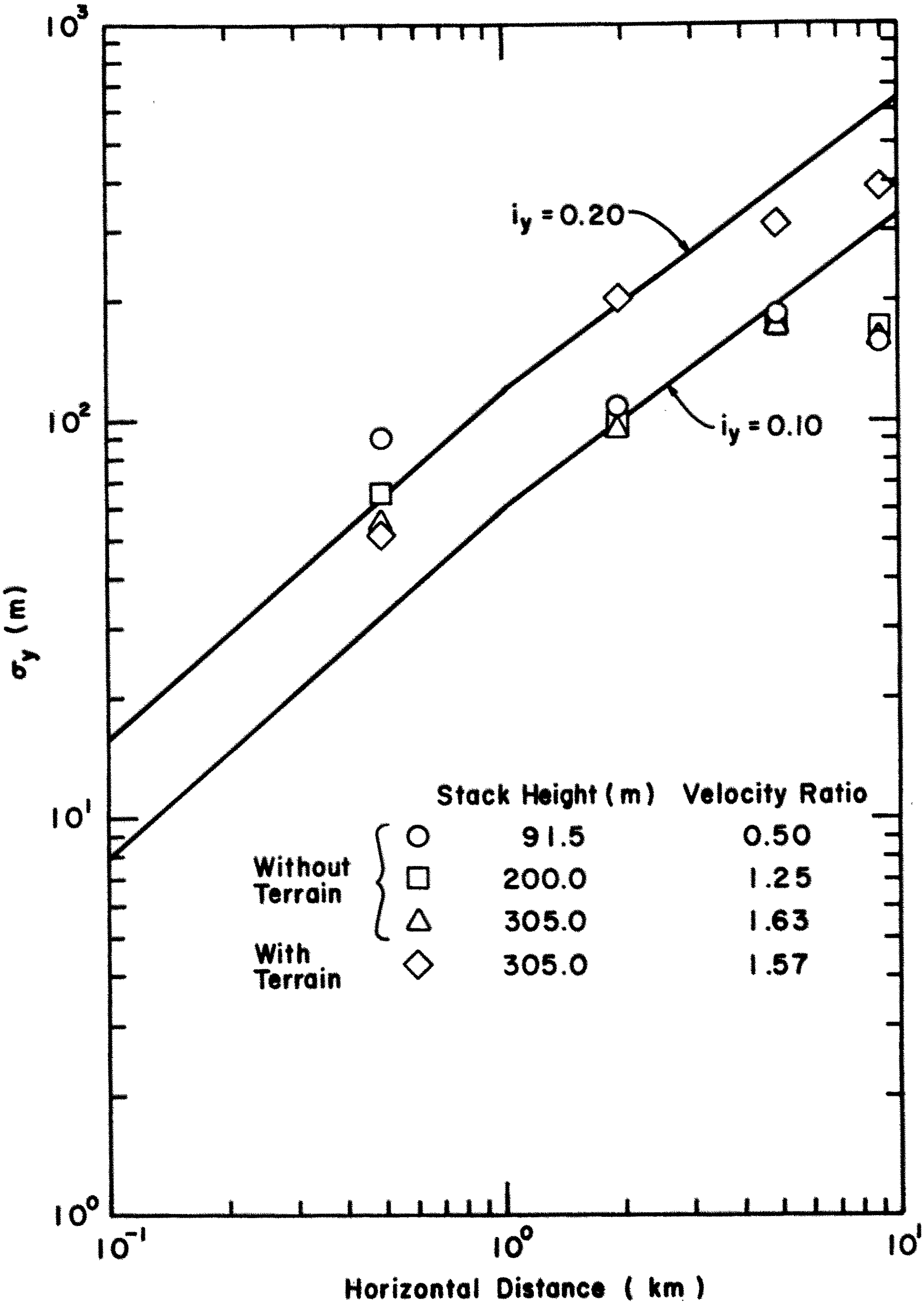

Figure 6.2-3. Comparison of observed σ_y variation with that predicted for a neutral atmosphere by Pasquill (1974, 1976).

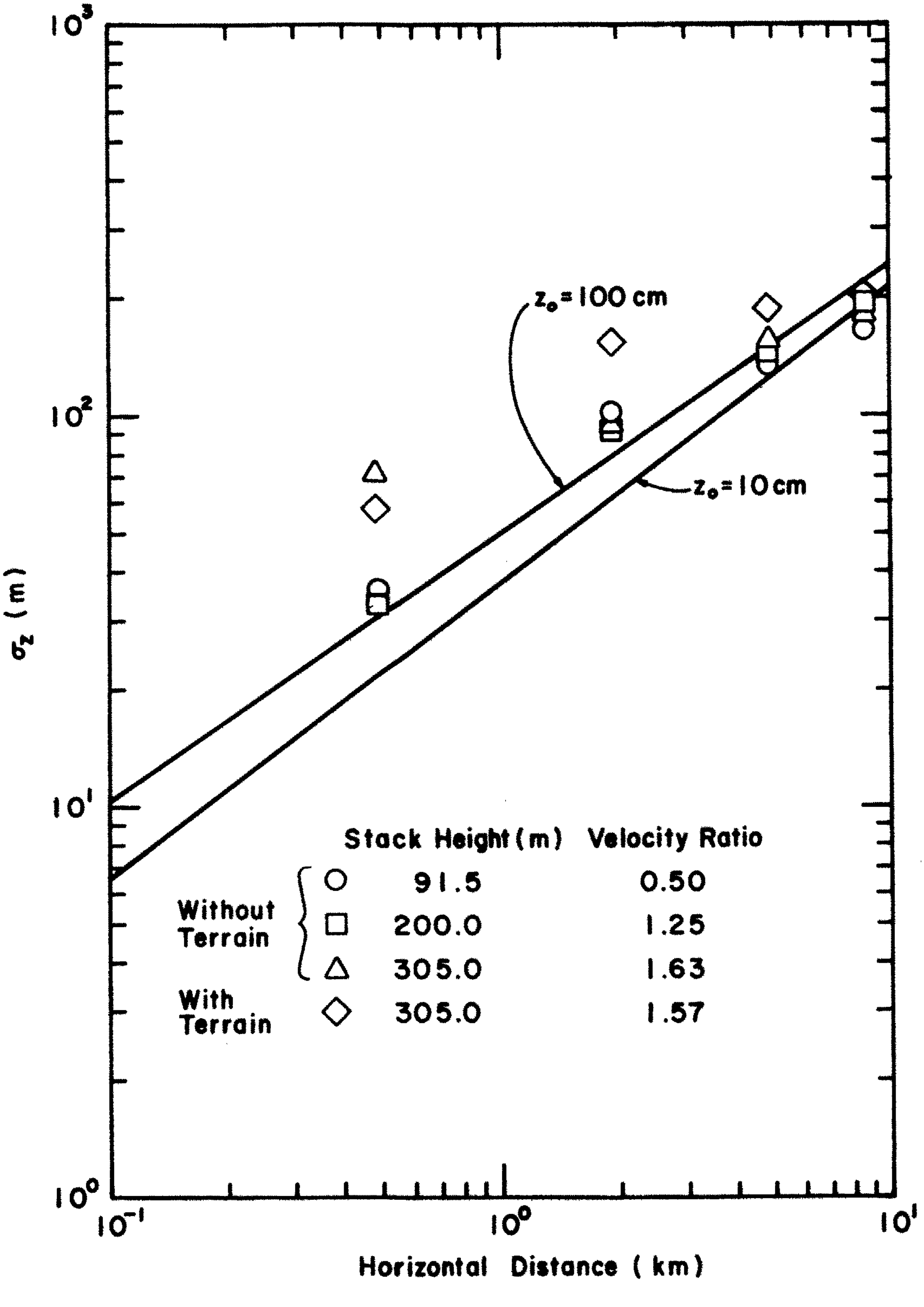

Figure 6.2-4. Comparison of observed σ_z variation with that predicted for a neutral atmosphere by Pasquill (1974, 1976).

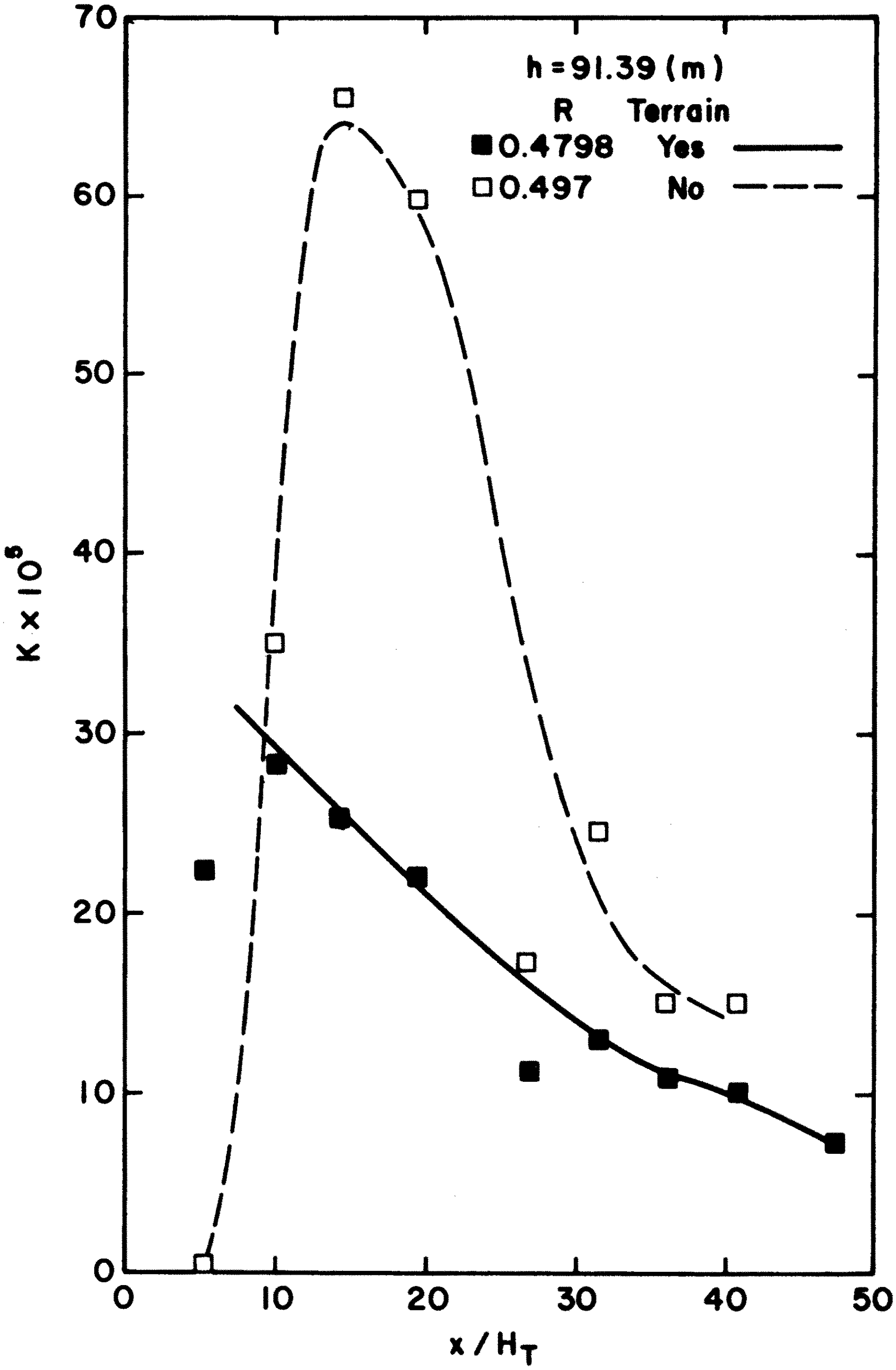

Figure 6.2-5. Maximum dimensionless concentration K versus dimensionless downwind distance (x/H_T) with and without the upwind terrain for a stack height of 91 m.

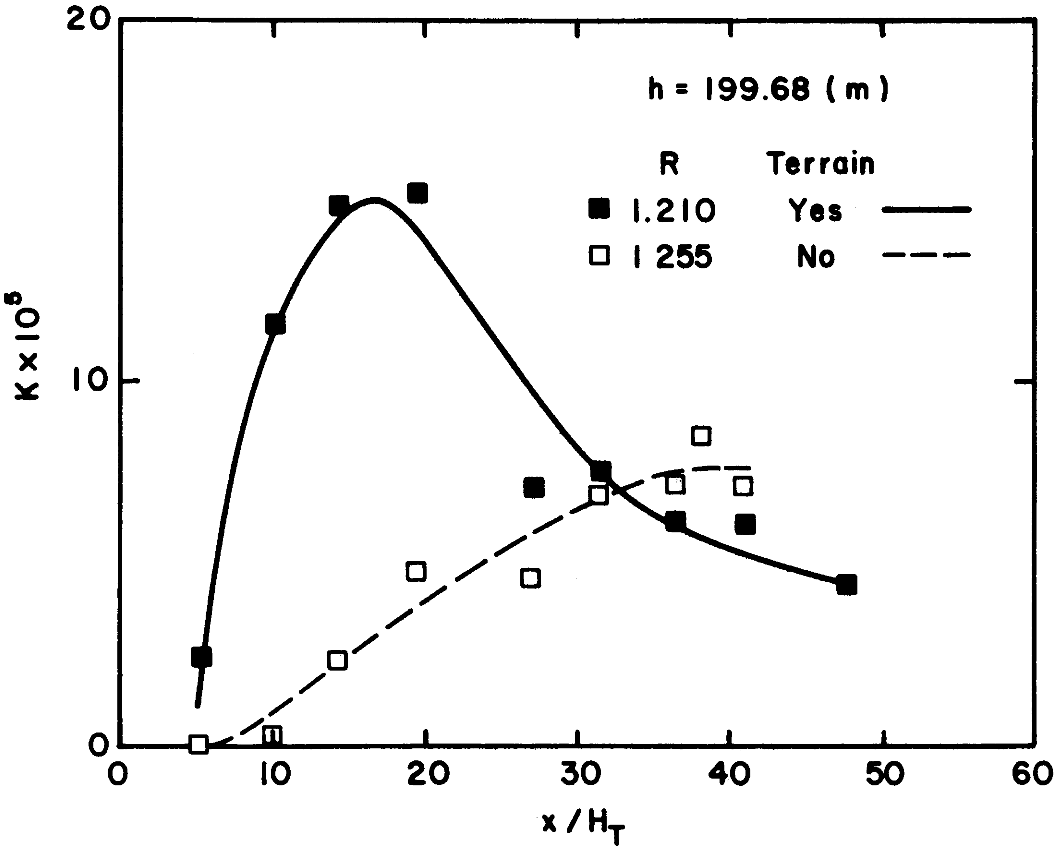

Figure 6.2-6. Maximum dimensionless concentration K versus dimensionless downwind distance (x/H_T) with and without the upwind terrain for a stack height of 200 m.

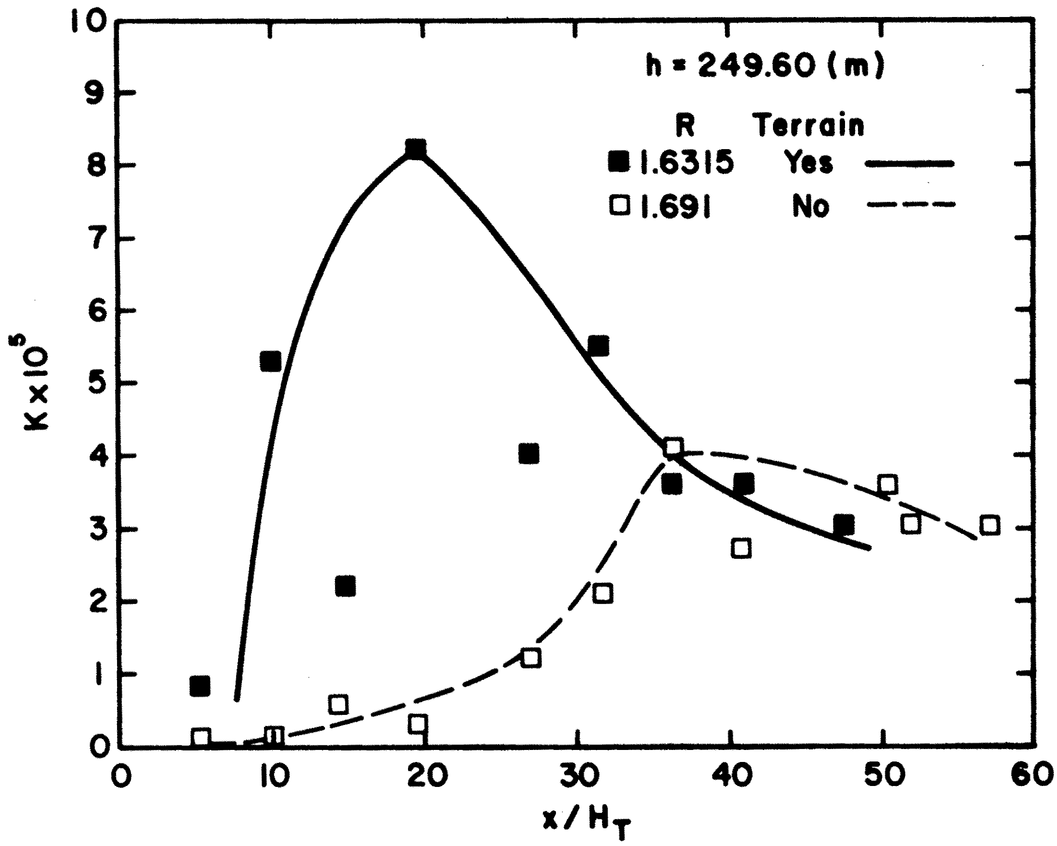

Figure 6.2-7. Maximum dimensionless concentration K versus dimensionless downwind distance (x/H_T) with and without the upwind terrain for a stack height of 250 m.

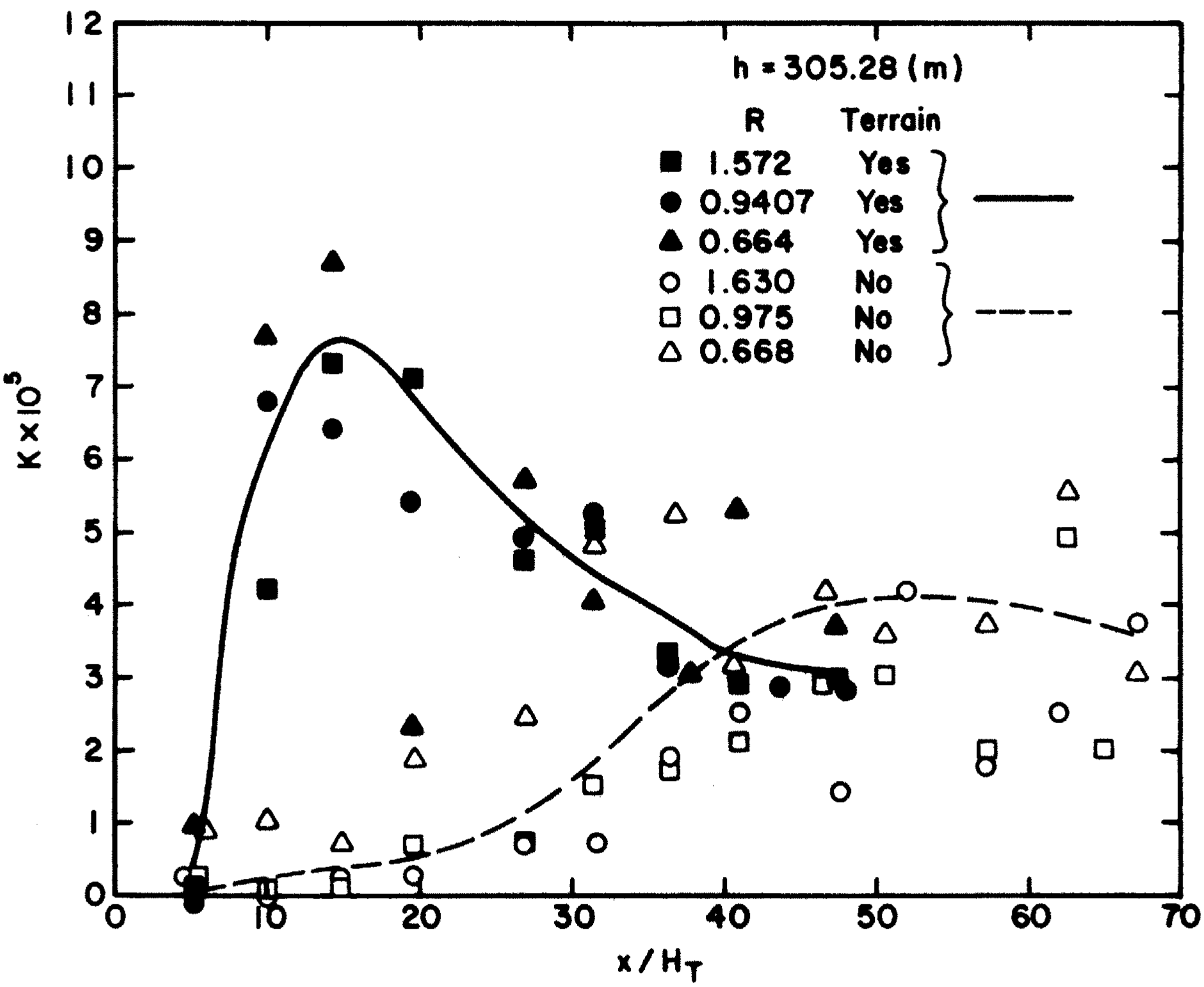

Figure 6.2-8. Maximum dimensionless concentration K versus dimensionless downwind distance (x/H_T) with and without the upwind terrain for a stack height of 305 m.

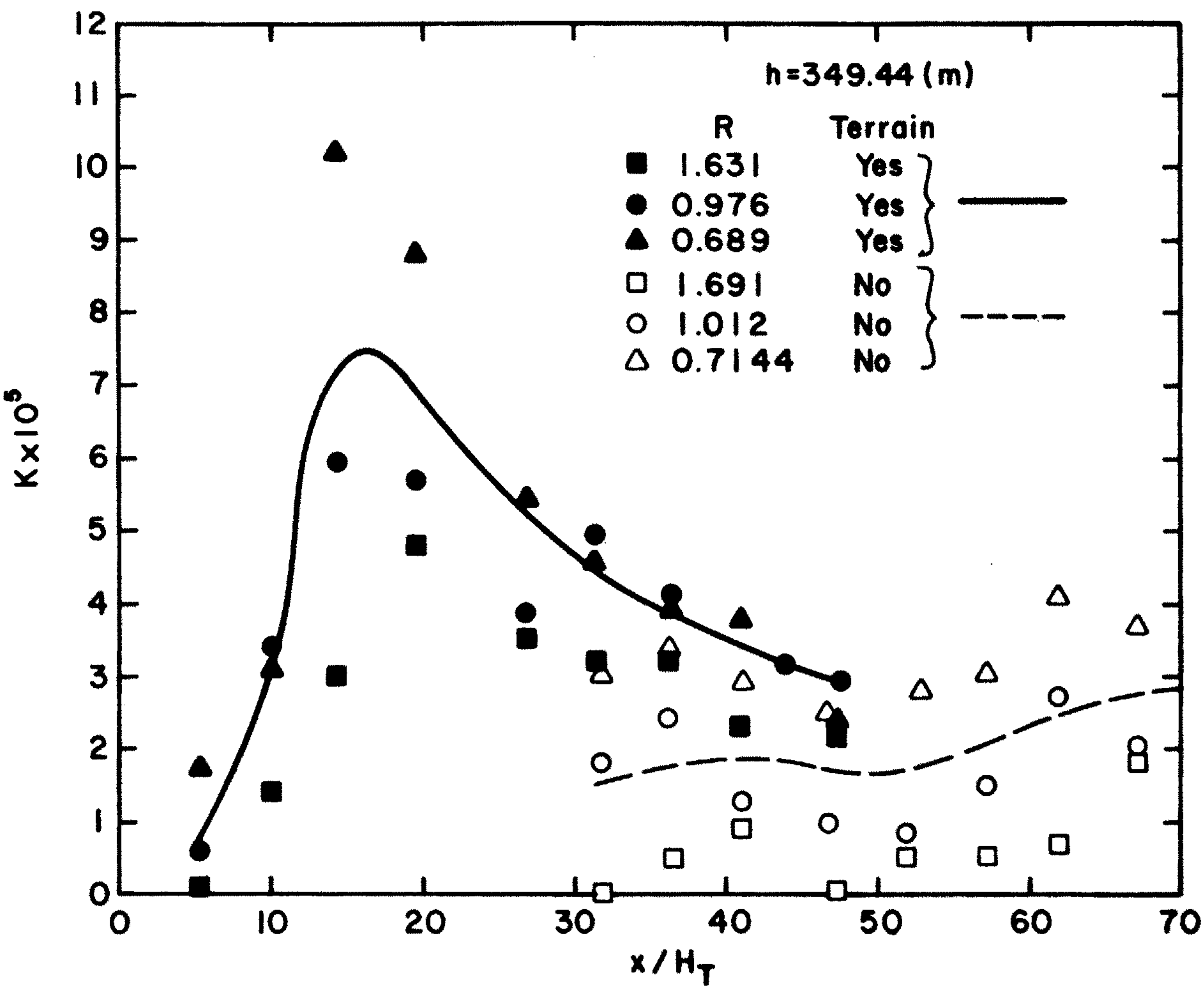

Figure 6.2-9. Maximum dimensionless concentration K versus dimensionless downwind distance (x/H_T) with and without the upwind terrain for a stack height of 349 m.

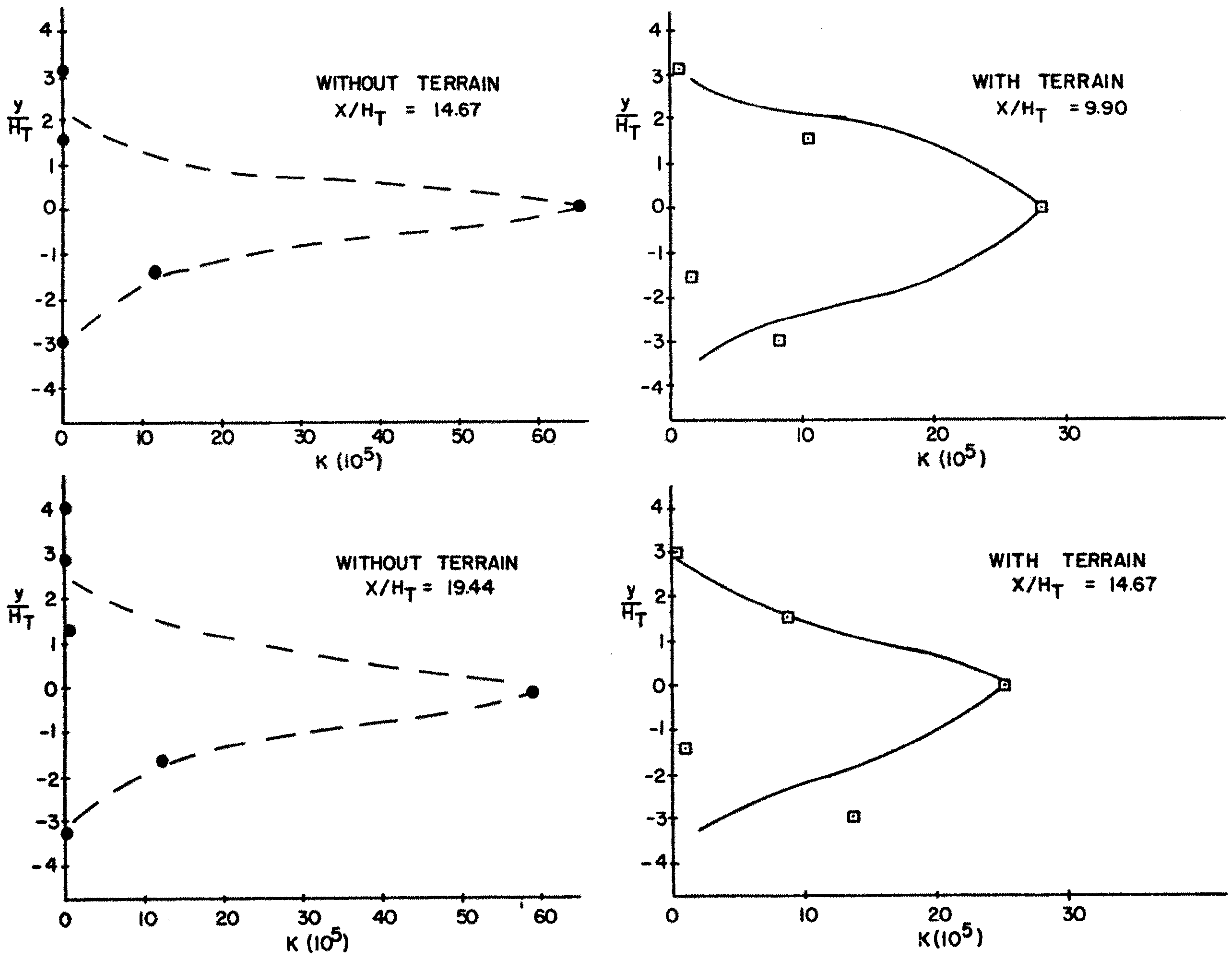

Figure 6.2-10. Dimensionless concentration K versus lateral distance (y/H_T) with and without the upwind terrain at the two downwind locations of maximum concentration for a stack height of 91 m.

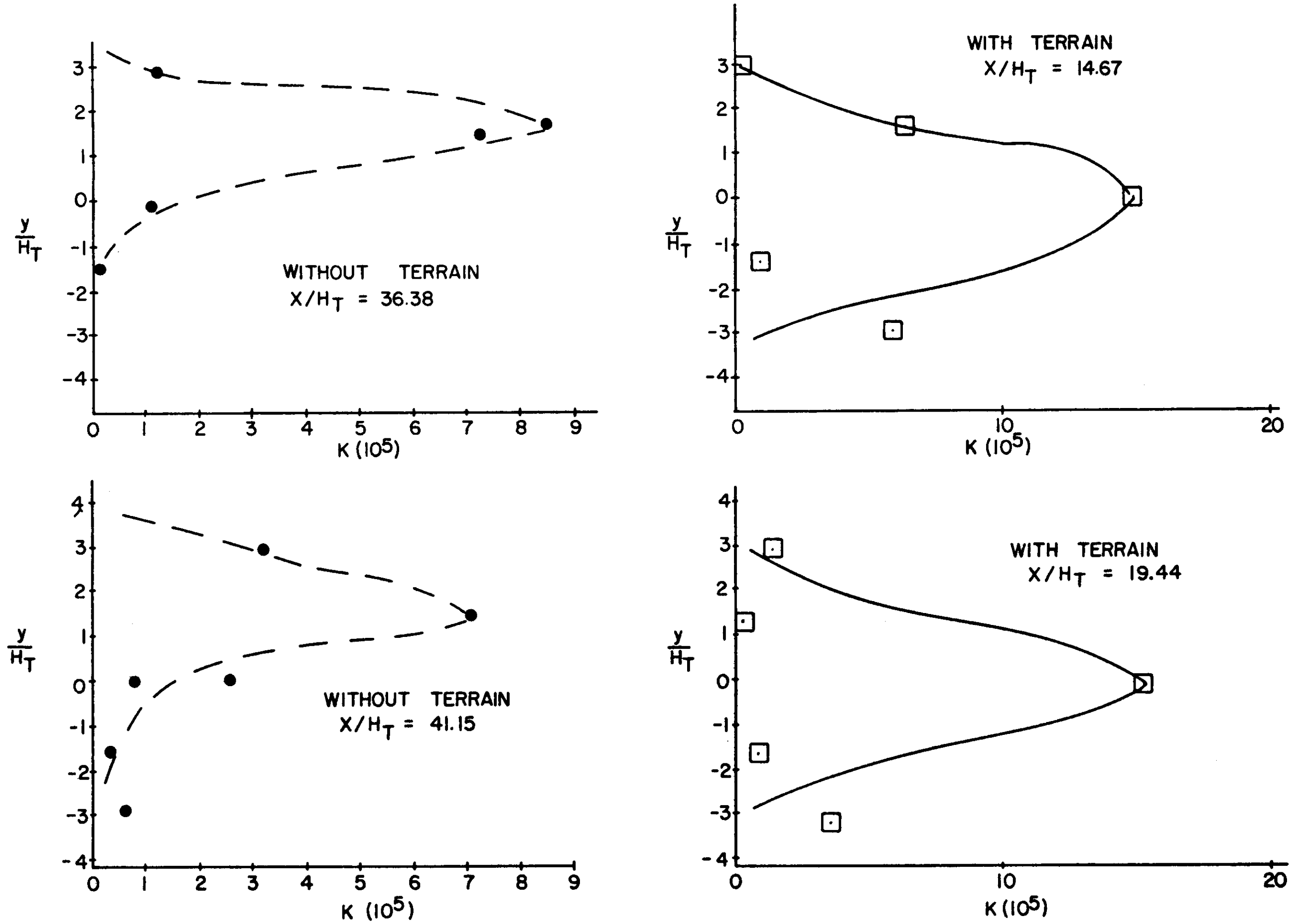

Figure 6.2-11. Dimensionless concentration K versus lateral distance (y/H_T) with and without the upwind terrain at the two downwind locations of maximum concentration for a stack height of 200 m.

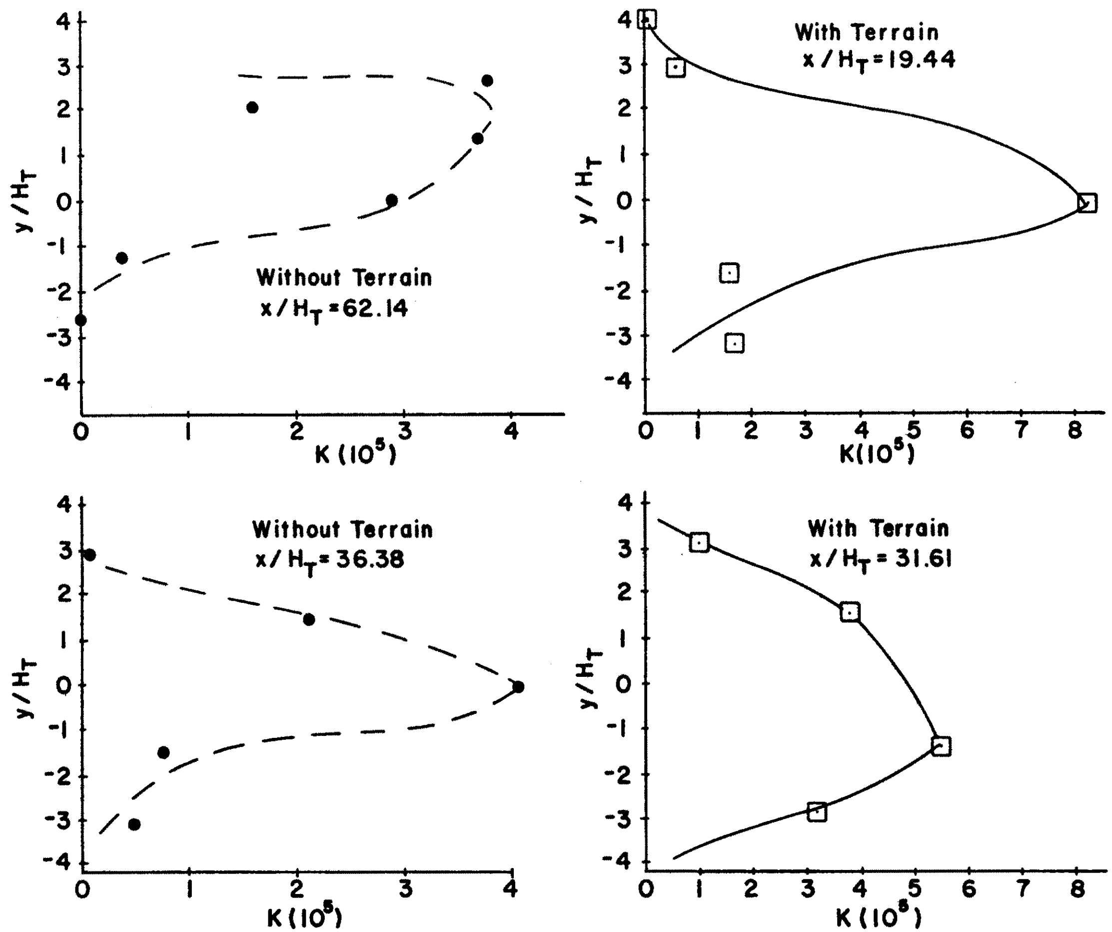

Figure 6.2-12. Dimensionless concentration K versus lateral distance (y/H_T) with and without the upwind terrain at the two downwind locations of maximum concentration for a stack height of 250 m.

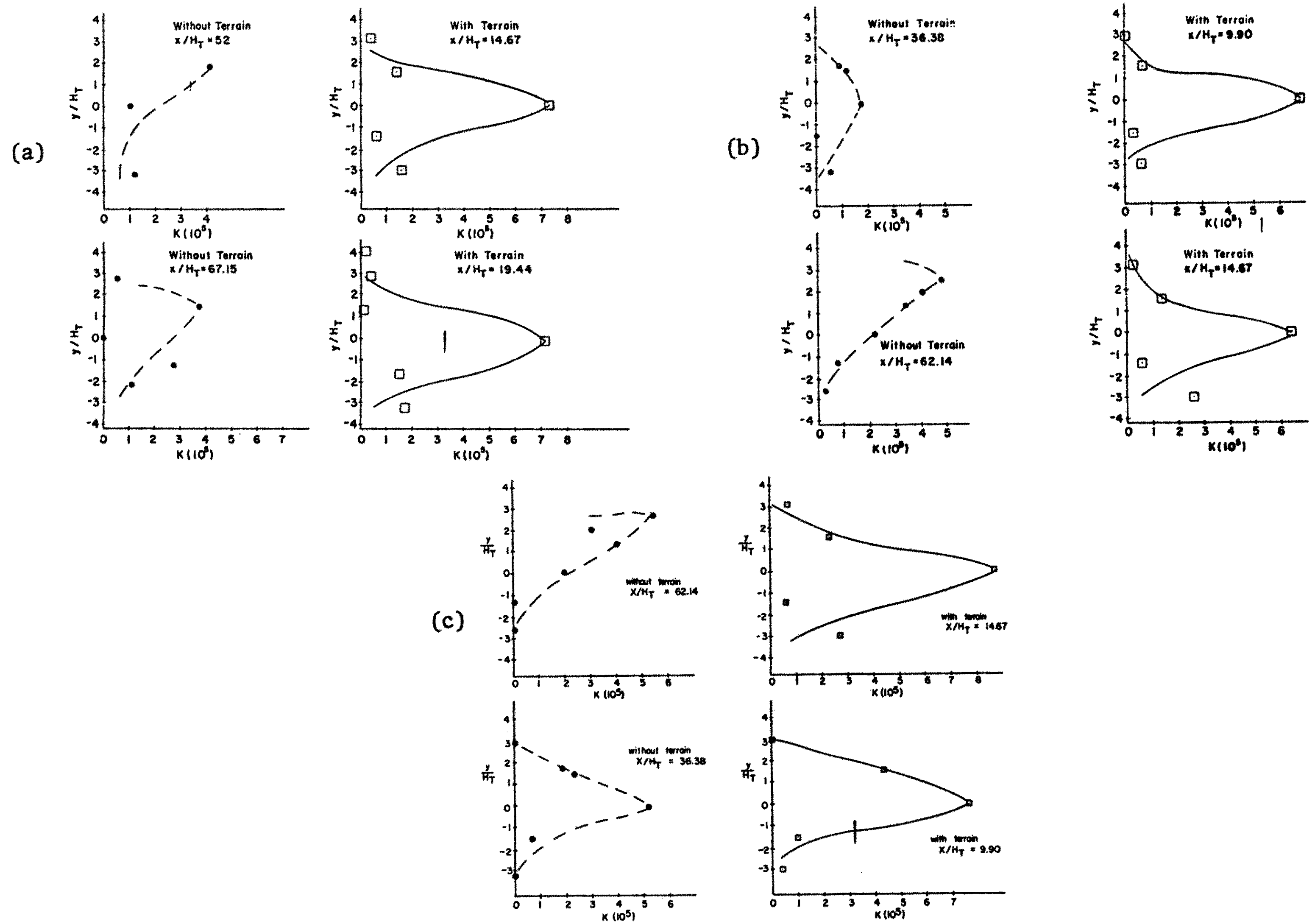

Figure 6.2-13. Dimensionless concentration K versus lateral distance (y/H_T) with and without the upwind terrain at the two downwind locations of maximum concentration for a stack height of 305 m and velocity ratios of (a) 1.57, (b) 0.94, and (c) 0.66.

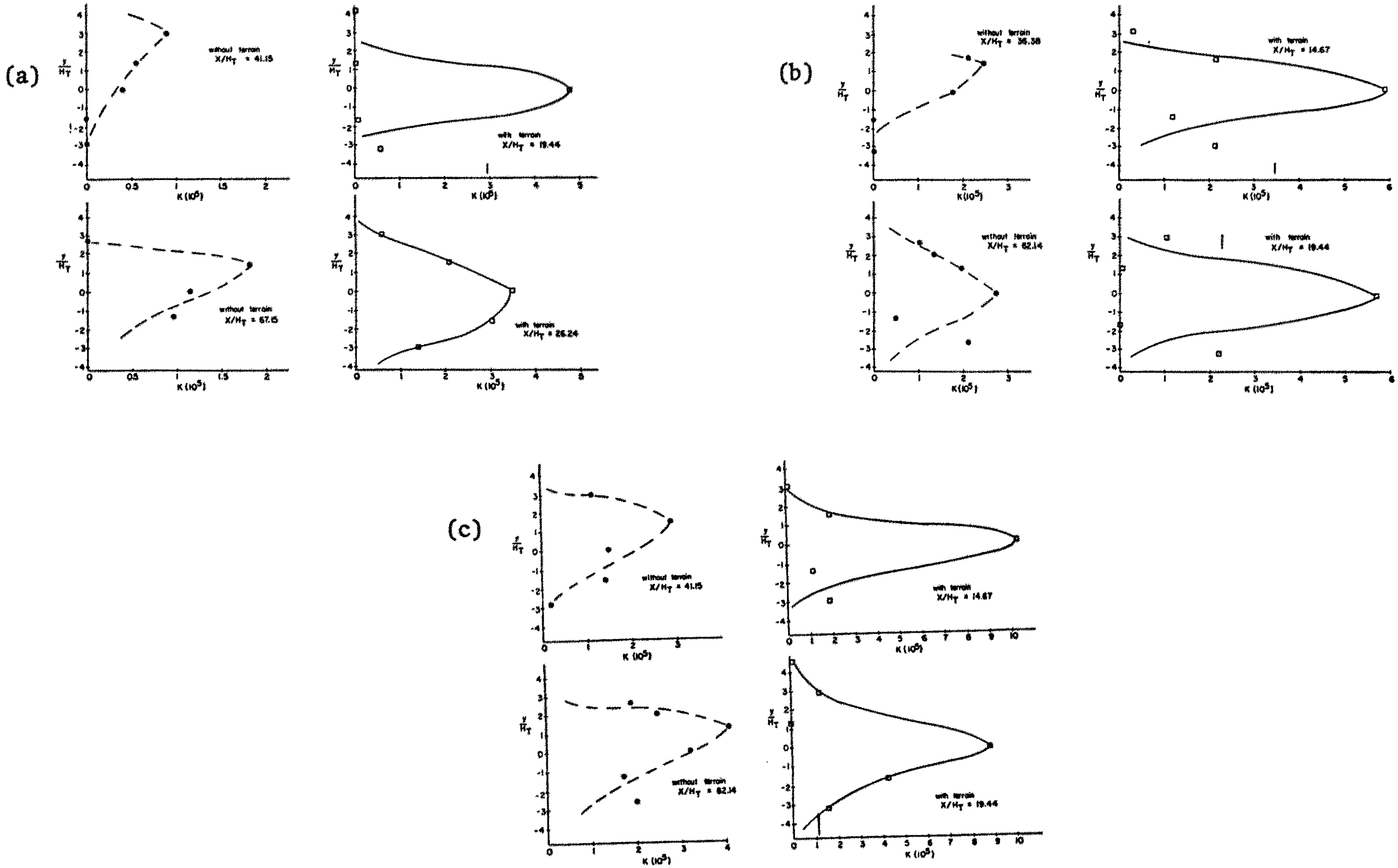

Figure 6.2-14. Dimensionless concentration K versus lateral distance (y/H_T) with and without the upwind terrain at the two downwind locations of maximum concentration for a stack height of 349 m and velocity ratios of (a) 1.63, (b) 0.98, and (c) 0.69.